# PHOSPHORYLATION-DEPENDENT CHANGES IN THE R-REGION INTERACTIONS CONTRIBUTE TO REGULATION OF THE CFTR CHLORIDE CHANNEL

**by**

**Diogo R. Poroca**

**Submitted in partial fulfilment of the requirements for the degree of Doctor of Philosophy**

**at**

**Dalhousie University**
**Halifax, Nova Scotia**
**August 2019**

# TABLE OF CONTENTS

# LIST OF TABLES

# LIST OF FIGURES

# ABSTRACT

Cystic Fibrosis Transmembrane Conductance Regulator (CFTR), the defective protein in cystic fibrosis, is an ion channel regulated by PKA and PKC phosphorylation of its regulatory region (R-region) through a mechanism still not completely understood, preventing a full comprehension of the process involved in CFTR activation. To provide novel insights into the CFTR activation mechanism, I analyzed *in situ* and *in vitro* interactions of the R-region with other parts of CFTR at different phosphorylation conditions (PKA, PKC, PKA+PKC). For *in situ* analysis, I used a split-CFTR construct expressing the front half (FH;N-tail/TMD1/NBD1), back half (BH;TMD2/NBD2/C-tail) and the R-region as three separate polypeptides expressed in BHK cells. I found that PKA stimulation increased both FH-R and BH-R interactions and PKC+PKA further increased only FH-R interactions whereas PKC stimulation alone had no effect. Inactivation of PKC consensus site S686 (S686A) significantly reduced basal BH-R interaction and prevented the further enhancing of FH-R interactions by PKC+PKA phosphorylation that was found with the wild-type R-region. The opposite phosphomimetic mutation S686D restored basal BH-R and rescued 80% of FH-R interactions after PKC+PKA stimulation compared to wild-type levels. As the channel function is mainly stimulated by PKA phosphorylation of the R region, and this response is doubled by PKC+PKA phosphorylation, results from this thesis suggest that PKC enhances PKA effect by increasing R-region interactions with the FH. Also, PKC site S686 was found to be crucial for the PKC enhancing effect which appeared to be mediated by a permissive interaction of the R-region with the BH, allowing FH-R interactions to be enhanced by PKC. Analysis of *in vitro* interactions of the R-region with six polypeptides corresponding to the N- and C-terminal tails and the four cytoplasmic loops (CLs) of CFTR showed that phosphorylation strongly increased R-region interactions with both N- and C-tails of CFTR. Moreover, PKA and PKC+PKA phosphorylation reduced R-region interactions with CLs 4 and 3, respectively, a mechanism that permits the channel activation by PKA and PKC enhancing effect. All together, these results demonstrate that phosphorylation induces an R-region shift from the cytoplasmic loops to both amino and carboxyl ends of the protein, to activate the channel.

# LIST OF ABBREVIATIONS USED

aa – amino acid

ABC – ATP-binding Cassette

ASL – Airway Surface Liquid

AMP – Ampicillin

AMPK – AMP (Adenosine Monophosphate)-activated protein kinase

BH – Back Half

BHK – Baby Hamster Kidney

BME – 2-mercaptoethanol

bp – Base Pair

CaCC – Calcium Activated Chloride Channel

CAL – CFTR-associated LigandCAM – Chloramphenicol

cAMP – 3',5'-Cyclic Adenosine Monophosphate

CF – Cystic Fibrosis

CFTR – Cystic Fibrosis Transmembrane conductance Regulator

CK2 – Casein Kinase 2

CL – Cytoplasmic Loop

CTCF – Corrected Total Cell Fluorescence

DTT – Dithiothreitol

ENaC – Epithelial Sodium Channel

ERM – Ezrin/Radixin/Moesin complex

FH – Front Half

FSK – Forskolin

IBMX – 3-Isobutyl-1-Methylxanthine

IPTG – Isopropyl β-D-1-Thiogalactopyranoside

kDa – Kilo Dalton

MST – Microscale Thermophoresis

MTX – Methotrexate

NBC – $Na^+$-$HCO_3^-$ Cotransporter

NBD – Nucleotide Binding Domain

NHERF – $Na^+/H^+$ Exchanger Regulator Factor

NKCC – $Na^+$-$K^+$-$Cl^-$ Cotransporter

PDZ – PSD95-Dlg1-Zo-1

PA – Ponasterone A

PKA – Protein Kinase A

PKC – Protein Kinase C

PCL – Periciliary Liquid

PLA – Proximity Ligation Assay

PMA – Phorbol 12-Myristate 13-Acetate

PP2A – Protein Phosphatase 2A

PP2C – Protein Phosphatase 2C

PYK2 – Proline-rich Tyrosine Kinase

RACK – Receptor for Activated C Kinase

SBP – Substrate Binding Protein

SR – Split-ΔR + R-region

SYK – Spleen Tyrosine Kinase

TMD – Transmembrane Domain

WT – Wild Type

# ACKNOWLEDGEMENTS

*I would like to thank Dr. Valerie Chappe for her supervision and guidance. I have learned a lot during this time and for sure I became a better scientist.*

*I would like to thank my supervisory committee members, Dr. Younes Anini, Dr. Xianping Dong, Dr. David Langelaan and Dr. Roger Croll for all suggestions and comments on the development of my PhD work. I also like to thank Dr. Ryan Pelis for his contribution as a supervisory committee member in the first 2 years of my PhD.*

*Access to equipment from the Labs of Dr. Stefan Krueger and Younes Anini was very appreciated.*

*I would like to thank Stephen Whitefield from the Cellular & Molecular Digital Imaging Facility for the confocal and fluorescence microscope training and Patricia Colp for the training at the Histology & Research Services Lab.*

*To my lab colleagues from Dr. Chappe Lab, Anna, Frederic and Audrey as well as the ones from Dr. Langelaan Lab, Calem, Makenzie, Connor, Kathleen and Alex, my truly gratitude for all I have learned from you and for the time we could work together.*

*To my friends in Canada and in Brazil, a sincere thanks for the good and relaxing times we had together. My PhD gave me the opportunity to meet Denise, a special person that will be ever in my life as my Canadian Mom!*

*A special thanks to Dr. David Langelaan who helped me a lot in part of my project and provided training, support, access to equipment in his lab and in the department of Biochemistry & Molecular Biology and specially for running a very collaborative environment with numerous fruitful chatting in his lab.*

*Another special thanks go to Dr. Yassine El Hiani for many conversations and advices during good and bad moments of this journey. Thanks a lot 'boss'!*

*I also thank all the funding agencies, Science without Borders-Brazil, Nova Scotia Graduate Scholarship and the Natural Sciences and Engineering Research Council (NSERC) of Canada, which have made this work possible.*

*To finish, my most important thanks goes to my family. Danielle, my wife, we have been through a lot during all those years and I am deeply grateful for all the support, patience, and understanding and apologize for all suffering I have caused in this very difficult and challenging time. I love you Mô! To Mom and Dad, thank you very much for the unconditional love and support. I could not have done it without you all!*

# CHAPTER 1: INTRODUCTION

## 1.1 CYSTIC FIBROSIS

Cystic Fibrosis (CF) is a life-limiting disease affecting epithelial cells from exocrine glands throughout the body. The basic defect in CF is a malfunction of the cystic fibrosis transmembrane conductance regulator (CFTR) chloride channel. CFTR regulates salt, and consequently water transport across epithelia and its defect causes mucus build up and clogging of exocrine ducts and airways (Davis, 2006; Elborn, 2016).

CF was first described 80 years ago by Dorothy Andersen (1938) by analysing post-mortem files of 49 patients previously diagnosed as celiac disease. She found ‘extensive fibrosis with the formation of cysts’ in the pancreas and denominated it ‘cystic fibrosis of the pancreas’, with distinctive features from celiac disease. Severe involvement of the lungs was soon associated with CF (Andersen, 1938). In 1946, Andersen and Hodges reported the study of the family history of 47 CF patients and found evidence to acknowledge CF as a genetic disease following mendelian autosomal recessive traits (Andersen & Hodges, 1946). In 1953, pediatrician Paul di Sant’Agnese and colleagues reported elevated levels of electrolytes in the sweat of 43 CF patients which became the basis of the ‘sweat test’, a powerful CF screening test still used today (Sant’Agnese et al, 1953). Three years later, Sant’Agnese described CF as a systemic disease affecting all exocrine glands, including not only the pancreas but also biliary ducts, sweat glands and airways (Sant’Agnese, 1956). In 1983,

Quinton demonstrated low chloride permeability in isolated CF sweat ducts as the primary deficiency in CF (Quinton, 1983). In 1989, the cDNA encoding the CFTR protein was isolated. The resulting protein, CFTR, is a 1480 amino acid polypeptide, member of the ATP binding cassette (ABC) superfamily of transporters. This family has a canonical architectural structure of two transmembrane domains (TMDs), each composed of six membrane spanning helices, and two nucleotide binding domains (NBDs), capable of binding and hydrolysis of ATP. In CFTR a unique and mostly disordered regulatory region (R region) is found between the two TMD-NBD halves and contains several phosphorylation consensus sites, including nine for protein kinase A (PKA) and seven for protein kinase C (PKC) (Riordan et al, 1989).

Because CFTR is expressed in tissues all over the body, its malfunction or absence affects several organs (Figure 1). In the lungs, mucus accumulation leads to chronic infection and inflammation that progressively deteriorate the organ. Mucus accumulation is a result of lower water content in the periciliary liquid (PCL) that is caused by the combination of lower or absent chloride secretion through CFTR and by hyperabsorption of sodium through the epithelial sodium channels (ENaC), which are normally downregulated by CFTR. The dense mucus formed accumulates in the airways and prevents normal ciliary clearance, creating an environment prone to inflammation and bacterial infection (Tang et al, 2014; Castellani & Assael, 2017). CFTR also mediates bicarbonate transport and the pH changes in airways liquids caused by CFTR dysfunction contributes to innate immune impairment with reduced bacterial killing efficiency

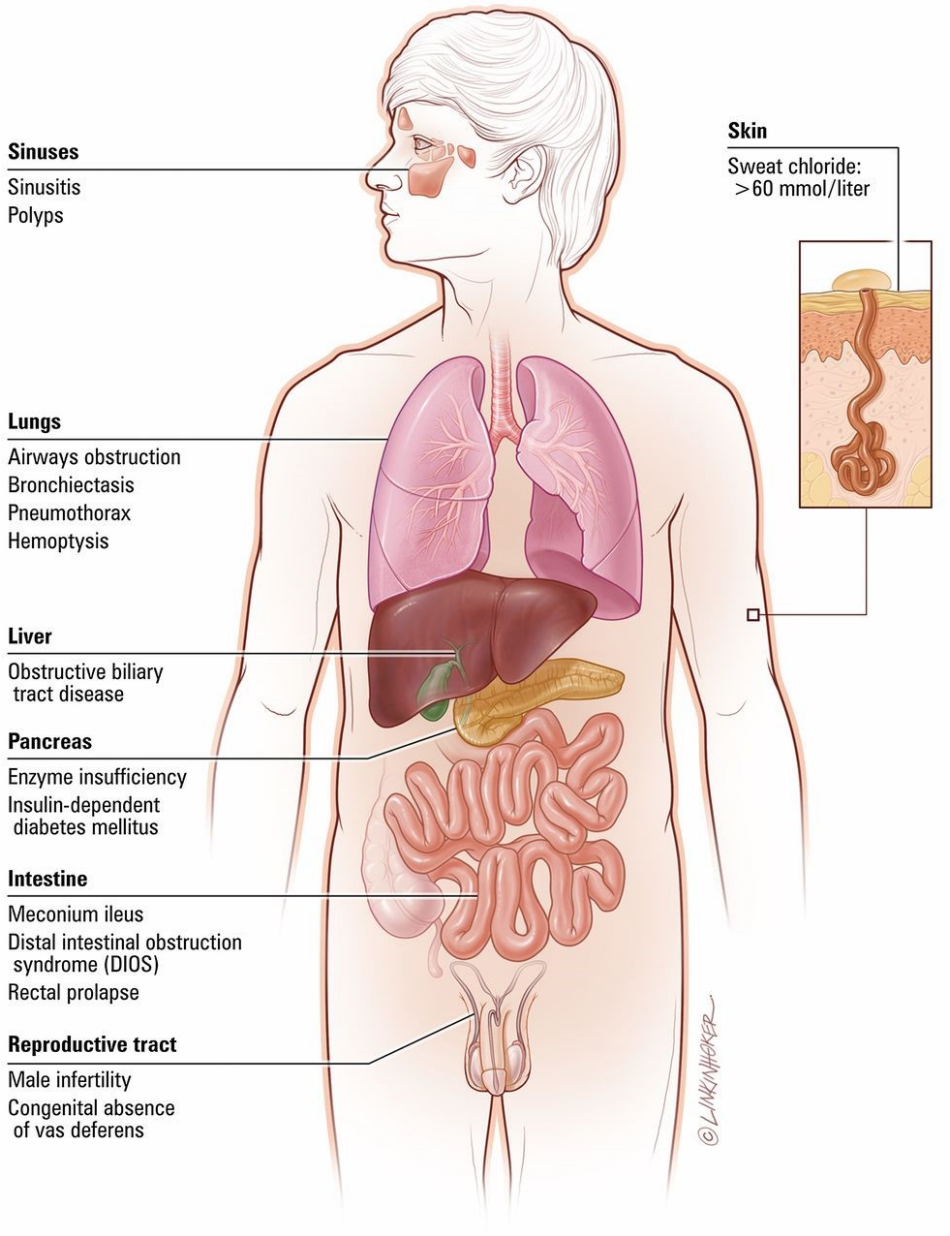


**Figure 1.** Organs affected by Cystic Fibrosis.

CF is a multisystem condition affecting many organs and causes several clinical complications. Reproduced from Paranjape SM & Mogayzel PJ (2014), with permission from the American Academy of Pediatrics.

and mucus hyperviscosity (Quinton, 2008; Hoegger et al, 2014). CF lungs also show exacerbated inflammatory responses with neutrophil infiltration and the presence of free neutrophil elastase and overproduction of pro-inflammatory cytokines, which can be found even in absence of bacterial infection (Cohen & Prince, 2012; Cohen-Cymberknoh et al, 2013). Lung infection is caused mostly by *Staphylococcus aureus* in children and as the disease progress, *Pseudomonas aeruginosa* becomes the most prevalent bacteria in adulthood. Patients with CF are also more prone to infections by non-tuberculous mycobacteria and fungi such as *Aspergillus*. Recurrent infections and inflammation result in progressively deterioration of airway tissues which eventually leads to respiratory failure and death, unless lung transplantation is possible (Cohen & Prince, 2012; Elborn, 2016; Castellani & Assael, 2017).

In the pancreas, the lower water content and acidic pH of pancreatic secretions due to CFTR dysfunction cause obstruction and progressive destruction of exocrine ducts, starting in fetal life. Ductal epithelial cells secrete bicarbonate which serves as a buffer to neutralize gastric acid and maintain optimal pH for digestive enzymes (Park & Lee, 2012; Gibson-Corley et al 2016). The deficient or absent pancreatic enzyme secretion leads to malabsorption of fat and proteins which causes malnutrition and poor growth in children with CF (Haller et al. 2014; Castellani & Assael, 2017). Exocrine pancreas impairment leads to high levels of trypsinogen in the bloodstream, which can be detected by the immunoreactive trypsinogen test, part of the neonatal screening now available in most countries where CF is prevalent (Levy & Farrell, 2015).

Liver disease occurs in a minority of patients. CFTR is expressed in the bile duct epithelia and regulates water and electrolyte content in the bile. CFTR dysfunction leads to acidic, thick and viscous bile which increases susceptibility to infection and causes periductal inflammation, progressing into biliary cirrhosis, periportal fibrosis and portal hypertension. At this stage patients are recommended for liver transplantation (Flass & Narkewicz, 2013; Kobelska-Dubiel et al, 2014; Ledder et al, 2014).

Congenital bilateral absence of vas deferens (CBAVD) is present in 90-95% of CF male, causing infertility. Other mutations in the *CFTR* gene that retain some channel activity and do not cause classic CF disease, are also reported to cause CBAVD (Castellani & Assael, 2017; Gajbhiye & Gaikwad, 2017).

Sweat glands secretion is severely affected by CFTR impairment and elevated levels of chloride and sodium in the sweat is a hallmark for CF diagnosis (Kobelska-Dubiel et al, 2014; Elborn, 2016). The sweat test is the gold standard in the diagnosis of CF and measures the levels of chloride in the sweat. Levels higher than 60mmol/L are indicative of CF, while levels lower than 30mmol/L are unlikely to be found in patients with CF. Patients with chloride levels in between those values need additional tests such as screening for genetic mutations (https://www.cff.org/What-is-CF/Testing/Sweat-Test/).

Life expectancy for patients with CF has seen a great improvement in the past decades; from a death sentence in early childhood in the 1950s to >50 years old today (Burgel et al, 2015). This increase in survival has been accompanied with comorbidities usually occurring in older patients. In the pancreas, later in life, islet

cells of endocrine pancreas are affected by pancreatic deterioration. CF related diabetes (CFRD) is turning into an important issue for CF patients, affecting up to 40-50% of adults. CFRD differs from conventional diabetes mellitus with mixed features of type 1 and type 2 diseases, and it is considered a bad prognosis for pulmonary disease progression (Kelly & Moran, 2013; Castellani & Assael, 2017).

Osteopenia is another condition commonly observed in older patients. Those patients show low bone mineral density that is attributed to late puberty, chronic inflammation, poor vitamin D absorption and reduced physical activity (Sermet-Gaudelus et al. 2011).

### 1.2 ABC Half-Transporters and Split-CFTR Channels

CFTR is a non-canonical member of the ABC superfamily of transporters and despite transporting ions bidirectionally as a channel, instead of transporting larger substrates unidirectionally, it shares a similar molecular mechanism to perform this task: ATP binding cassettes (ABCs or NBDs), with the capacity of binding and hydrolysis of ATP, are coupled to TMDs which are responsible for the translocation task (Higgins, 1992).

ABC proteins are divided in two main groups, importers and exporters. ABC importers or “uptake systems” are present only in the cytoplasmic membrane of prokaryotes and are mostly involved in the uptake of a plethora of nutrients that range from small carbohydrates, amino acids, and small peptides to metals, anions, iron chelators (siderophores), and vitamins. ABC exporters or “efflux

systems” are present in all live organisms and localize at the plasma membrane of both prokaryotes and eukaryotes as well as in membranes of intracellular organelles (Davidson & Chen, 2004; Biemans-Oldehinkel, 2006; Theodolou & Kerr, 2015).

The four core structural domains of a typical ABC transporter (two TMDs and two NBDs) can be organized in several different arrangements ranging from 4 distinct domains expressed separately to one single polypeptide containing the four domains, and almost every imaginable type of arrangement has been already described (Figure 2). In the nickel transporter from gram-negative and the oligopeptide transporter from gram-positive bacteria, each TMD and NBD are represented by a separate and distinct polypeptide. Some ABCs, like the glucose and maltose transporters, display two identical NBDs coupled with two distinct TMDs and occasionally, the two TMDs or NBDs can be fused as one polypeptide chain as it is the case of siderophore and ribose transporters, respectively. These complex structural organizations are found exclusively in prokaryotic importers. Several ABC transporters, mostly in eukaryotes but also found in bacteria, are organized as half-transporters where a TMD is fused covalently to a C-terminal NBD and the functional assembly consists either of two identical (homodimer) or two distinct (heterodimer) halves. This is the most common structural organization observed in eukaryotic exporters. The remaining eukaryotic exporters express the four core domains in a single long polypeptide with, normally, each NBD being C-terminal to each TMD and are called full-length

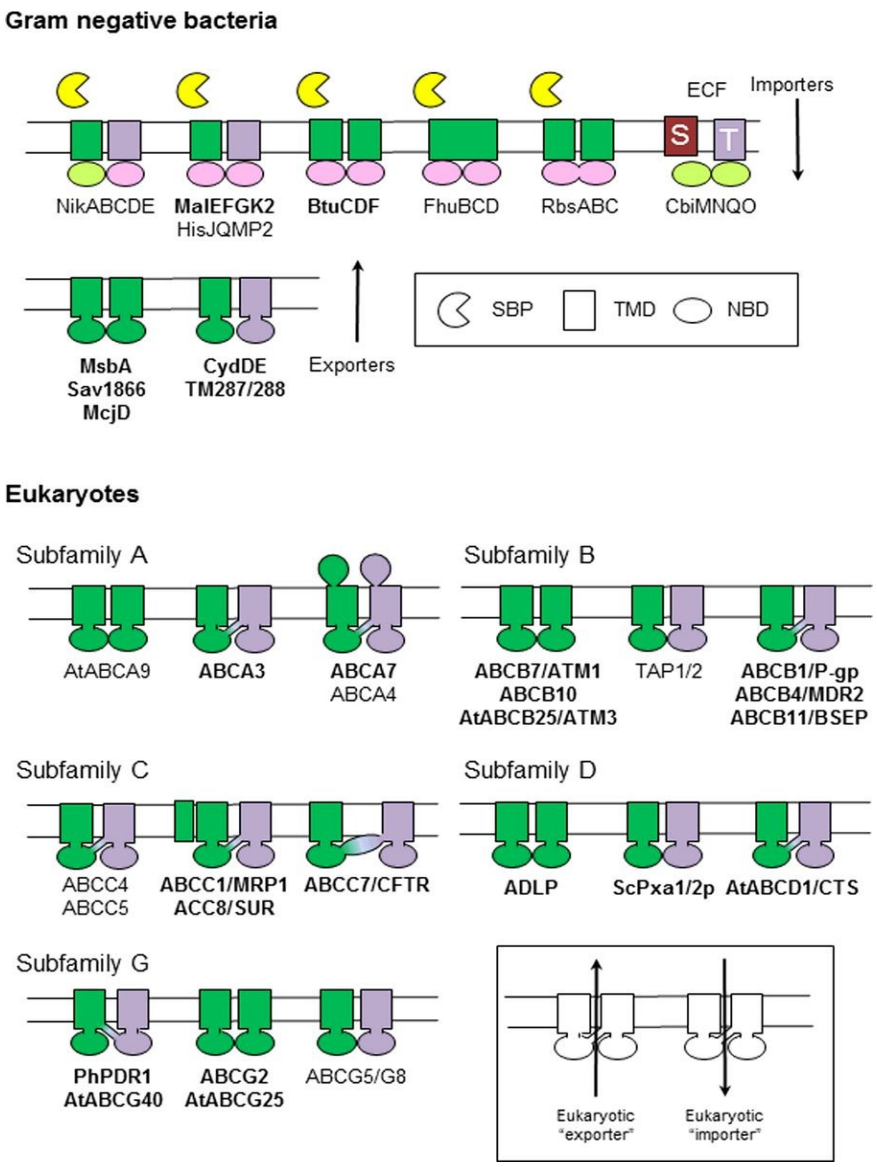


**Figure 2. Domain organization of ABC transporters from different organisms.**

In Gram-negative bacteria, importers comprise two TMDs, two NBDs (ATPase subunits) and a periplasmic SBP. Energy coupling factor (ECF) transporters comprise two NBDs, a transmembrane protein (T) and a substrate-specific integral membrane protein (S). All bacteria and archaea also contain homo- or heterodimeric exporters, in which a TMD is fused with an NBD. Eukaryotic ABC proteins are classified in eight subfamilies (A–H). The organization of core and additional domains is shown for different representative topologies in each subfamily. Not included are soluble subfamilies E and F and transporter subfamily H, which is absent from mammals, plants and fungi. Reproduced from ABC transporter research: going strong 40 years on, by Theodoulou & Kerr (2015), licensed under CC BY 3.0. No changes were made.

transporters (Higgins, 1992, Biemans-Oldehinkel, 2006; Theodolou & Kerr, 2015).

The four canonical domains suffice to perform the translocation of substrates, inwardly or outwardly, depending on the system. Extra, accessory domains are found in particular ABC transporters members, and serve as regulatory roles or for uptake of substrates. This is the case of CFTR and its regulatory region, or the substrate-binding protein (SBP) of several prokaryotic ABCs. The accessory domains can be identified as extra transmembrane segments or attached to the TMDs or NBDs and in most cases their deletion has no effect in the translocation function (Higgins, 1992; Biemans-Oldehinkel, 2006).

In humans, there are 48 ABC transporters subdivided in seven subfamilies, ABCA-ABCG, based on the similarities in amino acid sequence and phylogeny. Subfamilies ABCA and ABCC are entirely comprised of full-length transporters while ABCD and ABCG subfamilies are all half-transporters. ABCB subfamily members can be both half and full-length transporters. The last two subfamilies, ABCE and ABCF, have no TMDs associated with the NBDs and therefore, are not able to translocate substrates, although, their NBDs are phylogenetically similar to other ABC proteins (Dean & Annilo, 2005).

Although CFTR functions as a channel rather than either an importer or an exporter, its structural organization resembles the ABC exporters, such as the *Staphylococcus aureus* multidrug transporter Sav1866, which was often used as template for CFTR homology models before high resolution structures became available (Mornon et al, 2008; 2009; Serohijos et al, 2008; Norimatsu et al.

2012). Sav1866 is organized as a half-transporter with 2 homodimers, each composed of a TMD linked to an NBD. It displays a structural arrangement similar to CFTR, with the two half' TMDs intertwined with each other and tight interactions between both TMDs and NBDs (Dawson & Locker, 2006).

Since the basic functional mechanism of ABC proteins is conserved in all live organisms, from archaea to man, with diverse structural assemblies able to form functional systems, it is not unrealistic to assume that different structural arrangements of the same ABC protein could still generate functional transport systems. Indeed, the two NBDs of the *Salmonella typhimurium* peptide transporter (OppD and OppF), which are natively expressed as separate proteins, can be fused together to give a single functional polypeptide (Higgins,1992). Also, the yeast a-factor mating pheromone transporter, STE6, which is normally expressed as a single polypeptide of four domains, can be expressed as two halves, and are able to reassemble and mediate a-factor transport. Expression of each of the two halves alone did not generate functional transporters (Berkower & Michaelis 1991). Similar results were obtained with half-molecules of P-glycoprotein, a drug-exporter involved in resistance to cancer drugs, which exhibited drug-stimulated activity only when both halves were co-expressed (Loo & Clark, 1994).

This natural flexibility of ABC transporters structures has also been explored in CFTR research. Ostedgaard et. al (1997) demonstrated results similar to the yeast STE6 and P-glycoprotein transporters (Berkower & Michaelis 1991; Loo & Clark, 1994) by expressing CFTR as two halves, the N-terminal half comprising

amino acids 1-835, including the lasso motif, TMD1, NBD1 and the R-region, and the C-terminal half including amino acids encoding TMD2, NBD2 and the C-terminal tail (aa 836-1480). Co-expression of both CFTR halves elicited a cAMP-regulated channel activity, whereas expressing each half alone did not (Ostedgaard et al, 1997). Moreover, the authors suggested that the segments involved in the interaction between the two CFTR halves are located in the TMDs, as removal of the cytoplasmic regions, NBDs, R-region, and N- and C-tails, did not prevent association (Ostedgaard et al, 1997).

Earlier studies identified cAMP-regulated currents in oocytes expressing either a kidney-specific natively expressed N-terminal half of CFTR (TNR-CFTR; Morales et al, 1996) or an artificially truncated N-terminal construct (D836X) (Sheppard et al, 1994). The native kidney-specific form of CFTR, found to be expressed only in specific segments (renal medulla) of rat and human kidney, generated only 15-25% of the current observed in wild-type CFTR but retained the regulatory function over outwardly rectifying chloride currents (Morales et al, 1996), indicating that functional CFTR channels can also be reassembled as homodimers.

In a study aiming to identify the N- and C-terminal boundaries of NBD1, various combinations of CFTR half constructs were expressed in oocytes and channel activity similar to wild-type CFTR was observed in the constructs where the cutting site did not impair NBD1 function (Chan et al, 2000). In another study, the same group demonstrated that CFTR halves cut just before (aa 1-633 + 634-1480) or just after (aa 1-835 + 837-1480) the R-region boundaries could

reassemble to form functional channels, as well as a construct lacking the whole R-region segment (aa 1-633 + aa 837-1480) supporting the idea that the four core ABC transporter domains are enough to produce translocation (Csanady et al, 2000).

CFTR half constructs were also used in a study demonstrating PKA-induced interactions between CFTR domains. A split-CFTR construct similar to the one used by Csanady et al. (2000), comprising segments 1-634 and 837-1480, was co-expressed with a third polypeptide representing the R-region (aa 635-836). Co-expression of the R-region partially inhibited the constitutive activity observed in the split-channel (aa 1-634 + aa 837-1480). Moreover, physical and functional reassembly of the two halves were demonstrated by a combination of immunolocalization and functional studies (Chappe et al, 2005). Taken together, the natural existence of half-transporters in the ABC family (including CFTR in the kidney) and the studies using engineered half-transporters, including prokaryotic members, yeast and human (CFTR included), provide strong evidence for the usefulness of studies employing CFTR half-transporters to investigate how association between CFTR domains modulate channel function.

### 1.3 Cystic Fibrosis Transmembrane conductance Regulator

The *CFTR* gene is located on chromosome 7 (7q31), contains 27 exons and encodes a 1480 amino acids protein, the CFTR protein. Over 2,000 mutations in the CFTR gene have been reported (http://www.genet.sickkids.on.ca/Statistics Page/) and functional effects of many of them have been elucidated (Sosnay et

al, 2013; https://www.cftr2.org/). The majority of CFTR mutations are missense modifications, followed by frameshift, splicing and nonsense mutations. In frame deletions and insertions account for only 2% of the number of mutations. CFTR mutations are currently grouped into six classes based on their effect on the protein expression and function (Figure 2). Class I mutations lead to premature stop codons that interrupt CFTR translation prematurely, producing truncated and generally non-functional CFTR proteins. They are synthesis defect mutations that account for 10% of all CF causing mutations. Class II mutations lead to misfolded proteins that are targeted for degradation by the proteasome. They are trafficking/processing defect mutations and include the most prevalent CF mutation, F508del, which is present in ~90% of CF alleles. Class III mutations generate CFTR proteins that reach the cell surface but do not open for chloride transport. They cause a gating defect and account for 2-3% of CF mutations. Class IV mutations lead to defects in chloride conductance. CFTR reaches the cell surface but the flow of chloride ions through the channel is largely reduced. They are very uncommon, accounting for less than 2% of all mutations. Class V mutations cause a reduction in CFTR synthesis. They are mostly caused by splicing defects in the mRNA processing. Only few CFTR proteins are processed in the endoplasmic reticulum and few reach the cell surface. They are the least common group of CFTR mutations. Finally, Class VI mutations lead to CFTR proteins that are well folded, conduct chloride properly, but lack stability at the cell surface. In general, patients with classes IV, V and VI mutations have residual CFTR function, which grant them a mild phenotype. They are mostly

pancreatic sufficient and have mild lung disease. In contrast, patients with classes I, II, and III mutations have very low to no CFTR function and experience more severe phenotypes of the disease, including pancreatic insufficiency and rapid degradation of lung function (Elborn 2016; Castellani & Assael, 2017; Gajbhiye & Gaikwad 2017).

### 1.3.1 CFTR Synthesis and Trafficking

CFTR is a multidomain protein and its processing and trafficking includes several highly regulated steps which aim to guarantee that only functional, well folded forms of the protein are delivered to the plasma membrane (Younger et al, 2006; Riordan, 2008; Farinha & Canato, 2017). F508del-CFTR was found to be retained intracellularly and failed to be transported to the plasma membrane (Cheng et al, 1990). This finding pointed out to the importance of understanding the mechanisms of biosynthesis and trafficking of CFTR proteins, with the aim of finding strategies to rescue processing mutants. Briefly, CFTR biogenesis starts in the rough endoplasmic reticulum (RER), where the nascent polypeptide chain is targeted to the endoplasmic reticulum (ER) membrane translocon Sec61 complex through the signal recognition particle. Protein folding and core glycosylation happen co-translationally and only proper folded CFTR chains are sent to the Golgi apparatus where they are fully glycosylated, turning into the mature form that is transported from Golgi to the plasma membrane (Skach, 2000; Farinha & Canato, 2017)

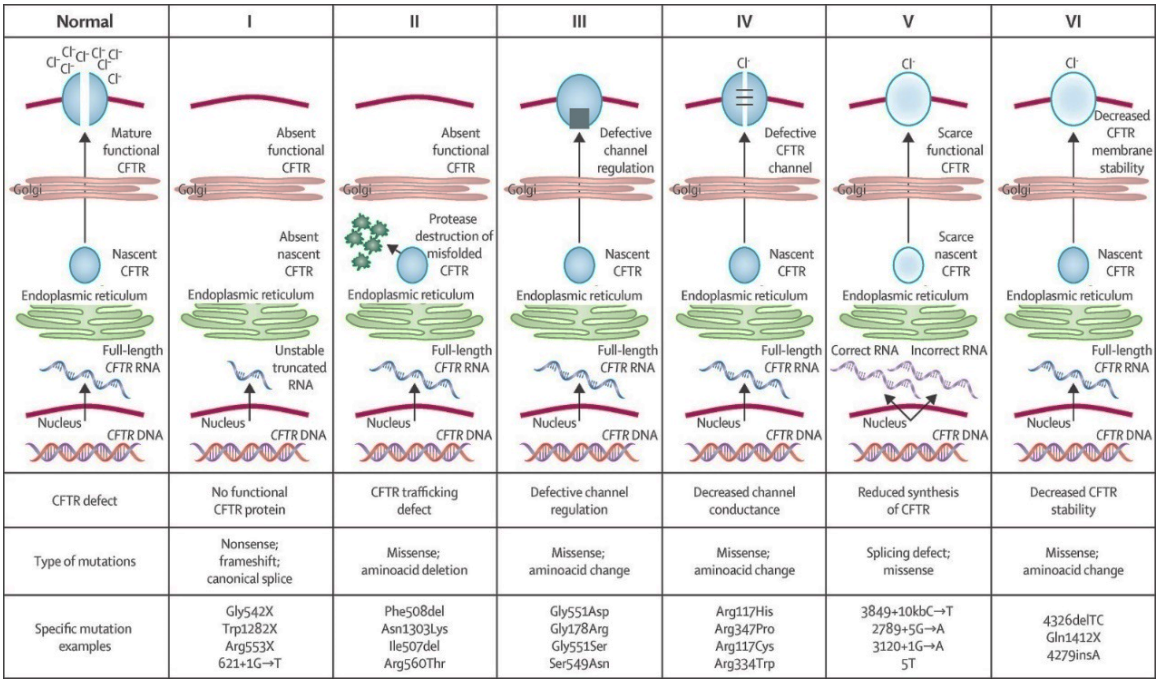


**Figure 3. Classes of CFTR mutations.**

Mutations in the cystic fibrosis transmembrane conductance regulator (*CFTR*) gene can be divided into six classes. Class I mutations result in premature stop codons with unstable mRNA and no protein production. Class II mutations are the commonest and cause retention of a misfolded protein at the endoplasmic reticulum, and subsequent degradation in the proteasome (e.g. F508del). Class III mutants can reach cell surface but do not open properly to transport chloride and are called gating mutations (e.g. G551D). Class IV mutants also reach cell surface but show a low level of conduction/flow of ions. Class V mutations cause splicing defects that substantially reduce mRNA and protein levels. Class VI mutations result in reduced amounts of functional CFTR at the cell surface because of high instability at the plasma membrane. Reproduced from Boyle MP & DeBoeck K (2013) with permission from Elsevier.

Successful maturation and folding of CFTR requires a co-translational folding of each individual domain (Kleinzen et al, 2005) in combination with post-translational steps which involves critical domain-domain interactions in order to achieve proper final native conformation (Serohijos et al, 2008; Du & Lukacs, 2009). This process is tightly controlled by the ER quality control (QC) machinery, which is comprised of several cytosolic and ER chaperones and lectins, responsible for preventing nascent domains from aggregation, facilitating CFTR folding and assembly or targeting a misfolded version for degradation via the ubiquitin-proteasome pathway (Pranke & Sermet-Gaudelus, 2014; Farinha & Canato, 2017). Although the exact mechanism by how ERQC discriminate native from non-native CFTR proteins is not fully understood, to date, four ERQC checkpoints have been described (Figure 4). The first checkpoint takes place in early stages of CFTR biogenesis and involves nascent polypeptide interaction with cytosolic chaperones Hsp70/Hsc70 and its co-chaperones Hdj-1 and Hdj-2 (Hsp40 family) (Meacham et al, 1999; Farinha et al, 2002). The chaperone pairs (Hsp70/Hdj-1 or Hsc70/Hdj-2) were found to bind to CFTR as soon as NBD1 is translated into the cytosol and this association is decreased after the translation of the R-region. Interaction of the co-chaperones with the mutant protein F508del-CFTR was found to be increased compared to wild type CFTR, indicating that proper folding and NBD1-R-region interaction is a critical step in CFTR biogenesis (Meacham et al, 1999). In a late stage of biogenesis, chaperone Hsp90 and its co-chaperone Aha-1 also regulate CFTR folding. Similarly, interaction of Aha-1 with F508del-CFTR, but not with wild type CFTR,

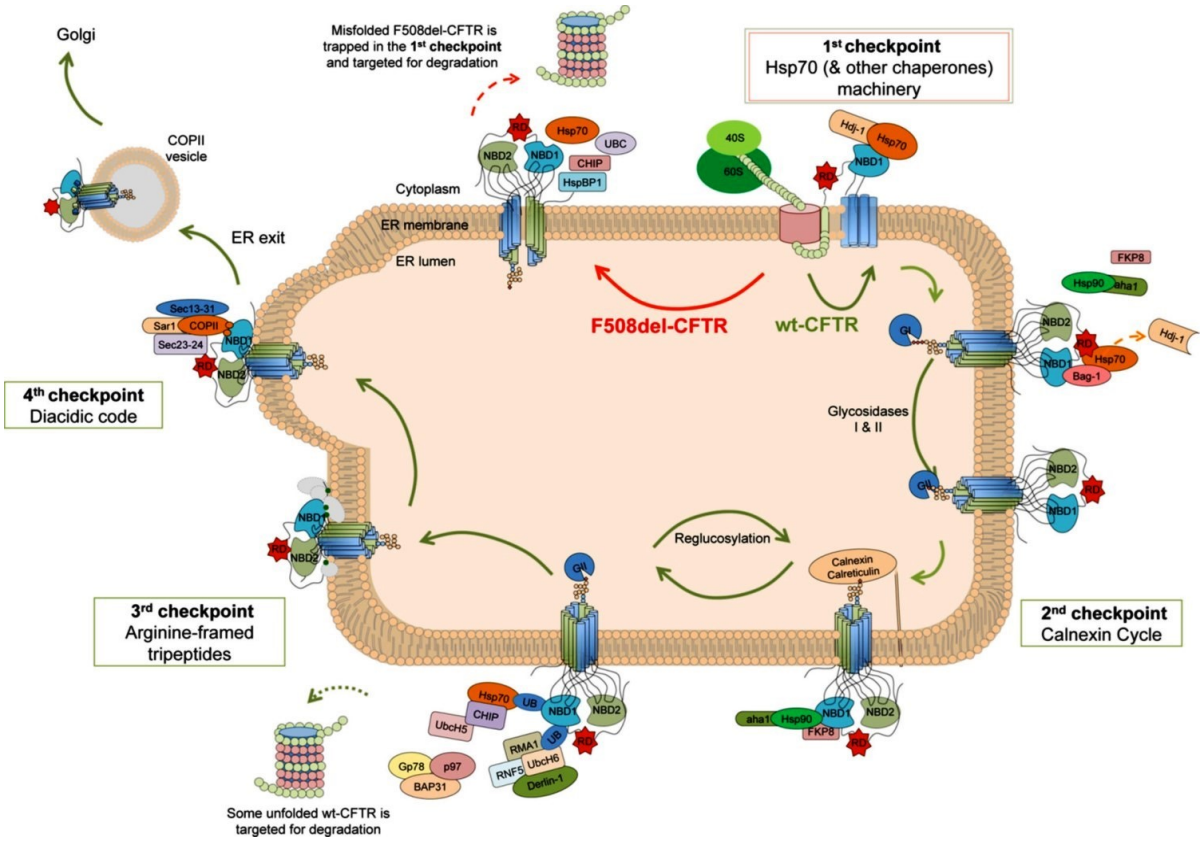


**Figure 4. Endoplasmic reticulum quality control (ERQC) machinery regulating CFTR folding and trafficking.**

When the nascent polypeptide emerges from the ribosome, it interacts with chaperones/co-chaperones (Hsc70/Hdj-2 or Hsp70/Hdj-1 or Hsp90/Aha-1) that assist its folding. Prolonged retention of unfolded CFTR (e.g. F508del-CFTR) by the chaperone system at this point enables CHIP to interact with Hsc70/Hsp70 (probably by displacing Hdj-1/Hdj-2) and causes the mutant to be degraded through the Hsc70-CHIP-UbcH5 pathway (first checkpoint). Then, the immature protein is glycosylated and interacts with the calnexin/calreticulin system. CFTR acquires its native conformation through successive rounds of release-deglucosylation and rebinding-reglucosylation to calnexin/calreticulin. Prolonged retention in the calnexin cycle may cause misfolded CFTR to be targeted for degradation (second checkpoint). CFTR retention in the ER is modulated through the exposure of retention/retrieval motifs (AFTs). As CFTR achieves a correct folding, these AFTs are internalized, preventing CFTR retention at the ER (third checkpoint) and ER export motifs (the diacidic exit code - DAD) are exposed, mediating its inclusion into COPII vesicles (fourth checkpoint). Misfolded F508del-CFTR is retained in the ER being trapped at the first checkpoint (dependent on the Hsp70 machinery) and subsequently degraded at the proteasome. Reproduced from Farinha CM & Canato S (2017), with permission from Springer Nature.

is increased (Loo et al, 1998). The Hsp70/40/90 system cooperates with other complexes, including CHIP (carboxy-terminal of Hsp70 interacting protein) E3 ubiquitin ligase/E2 enzyme UbcH5 (Matsumura et al, 2013), and E2 ubiquitin conjugating enzyme Ubc6e/RMA1 + the membrane associate Derlin-1, to ubiquitinate CFTR (Younger et al, 2006). Ubiquitination of CFTR recruits other partners, such as P97, which deliver CFTR to the proteasome to be degraded. The second checkpoint takes place during co-translational core-glycosylation and folding, and it involves the chaperones lectins, calnexin and calreticulin. Core-glycosylation involves enzymatic addition of a 14-unit oligosaccharide into two asparagine residues (894 and 900) in the extracellular loop 4, between TMs 7 and 8 (Pind et al, 1994; Patrick et al, 2011). Enzymatic removal of 2 monosaccharides turn the glycan structure recognizable by calnexin and calreticulin, that bind CFTR and assist in its folding. Upon removal of one more monosaccharide, calnexin/calreticulin dissociate and if correct folding is achieved, CFTR is directed out of the ER to gain complex glycosylation in the Golgi apparatus. In the case of improper folding, the monosaccharide that was last removed is re-attached to the oligosaccharide chain, making CFTR again recognizable by calnexin/calreticulin, starting another cycle that repeats until proper folding is eventually achieved, or if stuck in this cycle for too long, CFTR is tagged for ER associated degradation (Hammond et al, 1994). Most F508del-CFTR do not reach this second checkpoint as most of it is directed to degradation by the early Hsp-ubiquitin complex checkpoint (Farinha & Amaral, 2005).

The third and fourth checkpoints described are related to signals involved in the CFTR ER-to-Golgi transport. Arginine-framed tripeptides (AFTs) are specific signals that promote retention of CFTR in the ER. CFTR has four AFTs in its sequence, one at the lasso motif, two at NBD1 and one in the R-region (Michelsen et al, 2005). In order for the trafficking machinery to prompt CFTR for transport from the ER to the Golgi, those sites must be hindered by proper folding. Misfolded F508del-CFTR that eventually overcome the first two checkpoints is retained in the ER due to the exposure of the AFTs. Indeed, substitution of arginine by lysine in the four AFTs of F508del-CFTR promotes its escape from the ERQC (Chang et al, 1999). An ER export signal present in NBD1, the diacidic exit code (Asp-Ala-Asp - DAD), must be exposed for CFTR recognition by the Sec24 cargo selection complex, part of the COPII transport vesicles. Misfolded CFTR may have this exit code masked and, therefore, are not recruited into the COPII vesicles heading to the Golgi apparatus (Wang et al, 2004). In fact, mutations of both Asp residues to Ala, completely abolish CFTR processing (Farinha et al, 2015).

### 1.3.2 CFTR Function and Interactions in Epithelial Cells

CFTR has two main roles involved in electrolytes and fluid transport in a variety of epithelial tissues, such as the airways, secretory glands, and gastrointestinal tract: a role as an anion conduction pathway (channel) and a role as a regulator, modulating the function of other ion transporters and channels. Outcomes from CFTR activity are tissue specific and depend on the distinct tissue expression

and localization of the other ion transporters that cooperate with CFTR, which together generate the electrolyte potentials that govern the direction of transepithelial and paracellular fluid and salt transport, maintaining tissue integrity and homeostasis. In airways specifically, because of the contact with the air coming from the external environment, CFTR function is also related to body defense against pathogens (Frizzell & Hanrahan, 2012; Saint-Criq & Gray, 2017). Epithelial cells have an apical-basal polarity, that is, the basolateral and apical membranes possess distinct functions and are in contact with different body compartments. Depending on the tissue, the apical membrane is found facing the external environment or the lumen of internal cavities. The basolateral membrane of epithelial cells faces the interstitium, being responsible for the uptake of nutrients (including oxygen and ions) and disposal of waste metabolites from and to the bloodstream, respectively. Another characteristic of epithelial cells is the presence of tight junctions between cells, that keep them close together while creating distinct milieux compositions bathing the apical and basolateral membranes (Hong et al, 2014; Saint-Criq & Gray, 2017). Transepithelial transport of salt and fluids follow either a transcellular pathway, crossing both basolateral and apical membranes and the cytoplasmic environment, or a paracellular pathway, between the cells crossing the tight junctions. Paracellular transport is always passive, directed by the electrochemical gradient, while transcellular transport involves both passive and active electrolyte transports, carried by a series of ion channels, co-transporters and pumps (Figure 5) (Frizzell & Hanrahan, 2012; Hong et al, 2014; Saint-Criq & Gray, 2017).

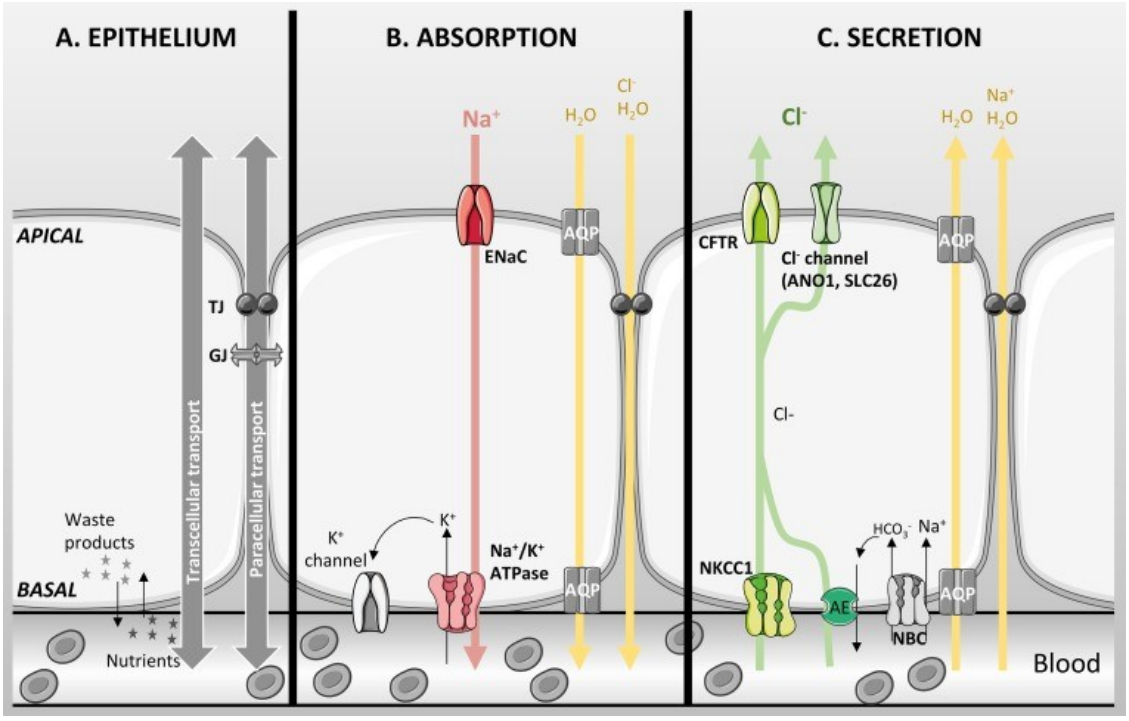


**Figure 5. Basic characteristics of an epithelial layer**

**A,** Epithelial cells are joined together by junctions [tight junctions (TJ), gap junctions (GJ)]. Uptake of nutrients and oxygen, and removal of cellular waste products occur on the basolateral surface. Water and ion transport can occur through the transcellular or paracellular pathways. **B,** In absorptive epithelia transport is mainly driven by active $Na^+$ absorption through ENaC in the apical membrane and the $Na^+/K^+$-ATPase in the basolateral membrane creating an electrochemical driving force for paracellular passive $Cl^-$transport. Water then follows either through aquaporins or the paracellular pathway. **C**, In secretory epithelia transport is mainly driven by $Cl^-$ secretion through CFTR and other $Cl^-$ channels in the apical membrane. NKCC1 and the coupled action of an anion exchanger and NBC in the basolateral membrane accumulate $Cl^-$ in the cell. Active $Cl^-$ secretion creates the driving force for $Na^+$ movement across the epithelium through the paracellular pathway and water transport occurs paracellularly and/or transcellularly. Red and green arrows show active transport, and yellow arrows show passive transport. Reproduced from Role of CFTR in epithelial physiology by Saint-Criq V & Gray MA (2017), licensed under CC BY 4.0. No changes were made.

In secretory epithelia, the primary energy source for active transcellular transport of electrolytes comes from the activity of the $Na^+/K^+$ ATPase at the basolateral membrane, creating an inward $Na^+$ chemical gradient that drives the activity of the basolateral secondary active co-transporter NKCC1 which brings 1 $Na^+$, 1 $K^+$ and 2 $Cl^-$ ions into the cytosol. $K^+$ is recycled back to the interstitium through basolateral $K^+$ channels, and $Na^+$ is continuously pumped out of the cell via $Na^+/K^+$ ATPase, resulting in chloride accumulation inside the cell (Frizzell & Hanrahan, 2012; Saint-Criq & Gray, 2017). In some epithelial cells, such as the airway cell line Calu-3 and serous cells of exocrine glands, an alternative mechanism for chloride accumulation through the cooperative activity of $Cl^-/HCO_3^-$, $Na^+/H^+$ exchangers and $Na^+/HCO_3^-$ co-transporter (NBC) was described (Shan et al, 2012; Huang et al, 2012). Accumulated chloride ions are then driven to the apical membrane where they are secreted mainly through CFTR, but other chloride channels such the calcium activated chloride channel (CaCC) TMEM16A (also called ANO1) (Caputo et al, 2008) and members of the solute carrier (SLC) 26A family (Bertrand et al, 2009) also take part in chloride secretion in some tissues. Active secretion of chloride into the lumen creates an electrogenic-driven paracellular passive transport of $Na^+$, generating salt (NaCl) accumulation that ultimately drives water passive transport either via the paracellular pathway or via aquaporins (Frizzell & Hanrahan, 2012; Saint-Criq & Gray, 2017). Lack of CFTR activity in epithelia abrogates the secretion of chloride ions, the primary electrochemical driving force involved in fluid secretion, which when impaired, constitutes the basic defect underlying the phenotypes

observed in patients with CF. CFTR also secretes bicarbonate and its importance in CF disease became notorious when some characteristics of the disease, such as hyperinflammatory responses and mucus processing impairment, that could not be explained solely by the defects in chloride secretion and hyperabsorption of sodium, were associated with defects in bicarbonate secretion (Choi et al, 2001; Quinton, 2001).

In the lungs, CFTR proper function maintains the volume, fluidity and composition of the periciliary liquid (PCL), one of the components of the airway surface liquid (ASL). Bicarbonate secretion via CFTR was shown to contribute to the maintenance of the other component of the ASL, the mucus layer (Trout et al, 1998) and also of the ASL pH (Coakley et al, 2003). Maintenance of ASL hydration and pH is tightly regulated by fluid and electrolytes transepithelial transport, and its impairment results in inefficient mucociliary clearance (Tarran, 2004), impaired bacterial killing (Pezzulo et al, 2012) and reduced fluid and mucus homeostasis (Hoegger et al, 2014).

Fluid secretion in the airways follows the basic secretory pathway described early in this section, with chloride accumulation at the basolateral membrane and its subsequent secretion through the apical membrane. The presence of epithelial sodium channels (ENaC) together with CFTR in the apical membrane of airway epithelia grant those cells the capacity of controlling ASL height and composition through the balance between sodium absorption and chloride secretion. In fact, several studies have proposed a negative regulation of ENaC by CFTR, preventing sodium absorption which would reduce ASL volume. This regulation

was first demonstrated to be lost in CF patients where, indeed, an excessive ENaC activity was observed (Gowen et al, 1986). Supporting evidences came from studies using mice overexpressing ENaC, which generated a CF-like phenotype including reduced ASL, exacerbated inflammation, and poor bacterial killing (Mall et al, 2004), and from electrophysiology measurements of epithelial alveolar cells from WT and CFTR knockout mice showing enhanced ENaC activity in the absence of CFTR (Lazrak et al, 2011). However, other studies could not confirm this functional association between ENaC and CFTR. By overexpressing CFTR in the background mice from Mall's group, the expected rescue of CF-like phenotype was not observed (Grubb et al, 2012), and the CF pig model do not display increased sodium absorption (Itani et al, 2011).

CFTR is also proposed to regulate other chloride channels and transporters, including CaCCs and members of the SLC26A family. Co-expression of exogenous CFTR caused a decrease in the currents of endogenously expressing CaCCs and this inhibitory effect was increased upon CFTR activation (Wei et al, 1999). Similar results were observed in human bronchial epithelial cells lines expressing CFTR and TMEM16A (a CaCC). This study also demonstrated mutual inhibition and physical association between the two channels (Ousingsawat et al, 2011).

CFTR bicarbonate conductance is a key factor for maintenance of ASL pH. Evidences of acidic ASL in CF were reported on studies measuring the pH of fluid secretions from primary airway cell cultures (Coakley et al, 2003) and submucosal glands (Song et al, 2006) from CF and non-CF patients as well as

from newborn CF and non-CF piglets (Pezzulo et al, 2012). The dysregulated pH caused by defective bicarbonate secretion has been implicated in deficient mucus properties, exacerbated inflammatory reactions and poor immune response to pathogens. Mucus is a polymer hydrogel produced by goblet cells and mucous cells of submucosal glands that covers and protect the airway lumen. Mucins, the main component of mucus, are released in the ASL as a condensed viscous form, inside granules linked to cations, mostly to calcium (Verdugo et al, 1987). It is proposed that when in contact to bicarbonate-rich ASL, calcium is sequestered from the mucins, which then are able to expand to form a fluid gel. Poor bicarbonate concentrations in the ASL from CF patients would prevent mucin expansion, thus, leaving mucus in an aggregate form, which combined with the reduced PCL, compromise mucociliary clearance, leaving CF lungs predisposed to microorganism colonization (Quinton, 2008; Tang et al, 2016). Acidic ASL also reduce the activity of resident antimicrobial peptides (AMPs), further complicating bacterial killing (Pezzulo et al, 2012). The cause of the exacerbated inflammatory response observed in CF is still a controversial subject. There is no consensus on whether the exacerbated inflammation is a result of continuous airway infection or is an intrinsic immune dysfunction of the epithelia due to CFTR dysfunction. A good body of evidence suggesting intrinsic dysregulation of inflammatory responses in CF airways showed the presence of high levels of interleukin-8 (IL-8), neutrophils agglomeration and abnormal activation of NF-κB (nuclear factor κ light-chain enhancer of activated B cells), even before any apparent infection (Tirouvanziam

et al, 2002; Verhaeghe et al, 2007). In contrast, other studies showed no differences in the levels of inflammatory markers in bronchoalveolar lavages of CF infants (Armstrong et al, 2005) or CF piglets (Wine, 2010) compared to controls, suggesting infection as the factor initiating and sustaining inflammation. Upon airways infection, bacterial PAMPs (pathogen-associated molecular patterns) trigger an exacerbated inflammatory response, characterized by TNF (tumor necrosis factor) and IL-8 expression, mucin secretion, neutrophils recruitment and protease release (Li et al, 1997; Sagel et al, 2002; Quinn et al, 2010). However, this exaggerated response is not efficient against pathogens, instead, it causes progressive damage to the airways. Neutrophil-released mediators, especially neutrophil elastase, which are crucial for bacterial killing in normal airways, are found in abundance in CF airways and are related to structural and functional destruction of the lungs, but inefficient against bacteria (Sly et al, 2009). In addition, levels of natural proteases inhibitors, such as secretory leucoprotease inhibitor, are reduced in CF lungs (Weldon et al, 2009). Intracellular signaling cascades involved in pro-inflammatory responses, including NF-κB, were found to be upregulated in CF cell lines compared to control cells whereas signaling cascades involved in resolution of acute inflammation and recruitment of adaptative immune responses were decreased in CF, which would explain the sustained inflammatory state of CF lungs (Cohen & Prince, 2012). Upregulated pro-inflammatory signals result in overproduction of reactive oxygen species (ROS) by the abundant neutrophils present in the airways, which in addition to exogenously ROS produced by colonized bacteria,

overwhelm the capacity of antioxidants to supress oxidative stress, and increase lung deterioration (Cohen-Cymberknoh et al, 2013). Two important ions that function as antioxidants are secreted by CFTR in the apical membrane of airway cells and contribute to control oxidative damage. Glutathione ($GSH^-$) is present in high concentrations (compared to the serum) in normal airways fluids (Day et al, 2004). Because its major function in the redox balance, an important mechanism against pathogens, absence of $GSH^-$ secretion in CFTR-deficient cell lines or in CFTR knock-out mice, has been connected to an inability to adapt to bacterial infections leading to increased inflammation and oxidative stress (Day et al, 2004; Rottner et al, 2009). Thiocyanate anion ($SCN^-$) is a precursor in the synthesis of a potent antioxidant agent, hypothiocyanite (OSCN). Lack of CFTR-mediate $SCN^-$ transport would decrease OSCN levels, contributing to the chronic bacterial settling observed in CF airway surface (Xu et al, 2009). Despite whether sustained exacerbated inflammatory responses in CF are intrinsically or extrinsically mediated, probably both, this is the main cause of lung damage and poor bacterial killing, which are the major factors involved in morbid-mortality associated with CF.

In the exocrine pancreas, CFTR secretes both chloride and bicarbonate and works in concert with apical $Cl^-/HCO_3^-$ exchangers of the SLC26A family to accumulate bicarbonate in the lumen of the ducts. Sodium then moves paracellularly toward the high concentrated (of $Cl^-$) pancreatic fluid which leads water to follow osmotically, creating an alkaline solution that is critical for clearance of the ducts and for the digestive enzymes to perform their catalytic

function. Accumulation of $Cl^-$ and $HCO_3^-$ inside the ductal epithelia is achieved by the work of NKCC1 and NBC co-transporters. Conversion of $CO_2$ to $HCO_3^-$ via carbonic anhydrase also helps cytosolic bicarbonate accumulation. In CF, lack of CFTR anion secretion results in pancreatic insufficiency due to ductal obstruction, which subsequently leads to atrophy and fibrosis, destroying the tissue (Frizzell & Hanrahan, 2012; Saint-Criq & Gray, 2017; Kunzelmann et al, 2017).

In the intestine, CFTR chloride and bicarbonate secretion is critical for the correct volume and composition of the luminal surface liquid that aids in nutrient uptake and enzyme activity. The transepithelial anion transport in the intestine follows similar pathways as in the airways with chloride crossing the epithelia transcellularly and sodium and water following through the paracellular pathway and osmotically, respectively. In CF, lack of CFTR function may lead to intestine obstruction (meconium) and constipation (Grubb & Gabriel, 1997; Frizzell & Hanrahan, 2012).

Defects in ion composition in the sweat glands was the first description related to CF disease back in the 1950s (Sant'Agnese et al, 1953). CFTR is expressed in both apical and basolateral membranes of sweat gland absorptive ducts (Quinton, 2007). In the apical membrane of epithelial cells, CFTR is co-expressed with ENaC but, in contrast to the airways, CFTR and ENaC work in conjunction to absorb salt from the ductal lumen into the interstitium (Reddy et al, 2003). Similar to the airways, sodium enters the cells through apical ENaC down the electrochemical gradient and it is pumped out to the interstitium via

basolateral Na/K pumps, which creates the electrical gradient that drives chloride transcellular absorption. In CF, lack of CFTR activity leads to the formation of a high salt concentrated sweat, due to the inefficient chloride absorption, which prevents sodium absorption (Quinton, 2007; Bovell, 2015, Saint-Criq & Gray, 2017).

Besides the functional and physical interaction with other channels and transporters, CFTR can associate with other intracellular partners. The four last amino acids at the C-terminal end of CFTR (DTRL) is a site for binding of PDZ (PSD95, Dlg1, Zo-1) domain-containing proteins. Mutations at the PDZ binding site results in partial mislocalization of CFTR, indicating a role for this motif in anchoring the CFTR protein at the apical membrane (Wang et al, 1998). Indeed, two of the PDZ-domain containing proteins reported to interact with CFTR, NHERF ($Na^+/H^+$ Exchanger Regulator Factor)1 and NHERF2, are cytosolic proteins concentrated at the apical membrane of airways cells (Vankeerberghen et al, 2002). NHERF1 contains two PDZ domains (PDZ1 and PDZ2) that bind to CFTR (with different affinities) when the C-terminal of NHERF1 is attached to ezrin, a PKA anchoring protein, or phosphorylated by PKC (Li et al, 2007; Alshafie et al, 2014). NHERF2 (E3KARP), a related PDZ-protein, has been shown to interact with CFTR and ezrin, and together with NHERF1, function as a scaffold protein suggested to localize ezrin, and consequently PKA, near the R-region of CFTR (Sun et al, 2000). Ezrin also binds to actin (Sato et al, 1992), which perhaps helps stabilize the protein complex at the cell surface. NHERF3 (CAP70), a four PDZ-domain protein, was reported to be able to link two CFTR

molecules and potentiate chloride currents (Wang et al, 2000). CAL (CFTR-associated ligand), is a Golgi-associated protein that binds CFTR through its sole PDZ domain and confine it inside the cell, reducing its expression at the plasma membrane (Cheng et al, 2002). RACK1, another scaffold protein proposed to be part of the CFTR interactome, is a receptor for activated C kinase, which binds to NHERF1 forming a complex that helps stabilize CFTR at the cell surface and brings PKC close to CFTR (Auerbach & Liedtke, 2007; Alshafie et al, 2014). Shank2E is also able to bind the C-terminal of CFTR through its PDZ-domain, but in contrast to NHERF proteins that recruit the ezrin/PKA complex, Shank2E form a complex with the cyclic nucleotide phosphodiesterase PDE4D, which prevents cAMP/PKA signals in epithelial cells, thus inhibiting CFTR activity (Lee et al, 2007). A competition between positive regulators, such as NHERFs, and negative regulators, such as CAL and ShanK2E for binding to CFTR modulates its surface expression and activity (Cheng et al, 2002; Kim et al, 2004; Alshafie et al, 2014).

Acidic residues located at the N-terminal lasso motif of CFTR were described to interact with SNARE proteins. Syntaxin 1A, a t-SNARE protein, inhibits both CFTR trafficking and activation by cAMP when attached to the lasso motif. Binding of syntaxin 1A was described to disrupt the interaction between the lasso motif and the R-region of CFTR, suggesting that this interaction is involved in CFTR activation. Binding of syntaxin 1A to Munc-18a disrupts its association with CFTR, which, in turn, relieves the inhibition (Naren et al, 1997; Naren et al, 2000).

### 1.3.3 CFTR STRUCTURE

CFTR was classified as a member of the ATP binding cassette (ABC) superfamily of proteins after its DNA sequence (Riordan et al, 1989) revealed the presence of well conserved canonical sequences encoding the ABC (usually referred to as NBD) domains, a hallmark of the family. ABC proteins are found in all kingdoms of life and most members transport a variety of substrates through cell membranes (Higgins et al, 1992; Dean et al, 2001). A structural architecture comprising two transmembrane domains (TMDs) and two cytoplasmic nucleotide binding domains (NBDs, the ABC domain) is a characteristic of this family. In contrast to the NBDs, which contain several conserved signature sequences involved in ATP binding and hydrolysis, the TMDs are much more diverse in sequence and arrangement. Expression of the four core domains in ABC proteins vary among species: four separate polypeptides assembling to form a functional unit are observed exclusively in prokaryotes, and 2 half-molecules (TMD/NBD) that re-assemble post-translationally to form functional proteins or single polypeptide chains containing all four domains are seen in eukaryotes (Higgins, 1992; Dean et al, 2001; Davidson & Chen, 2004; Dean & Annilo, 2005).

In humans, there are 48 ABC proteins, divided into seven subfamilies (ABCA-ABCG), and CFTR is included in the ABCC subfamily (Dean & Annilo, 2005). CFTR is unique among ABC proteins as it functions as an ion channel rather than a substrate transporter (Bear et al, 1992). In CFTR, the four canonical domains are organized structurally in two hetero-halves (TMD1-NBD1 and

TMD2-NBD2) connected by a unique and intrinsically disordered regulatory region (R-region), which contains multiple PKA and PKC phosphorylation consensus sites (Riordan et al, 1989). CFTR also contains an amino-terminal segment of 77 residues (lasso motif) and a carboxy-terminal segment of ~40 residues, which is mostly disordered (Liu et al, 2017). The final domain organization of CFTR is, from amino-terminal to carboxy-terminal: lasso motif, TMD1, NBD1, R region, TMD2, NBD2 and C-terminal tail, all expressed in a single polypeptide chain of 1480 amino acids (Figure 6 A). The 12 membrane spanning helices of the TMDs are responsible to form the pore of the channel for ion conductance and the ion selectivity filter. Through four intracellular extensions, called cytoplasmic loops (CLs), TMDs connect with the NBDs, which are responsible for CFTR channel opening and closing (gating) through binding and hydrolysis of ATP molecules. The mostly disordered R-region (Ostedgaard et al, 2000; Baker et al, 2007, Bozoki et al, 2013), modulates CFTR activity by means of phosphorylation and dephosphorylation of several PKA and PKC consensus sites. Details on the structure of each of the CFTR domains will be discussed in the next sections.

#### *1.3.3.1 The Nucleotide Binding Domains and Channel Gating*

The NBDs of CFTR house the canonical consensus motifs of ABC proteins. Binding and hydrolysis of ATP in between NDBs is the driving force for substrate transport in ABC transporters. In CFTR, channel gating is regulated by ATP binding at two distinct sites, each site sharing conserved sequences and motifs

from both NBDs. The ATP-bound NBDs dimerize in a head-to-tail conformation (Mense et al, 2006; Vergani et al, 2007) with the A-loop, Walker A motif (GXXGXGKS/T, with X being any residue), Walker B motif (ϕϕϕϕDE, with ϕ being a hydrophobic residue), Q-loop and H-loop from one NBD (the 'head') cooperating with the signature sequence (LSGGQ) and D-loop of the adjacent NBD (the 'tail') in the task of binding and hydrolysis of ATP (Figure 6 B). The A-loop tryptophan 401 in NBD1 and tyrosine 1219 in NBD2 interact with the adenosine base of each ATP; the Walker A motif lysine interacts with the phosphates α and β of ATP; the Walker B motif arginine interacts and coordinate the $Mg^{+2}$ ion, a cofactor for ATP hydrolysis; the Q-loop glutamine interacts with the γ phosphate of ATP; the H-loop histidine interacts with the D-loop, the Walker B glutamate and with the γ phosphate of ATP; the D-loops from both NBDs mediates cross-talk between the two ATP sites; and the signature sequence further stabilizes ATP binding (Ter Beek et al, 2014; Hwang et al 2019). The two NBDs in CFTR only share ~30% sequence identity (Klein et al, 1999) and some of those differences directly affect the capacity to hydrolyze ATP. The ATP site 2, composed by NBD1 signature sequence and NBD2 walkers A and B motifs, is well conserved and catalytically competent whereas in the ATP site 1, the signature sequence in NBD 2 is modified to LSHGH and the walker B motif of NBD1 lacks the catalytic glutamate responsible for ATP hydrolysis (Hung et al, 1998), which renders the site 1 hydrolysis incompetent (Aleksandrov et al, 2002; Basso et al, 2003). Other difference, not related to ATP hydrolysis, is the presence of a disordered region in NBD1, the regulatory insertion (RI), which

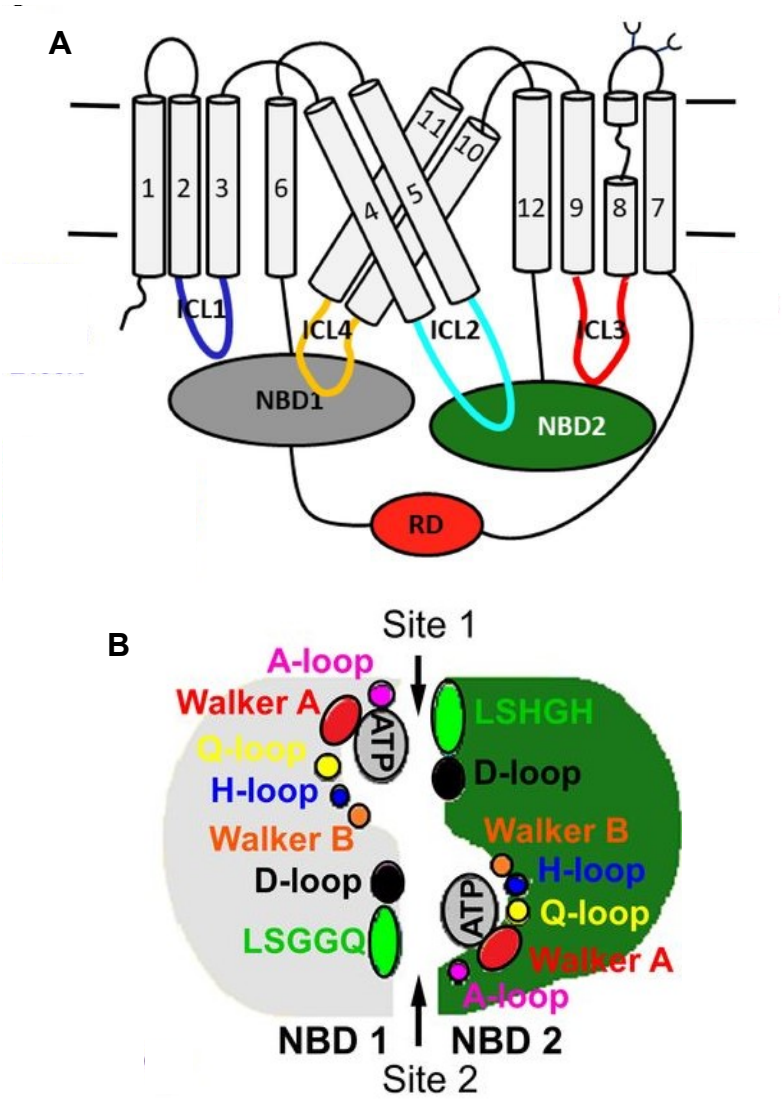


**Figure 6. CFTR topology and its conserved motifs.**

**A,** Representation of CFTR topology showing its 12 TMs, two NBDs (gray, NBD1; green, NBD2), the R domain in red, and cytoplasmic loops 1-4 in dark blue, cyan, red and yellow, respectively. Note the two interfaces between ICL2-NBD2 and ICL4-NBD1 described in the text. **B,** Conserved sequences and motifs in CFTR's NBDs. Head and tail subdomains of NBDs with two ATP molecules sandwiched in the dimer interface and characteristic motifs highlighted in different colors as indicated. Reproduced with adaptations from Structural mechanisms of CFTR function and dysfunction by Hwang T-C, Yeh J-T, Zhang J, Yu Y-C, Yeh H-I, Destefano S (2018), licensed under CC BY-NC-SA 4.0. **'A'** was taken from figure 8 and **'B'** was taken from figure 12.

contains a single consensus site for PKA phosphorylation at S422 (Lewis et al, 2004). In a construct where most of the RI was absent, channel responses to ATP and phosphorylation were largely similar to the WT, except for slightly shortened open bursts and faster closing, indicating that this segment may be involved in stabilizing the channel in the open state (Csanady et al, 2005). The RI was also demonstrated to interact with NBD1 at the dimerization interface and that interaction was disrupted by phosphorylation, facilitating the NBD dimer formation. Furthermore, the phosphorylated RI was implied to interact with the first cytoplasmic loop (Kanelis et al, 2010).

Two gating mechanisms are currently proposed for CFTR. The first defends a strict coupling between a gating cycle and an ATP hydrolysis cycle. Here, each gating cycle begins with NBDs dimerization, induced by ATP binding, and finishes with dimer dissociation, triggered by ATP hydrolysis in the competent catalytic site (Gunderson & Kopito, 1995; Csanady et al, 2010; Liu et al, 2017). In this mechanism CFTR is proposed to undergo a cycle of four functional states ($C_1$, $O_1$, $O_2$ and $C_2$), where $C_1$ represents a closed state before NBDs dimerization and ATP binding at the two composite sites promotes the open state ($O_1$) until the ATP at the competent site is hydrolyzed (state $O_2$), causing partial dimer dissociation ($C_2$), and finally total dimer dissociation (state $C_1$). The fact that preventing ATP hydrolysis, either by mutations at the competent catalytic site (Gunderson & Kopito, 1995; Vergani et al, 2005) or by using non-hydrolysable ATP analogs (Gunderson & Kopito, 1994; Hwang et al, 1994) abolishes the transition between states $O_1$ and $O_2$, keeping the channel in a

steady open state, support the idea of the strict coupling mechanism. It was also demonstrated that ATP binding to the catalytic competent site is critical for channel opening, whereas binding to the degenerated site is less important (Vergani et al, 2003; Zhou et al, 2006).

Although 95% of CFTR openings terminate with ATP hydrolysis (Csanady et al, 2000), an alternative mechanism must exist to explain the spontaneous (uncoupled) openings observed, although infrequently, in CFTR functional experiments in the absence of ATP (Bompadre et al, 2005). The second mechanism defends a nonstrict coupling between gating and ATP hydrolysis cycles. This theory is based on several studies that identified structural and functional features that can not be explained by the first theory. For instance, CFTR channels can open without the presence of ATP. This uncoupled (spontaneous) gating can also be observed in mutants with a dysfunctional site 2 (CF causing mutation G551D) (Bompadre et al, 2007), and even in truncated constructs lacking the NBD 2 (Cui et al, 2007; Wang et al, 2007), indicating that ATP hydrolysis at site 2 or NBD dimerization are not essential for CFTR gating. Some mutations, such at position 978 in the cytoplasmic loop 3 or at position 355 in TM6, promote strong spontaneous gating events (Bai et al, 2010; Wang et al, 2010). Another study identified a transitory open state where ATP site 2 was already empty after an ATP hydrolysis cycle (Jih et al, 2012a). In a follow up study, the same group, using a construct bearing a mutation neutralizing the positive charge of a residue lining the cytoplasmic vestibule of the pore (R352Q), demonstrated that this mutant followed the similar pattern of $C_1$, $O_1$, $O_2$ and $C_2$

states, but with several cycles between $O_1$ and $O_2$ before full closure of the channel, suggesting the presence of several ATP hydrolysis cycles within the same opening burst and the existence of intermediate open state(s) between ATP hydrolysis and channel closure (Jih et al, 2012b).

Regardless of the mechanism involved, the movement of the NBDs (the gating power stroke) during a dimerization/dissociation cycle are translated to the pore (containing the gate) through the TMDs cytoplasmic extensions (cytoplasmic loops) in order to promote the conformational changes in TMDs necessary for channel gating (He et al, 2008). CFTR contains four cytoplasmic loops formed by the helical extensions of TM 2-3 (CL1), TM 4-5 (CL2), TM 8-9 (CL3) and TM10-11 (CL4) with one cytoplasmic loop from each TMD (CL2 and CL4) traversing the protein to make tight connections with the NBD located in the opposite half (Dawson & Locker, 2006). Thus, CL1 and CL4 interact with NBD1 while CL2 and CL3 interact with NBD2, forming two structural halves in CFTR: one formed by TM helices 1, 2, 3, 6 (from TMD1), 10, 11 (from TMD2) and NBD1, and the other formed by TM helices 7, 8, 9, 12 (from TMD2), 4, 5 (from TMD1) and NBD2 (see Figure 5 A). The recent crystal structures show asymmetrical interaction between the CLs and NBDs. CL2-NBD2 and CL4-NBD1 interfaces are tightly connected in a ball-in-a-socket fashion, while CL1 and CL3 make less connections with NBD1 and NBD2, respectively, and do not form ball-in-a-socket associations (Zhang et al, 2016; Liu et al, 2017; Hwang et al, 2019). Upon NBD dimerization, CL2-NBD2 and CL4-NBD1 tight associations remain relatively unaltered, while CL1-NBD1

and CL3-NBD2 loosen connections are reduced (Zhang et al, 2017; Zhang et al, 2018).

*1.3.3.2 The Transmembrane Domains and Channel Pore*

Each of the TMDs of CFTR consist of six membrane spanning helices (TM 1-6 and TM 7-12), which bundle together to form the anion pathway and channel gate. Although structural features of CFTR resemble the other ABC transporters, its function as an ion channel rather than an active transporter prevent a direct comparison of the transport mechanism with other ABC transporters. The CFTR pore must be simultaneously open to both intracellular and extracellular sides of the membrane in order to promote passive ion diffusion down the electrochemical gradient, in contrast to other ABC transports that alternate the opening of an intracellular or an extracellular gate depending on the protein conformation. Several studies suggest a continuous pathway for ion flux through CFTR, consisting of a lateral cytoplasmic entrance between TM4 and TM6, lined by several positively charged amino acid side chains, which attract negatively charged ions to the cytoplasmic entrance of the pore (El Hiani & Linsdell, 2015; El Hiani et ai, 2016), a large cytoplasmic vestibule (Bai et al, 2011), a narrow constriction predicted to function as a gate and selective filter, located close to the extracellular membrane surface, and involving residues T338-S341 in TM 6, L102 in TM 1 and N1138 in TM 12 (Gao et al., 2013, Gao & Hwang, 2015; Linsdell, 2016; Zhang et al, 2018), and a shallow extracellular vestibule (Norimatsu et al, 2012). In the past decade, several studies using the substituted

cysteine accessibility method (SCAM) have predicted contributions of TMs 1, 3, 4, 5, 6, 9, 10, 11, and 12 to the channel pore (Fatehi and Linsdell, 2008; Bai et al., 2010; El Hiani and Linsdell, 2010; Wang et al., 2011; Bai et al., 2011; Qian et al., 2011; Norimatsu et al., 2012; Gao et al., 2013; Wang et al., 2014; Zhang and Hwang, 2015; El Hiani and Linsdell, 2015; Gao and Hwang, 2015; El Hiani et al., 2016; Negoda et al, 2017).

Although most of the biochemical and biophysical studies on the structure and function of the TM segments of CFTR were confirmed by comparison with the CFTR structures solved, with the exception of the asymmetrical feature of TM 8 helix which is broken down in two parts and dislocated toward the center of the pore, some residues identified by SCAM as pore lining are not facing the pore in any of the structures solved so far. L102, proposed to be part of the constriction area of the pore (Gao et al., 2013) is only facing the pore in the human (Zhang et al, 2018), but not in the zebrafish (Zhang et al, 2017) phosphorylated ATP-bound structure. In fact, the structures solved in the phosphorylated ATP-bound state (Zhang et al, 2017; Zhang et al, 2018), which were supposed to reflect an open state of the channel, do not display a fully conductive pathway as the extracellular access of the pore is blocked by the tilted TM 8 and by TM 12 in zCFTR, and only a very small opening, that is too small to permit flow of water or ions, is observed in hCFTR (opening radius of 1,2Å compared to the chloride ion radius of 3.6Å). To date, a CFTR structure where both sides of the pore are accessible to the aqueous environment is not available (Hwang et al, 2018; Csanady at al, 2019).

Although the CFTR pore displays high predilection for anions compared to cations, it does not discriminate different anions (Linsdell et al, 2000; McCarty & Zhang, 2001). In CFTR, the narrowest region of the pore (residues 338-341 in TM 6) is suggested to be the selective filter for both charge and size (Hwang et al, 2018). The fact that this region is only permeable to anions with similar size as chloride, i.e. bicarbonate or nitrate, and that mutations at residues 338 and 341 as well as at residues nearby that region, such as 337, 1118 and 1134, changes the selectivity properties of CFTR, are evidences supporting this idea (Linsdell et al., 2000; Linsdell, 2001; McCarty and Zhang, 2001). In addition to this region, the positively charged residues that line the lateral opening and the internal vestibule of the pore are suggested to contribute to anion selectivity by attracting anions over cations to the pore entrance (Linsdell, 2016).

#### *1.3.3.3 The Regulatory Region: An Intrinsically Disordered Protein*

The unique R-region of CFTR is a disordered segment located in between and connecting the two CFTR halves. The sequence encoding the R-region is not found in any other ABC family member or in any other known protein (Riordan et al, 1989), and its origin was attributed to an evolutionary loss of a splice donor site which rendered an extension of exon 14 and appearance of exon 15 in the *CFTR* gene sequence, that are not found in other ABC members. This way, a non-coding intronic region became the coding sequence of the R-region, conferring the internal regulated channel function of CFTR (Sebastian et al, 2013). R-region phosphorylation is the primary critical step for CFTR activation,

followed by ATP binding at the dimerized NBD domains (Tabcharani et al, 1991; Gadsby & Nairn, 1999; Ostedgaard et al, 2000). Several phosphorylation consensus sites are found in the R-region, including ten for cAMP-protein kinase (PKA) and seven for protein kinase C (PKC) (Riordan et al, 1989). Besides modulation through PKA (Cheng et al, 1991; Anderson et al, 1991) and PKC phosphorylation (Hwang et al, 1989; Picciotto et al, 1992), other kinases, including cGMP-dependent kinases (French et al, 1995), tyrosine kinases (Fischer et al, 1996; Billet et al, 2015) and AMP-activated kinases (AMPK) (Hallows et al, 2000; King et al, 2009), can also phosphorylate and modulate CFTR function. Although the overall sequence of the R-region is not well conserved across species, the presence and distribution of the phosphorylation sites is highly conserved (Riordan et al, 1989).

Structural studies of the R-region show that this region of CFTR is mostly unstructured (disordered), assuming a random coil conformation rather than a well defined secondary structure, in contrast to all other CFTR domains (Ostedgaard et al, 2000, Baker et al, 2007; Marasini et al, 2013). There is still no full consensus on the R-region sequence boundaries. This is mainly due to the difficulty of establishing the exact limit between the C-terminal portion of NBD1 and the N-terminal portion of the R-region. On the other hand, because of easy identification of the starting point for TMD2, the C-terminal boundary of the R-region is more defined around residue D836. This uncertainty has led to early studies using shorter constructs (aa 708-831) to evaluate the structural properties of the R-region (Ostedgaard et al, 2000). By that time, studies using

constructs bearing a deletion between residues 708-835 were able to generate currents similar to wild-type channel (Rich et al, 1991) and supported the use of the aforementioned construct. Circular dichroism (CD) spectra analysis of this shorter R-region segment shows a mostly disordered conformation with only 5% of the protein composed by helical content. Those characteristics were not altered by PKA phosphorylation, suggesting it does not promote structural changes (Ostedgaard et al, 2000). NMR spectroscopy studies of a longer construct (654-838) also showed that the R-region is predominantly disordered, and that phosphorylation does not disturb the overall disorder. Phosphorylation promoted, nevertheless, isolated chemical shifts at the phosphoserines and to some adjacent residues, not enough, however, to promote global folding of the protein. This study identified the segments within the R-region with higher tendency to form elements of secondary structures. Residues within segments 654-670, 755-778 and 801-818 displayed the highest α-helix propensity, with up to 30-40%. Phosphorylation decreased the helical content of those segments of the R-region (Baker et al, 2007). Small angle X-ray scattering (SAXS) structural analysis of a R-region construct bearing residues 654-838 generate conflicting results. Although the data demonstrated that the R-region is mostly unstructured, a higher level of secondary structure was reported. Moreover, phosphorylation increased the rate of secondary structures, with the random coil fraction varying from ~30-18% and secondary structures varying from ~50-70% before and after phosphorylation, respectively (Marasini et al, 2013). All data discussed above was obtained from isolated recombinant proteins in solution and may not

represent the R-region state in the context of the full CFTR protein anchored at the plasma membrane. As the available crystal structures of the full-length CFTR did not resolve most of the R-region, to date, there is no certainty of the structural conformation(s) that the R-region assumes when integrated into the full CFTR sequence.

Proteins like the R-region that are biologically active, but retain an unstructured conformation are classified as intrinsically disordered proteins (IDPs). In contrast to the stable secondary structure of folded proteins, IDPs appear in several interchangeable conformations, with rapid alternation among individual conformations. This intrinsic lack of well folded secondary and tertiary structure provides functional advantages for these proteins, including the ability of binding to multiple partners. Therefore, IDPs are key participants in several protein-protein interactions, as well as signalling and regulation processes in the cell (Wright & Dyson, 1999; Dyson & Wright, 2005). This rapid interconversion of multiple conformations may give IDPs an advantage in interaction processes, increasing the overall radius of the protein, thus facilitating the initial contact with the binding partner, which can trigger further contacts with the same partner or provide accessibility to other binding partners (Shoemaker & Portman, 2000). One study analysing structural disorder prediction in four eukaryotic interactomes, including the human, showed that hub proteins (those interacting with ten or more binding partners) are significantly more unstructured than end proteins (those that interact with only one partner). The same study demonstrated that functions related to transcription, regulation and development

are performed by proteins with high level of disorder, whereas proteins with membrane localization and the ones with catalytic and transport functions are depleted of disorder, suggesting a positive correlation between the functional promiscuity of hub proteins and the presence of intrinsic structural disorder, with disorder serving as a 'stimulus' for protein interactivity (Haynes et al, 2006). Many IDPs experience folding transitions upon binding to a partner assuming one main conformation at the bound state (Dyson & Wright, 2005). However, other alternative configurations may arise after a binding event, including interaction systems where:(1) the IDP assumes more than one bound conformation upon binding;(2) only the segment of the IDP involved in the binding event becomes folded but the flanking regions remain unfolded;(3) two folded bound segments of the IDP are connected by a segment that remain unfolded and serve as a linker;(4) the majority or the whole IDP remains highly dynamic even in the bound state, and displays only local ordering based on weak transient interactions with their binding partners (Tompa & Fuxreiter, 2008). The R-region seems to fit in one or a mix of the alternative configurations for interacting systems, as proposed by Ostedgaard et al, (2000) in four speculative models for the interactions of the R-region with the rest of CFTR.

Amino acid sequence analysis of several naturally folded and non-folded proteins identified that IDPs usually have a low mean hydrophobicity and a high net charge, which confers the protein a low driving force for compaction and electrostatic repulsion, features that favor a disordered state (Uversky, 2011). In fact, the R-region sequence (aa 635-836) contains only 40% of hydrophobic

residues, and 30% are charged residues. Most positive charged residues are distributed among the phosphorylation consensus sites, while the negative charged residues are clustered in two distinct areas named NEG1 (aa 725-733) and NEG2 (aa 817-838). The sequence of NEG2 is well conserved among species and mutations in some residues within NEG2 cause CF, suggesting an important role for this segment in channel function. Moreover, ΔNEG2-CFTR channels displays low constitutive activity and are insensitive to PKA (Xie et al, 2002). Phosphorylation further increases the net charge of the R-region by addition of phosphate groups and this feature was reported the be the most common mechanism in which IDPs change the binding affinity to different binding partners (Iakoucheva et al, 2004), reinforcing the association between regulatory processes and unstructured proteins.

Several studies attempted to understand the functional role of the R-region in CFTR function by expressing constructs lacking different portions of the R-region sequence and examining the consequences in function. As for the structural studies, early functional studies on the function of the R-region used constructs lacking a shorter segment of the R-region, aa 708-835. Those studies demonstrated that CFTR-ΔR (708-835) channels were constitutively active in the presence of ATP and did not requir phosphorylation, in contrast to full length channels that require both ATP and phosphorylation to be active (Rich et al, 1991; Ma et al, 1997). Based on this data, it was proposed that the R-region was an inhibitory particle and its phosphorylation relieved this inhibition. However, this proposition was brought into question based on studies showing that co-

expression of half-CFTR proteins which included the R-region, also generated constitutive activation [aa 1-833 + aa 834-1480 (Csanady et al, 2000) or Δ1-836 + M837X (King & Sorscher, 2000)], and addition of variants of exogenous unphosphorylated R-region segments (aa 645-834 or 590-858 or 708-831) to CFTR-ΔR (708-835) channels were not able to re-establish the inhibition and block spontaneous activity (Winter & Welsh, 1997, Ma et al, 1997, Ostedgaard et al, 2000). On the other hand, the addition of the same R-region fragments, but now after phosphorylation, was able to increase the constitutive activity observed in CFTR-ΔR (708-835), confirming that besides an inhibitory role, the R-region is also able to stimulate channel activity, but only when it is phosphorylated (Winter & Welsh, 1997, Ma et al, 1997, Ostedgaard et al, 2000). Another study has demonstrated, however, that addition of a R-region segment (aa 635-836) was able to reduce, the constitutive activity of half-CFTR channels (aa 1-634 and aa 837-1480). Phosphorylation of the R-region increased the constitutive activity (Chappe et al, 2005).

The idea that the R-region can both prevent constitutive activity and stimulate activity after phosphorylation led to studies aiming to find parts of the R-region that are involved in this dual role. As mentioned above, constructs lacking NEG2 (aa 817-838), displayed constitutive activity that could not be enhanced by phosphorylation. Addition of exogenous NEG2 peptides was able to stimulate full-length CFTR channels suggesting that this segment is critical for the stimulatory role of CFTR (Xie et al, 2002). Another study, using several deletions

of the R-region, proposed that the region comprising aa 760-783 holds the inhibition role of the R-region (Baldursson et al, 2000).

These data strongly support the idea that the R-region holds both inhibitory and stimulatory roles, and the addition of negative charges or the conformational changes induced by phosphorylation is the determinant of whether it functions in a stimulatory or inhibitory mode. Further evidence for the inhibitory role was found in the recent crystal structure, which shows the unphosphorylated R-region located in between the two CFTR 'halves' preventing NBD dimerization, but, unfortunately, the structures did not show any evidence for the stimulatory role of the R-region as the phosphorylated R-region is mostly not visible (Liu et al, 2017; Zhang et al, 2018) (Figure 7).

### 1.3.4 CFTR Regulation by Phosphorylation

Although gating of CFTR channels is promoted by ATP binding, the primary stimulus to activate CFTR channels is phosphorylation. Cytosolic concentrations of ATP always exceed the threshold for CFTR opening, so the physiological regulation of CFTR activity comes from the balance between phosphorylation and dephosphorylation. Several kinases were reported to modulate CFTR, but cAMP-activated kinase (PKA) is the main regulator of CFTR activity (Cheng et al, 1991; Anderson et al, 1991). On the other side, several phosphatases such as phosphatases 2A (PP2A) and 2C (PP2C) have been found to be the most effective in dephosphorylating CFTR (Berger et al, 1993; Luo et al, 1998).

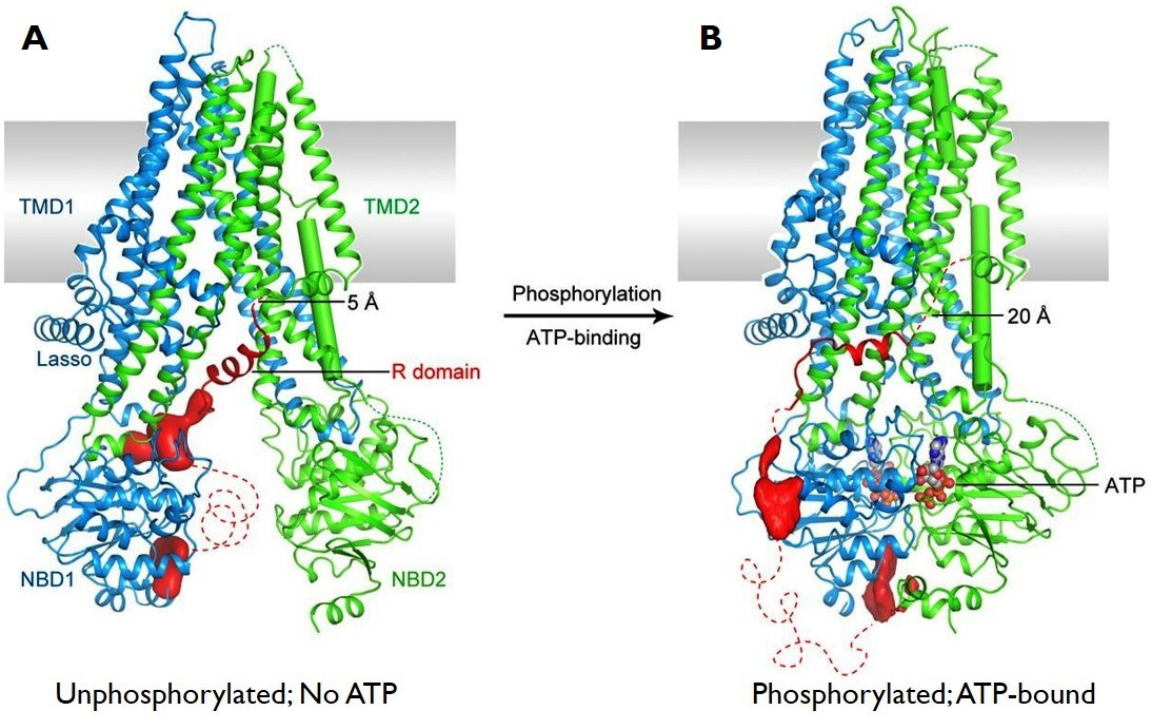


**Figure 7. Human CFTR structures.**

Ribbon representation of the unphosphorylated, ATP-free (**A**) and the phosphorylated, ATP bound conformation (**B**). Note the red dashed lines representing parts of the R-region that could not be resolved. Red EM densities correspond to unstructured parts of the R-region. The distances between the last visible residue in the R region and the first residue in TMD2 are indicated. TM 8 is highlighted in cylinder. ATP is shown in ball-and-stick and colored by heteroatom. **A**: Reproduced with adaptations from Liu F, Zhang Z, Csanády L, Gadsby DC, Chen J, (2017), with permission from Elsevier. **B**: Reproduced with adaptations from Molecular structure of the ATP-bound, phosphorylated human CFTR by Zhang Z, Liu F, Chen J (2018), licensed under CC BY-NC-ND 4.0.

PKA recognizes specific amino acids sequences, consensus sites, and catalyzes the incorporation of phosphate groups at the side chains of serine or threonine residues. Consensus sites for PKA can be monobasic (R-X-S/T; X represents any amino acid) or dibasic (R-R/K-X-S/T). CFTR contains ten dibasic consensus sites as well as several monobasic sites. Among the dibasic sites, eight were found to be phosphorylated at least *in vitro*, seven located within the R-region (S660, S700, S712, S737, S768, S795 and S813) and one (S422) located at the RI, a small disordered region within NBD1. Only two of the monobasic PKA sites were found to be phosphorylated at least *in vitro* (S670 and S753). From all PKA sites, at least six (S660, S700, S737, S768, S795 and S813) were found to be phosphorylated in vivo (Cheng et al, 1991; Picciotto et al, 1992; Hegedus et al, 2009). Among the two remaining dibasic sites, S686 is actually a substrate for PKC phosphorylation and T788 was only seen to be slightly phosphorylated (15%) by PKA in one study (Baker et al, 2007).

Mutational analysis of PKA sites demonstrated that none of these sites is essential for CFTR function and favors the idea of an additive mechanism for the phosphorylated-dependent activation of CFTR. However, it seems that each site does not contribute equally for the maximal response. Mutation of four sites with alanines (S660A, S737A, S795A and S813A) reduced substantially CFTR response to cAMP. Including mutations of the other 4 dibasic sites within the R-region (S686A, S700A, S712A, S768A), or even removing all ten dibasic PKA sites in CFTR (by also including S422A and T788A) further reduced the channel response, and a low level of activity was still observed, probably because of

phosphorylation of the monobasic sites (Chang et al 1993, Rich et al, 1993). Only after removing fifteen PKA sites (by including five monobasic sites) no further reduction in channel activity was observed (Seibert et al, 1999). Those results pointed to a mechanism of redundancy where CFTR maximal function would be achieved by graded addition of negative charges (phosphorylation) in an increasing number of sites. Evidences in favor of this mechanism were obtained by experiments showing that mutants carrying six or eight (but not less than six) aspartate residues in place of serine residues (to mimic incorporation of negative charges similar to phosphorylation) displayed a low, but measurable, activity in the absence of PKA (Rich et al, 1993). On the other hand, evidence against this simple accumulative mechanism came after the finding that two of the dibasic sites (S737 and S768) play inhibitory roles (Wilkinson et al, 1997; Csanady et al, 2005), and from structural studies demonstrating that PKA phosphorylation promotes conformational changes in R-region peptides, altering significantly its secondary structure, the CD spectra and the mobility in SDS-PAGE (Dulhanty & Riordan, 1994; Dulhanty et al, 1995; Ostedgaard et al, 2000, Baker et al, 2007; Marasini et al, 2013). Thus, the fact that addition of negative charges can cause stimulatory or inhibitory effects, and that phosphorylation does cause marked conformational changes in the R-region that could be involved in the regulatory mechanism, supports a mechanism where individual phosphorylation sites may play specific functions, rather than just being responsible for an accumulation of negative changes (Gadsby & Nairn, 1999; Csanady et al, 2005).

The exact mechanism by how PKA phosphorylation of the R-region regulates the activity of CFTR still remains unclear. To date, two main mechanisms were proposed based on the available biochemical, structural and functional data. The first argues that the R-region modulates function by controlling NBDs dimerization. In support, NMR studies and CFTR structures demonstrated that the R-region interacts with both NBDs and that PKA phosphorylation relieves those interactions. (Baker et al, 2007; Bozoki et al, 2013; Liu et al, 2017). Also, the efficiency of NBDs dimerization was found to be positively affected by PKA phosphorylation (Mense et al, 2006; He et al, 2008). In this mechanism, PKA phosphorylation would both relieve R-region binding to NBDs and stimulate NBD dimerization, therefore, activating the channel. The second mechanism defends that the R-region modulates function by interactions with the pore machinery either indirectly, through interaction with the CLs or directly interacting with the TMDs, regulating channel gating independently of the NBDs. As supporting evidence is the finding that CFTR constructs lacking NBD2 are still active and activation is independent of ATP, but dependent of PKA stimulation (Cui et al, 2007; Wang et al, 2007). Also, gating deficient channels harboring G551D mutation are still active in the presence of PKA (Bompadre et al, 2007). This mechanism is based on spontaneous channel openings that are observed in the absence of ATP in several expression systems. As NBD2-truncated and G551D channels are not able to NBD dimerization and hydrolyze ATP, respectively, an alternative mechanism is necessary for channel activation. That would be achieved by PKA-induced direct connections of the R-region with CLs or TMDs,

which has been observed in the CFTR crystal structures (Zhang et al, 2016; Liu et al, 2017). In addition, an ancillary mechanism is based on PKA phosphorylation at S422, localized at the RI in NBD1, proposed to modulate an interaction between NBD1 and the CL1 of TMD1. Upon phosphorylation of S422, a potential site on NBD1, responsible for binding to CL1 is exposed and this binding is proposed to complement the effects ensued by PKA phosphorylation of the R region (Kanelis et al, 2010). However, a study using half-CFTR channels missing most of the RI (1-414 and 433-1480) behaved largely similar to wild type channels (Csanady et al, 2005), suggesting that segment, and therefore S422, plays minimal, if any, role in CFTR activation by PKA.

All of the above mechanisms are reasonable and perhaps a combination of them are responsible for PKA stimulation of CFTR activity. The high number of PKA sites in CFTR, and the fact that phosphorylation of individual sites elicits different channel responses (Winter & Welsh, 1997; Wilkinson et al, 1997, Baldursson et al, 2000) support such a cooperative mechanism.

Besides PKA, which is clearly the major regulatory pathway for CFTR activation, CFTR is also phosphorylated by other kinases, including protein kinase C (PKC) and AMP activated protein kinase (AMPK). The R-region has seven PKC consensus sites (S641, T682, S686, S707, S790, T791 and S809). From those, five (S641, T682, S686, S707 and S790) have been phosphorylated *in vitro* and only S686 was found phosphorylated *in vivo*. PKC also phosphorylates S660 and S700, but in a lower rate than PKA does (Picciotto et al, 1992; Jia et al, 1997; Chappe et al, 2004). In contrast to PKA, PKC phosphorylation of the R-region did

not induce changes in the CD spectra or in SDS-PAGE mobility (Picciotto et al, 1992, Dulhanty & Riordan, 1994). PKC phosphorylation itself only elicits small activation of CFTR. However, PKC phosphorylation prior to PKA stimulation was found to potentiate PKA responses by approximately two-fold (Tabcharani et al, 1991; Berger et al, 1993, Chappe et al, 2003). Moreover, a low level of constitutive PKC phosphorylation is argued to be essential for CFTR activation by PKA (Berger et al, 1993; Jia et al, 1997). This effect is better observed in prolonged cell patches, or when cells are treated with PKC inhibitors. In both cases, PKA stimulation is almost completely abrogated, apparently because PKC phosphorylation is removed by either the action of phosphatases in prolonged patches or because of the effect of the inhibitors. Moreover, when comparing cell responses to PKA stimulation, cells that were pre-treated with PKC inhibitors show reduced responses compared to control cells (Jia et al, 1997). Thus, PKC seems to work in synergy with PKA, however, the mechanism involved in this cooperative work is unknown. Later studies have examined the role of PKC sites in CFTR function. Mutation of nine PKC sites in CFTR (seven of the R-region and two localized at NBD1; T582A and T604A) dramatically reduced responses to PKA and abrogated the enhancing effect on PKA response. Moreover, after treatment with phosphatases, PKC elicited a small response in wild-type channels but not in the PKC mutant (Chappe et al, 2003). The results suggested that both the small response in absence of PKA and the modulation of PKA response are a result of direct PKC phosphorylation of CFTR rather than an indirect regulation via other molecules. In a detailed investigation on the role of

individual PKC sites, S641 and T682 were described as inhibitory sites, similarly to PKA sites S737 and S768, and S686 was described as essential for PKC modulation of PKA response (Chappe et al, 2004). Channels lacking S641 had increased responses to PKA and channels lacking T682 had very high responses to PKC. In contrast, channels lacking S686 could not be stimulated by exogenous PKC and lost the PKC enhancing effect on PKA response (Chappe et al, 2004), suggesting that S686 may play a significant role in CFTR regulation by PKC. The two PKC sites localized within NBD1 (T582 and T604) were found to be important for channel function as their mutation to alanine drastically reduced the channel response to phosphorylation (Chappe et al, 2004).

In addition to the modulation of CFTR activity, PKC is also involved in CFTR expression and trafficking. The PKCε isoform is a key component in the VIP (vasoactive intestinal peptide) signaling cascade that promotes CFTR membrane localization. Phosphorylation by PKCε of the actin-binding protein complex ezrin/radixin/moesin (ERM) is critical for its binding to NHERF-1 and CFTR, forming a complex that stabilized CFTR at the cell membrane (Alshafie et al, 2014).

AMPK is a metabolic-stress sensitive kinase that modulates ion transport activity in response to cell metabolic status. AMPK localizes at the apical membrane in epithelial cells, binds to the C-terminal tail of CFTR at residues 1420-1457 and phosphorylates the two inhibitory PKA sites (S737 and S768; mostly at the latter one) in response to high levels of AMP, providing a link between CFTR function and metabolic status. When activated, AMPK prevents channel activation by

PKA and PKC, but also inhibits constitutive low activation of CFTR. Inhibition of AMPK or mutations at both S737 and S768 to alanine increased baseline activity of CFTR, and the response of CFTR to cAMP agonists (Hallows et al, 2000; King et al, 2009, Kongsuphol et al, 2009). Thus, the basal activity of CFTR found in several expression systems is proposed to be regulated by the levels of endogenous AMPK in the cell, with high activation of AMPK, reflecting metabolic stress, keeping CFTR silent and low activity of AMPK, enabling constitutive activity of CFTR (Kongsuphol et al, 2009). In cells expressing a highly activated AMPK mutant, CFTR stimulation by PKA is completely abrogated, and this effect is not seen in cells expressing a dominant-negative version of AMPK. Interestingly, CFTR phosphorylation by AMPK at sites S737 and S768 did not prevent R-region phosphorylation at the other phosphorylation sites, but still kept CFTR channels closed, suggesting that AMPK phosphorylation renders CFTR in a state or conformation where PKA or PKC phosphorylation are not able to promote channel activation (King et al, 2009).

Casein kinase 2 (CK2) is a constitutively active serine/threonine protein kinase described to regulate both CFTR biosynthesis and function. CK2 co-localize with CFTR and its inhibition was found to reduce both channel function and protein processing. CK2 was described to phosphorylate CFTR at S422 at NBD1 and T1471 at the C-terminal tail (Treharne et al., 2009; Luz et al., 2011; Venerando et al., 2013). CFTR phosphorylation by spleen tyrosine kinase (SYK) at Y512 has been found to reduce its membrane localization by a mechanism still unknown. It is proposed that SYK and CK2 work cooperatively, with phosphorylation at Y512

by SYK being required prior to phosphorylation by CK2. Inhibition of SYK or mutation of Y512 has been demonstrated to strongly increase CFTR currents by preventing its removal from the plasma membrane. Mutations that mimic phosphorylated (Y521E) or unphosphorylated (Y521F) states have led to reduction and increase of CFTR levels at the membrane, respectively (Luz et al, 2011; Mendes et al, 2011). Two other tyrosine kinases, Pyk2 (proline-rich tyrosine kinase 2) and Src (proto-oncogene tyrosine-protein kinase) are also able to phosphorylate and stimulate CFTR function, reaching 80% of the response obtained by PKA phosphorylation (Fisher et al, 1996; Billet et al, 2015). The proposed sites for both Src and Pyk2 phosphorylation are residues Y625 and Y627, localized in the end of NBD1. Mutation of these sites for phenylalanine robustly decreased channel function, but did not abrogated completely, suggesting other sites are still to be identified (Billet et al, 2016).

CFTR dephosphorylation, and consequently deactivation, is carried out by protein phosphatases, however, there is no single phosphatase able to completely dephosphorylate CFTR. CFTR exposure to PP2A, PP2C and alkaline phosphatase is able to decrease CFTR activity by >90% (Thelin et al, 2005). PP2A and PP2C, deactivate CFTR in distinct ways. While deactivation by exogenous PP2C requires $Mg^{+2}$, and resembled the spontaneous deactivation observed in cells after removal of PKA agonists, with no changes in the burst duration, deactivation by PP2A requires no cofactors and causes a dramatic reduction in channel burst durations, indicating they may act at different phosphorylate sites (Luo et al, 1998). PP2A directly binds to peptides comprising

residues 1451-1476 at the C-terminal of CFTR and residues 672-855 at the R-region of CFTR by means of two different regulatory subunits of the protein, B'ε and PR65 respectively (Thelin et al, 2005; Vastiau et al, 2005). PP2C efficiently dephosphorylates a R-region peptide (aa 654-837) and was found to interact with CFTR but specific interaction sites are still unknown (Zhu et al, 1999).

In order to be activated or deactivated by kinases or phosphatases, CFTR must be exposed to those components and this is achieved by the formation of compartmentalized protein complexes anchored to the cytoskeleton, which bring together scaffold proteins, adaptors, phosphodiesterases, other transporters and several regulatory factors and enzymes, including kinases PKA, PKC and AMPK and phosphatases PP2A and PP2C, that interact with CFTR promoting its regulation in the apical cell surface. Among other molecules, the CFTR interactome is composed of NHERF1 binding to the C-terminal PDZ motif of CFTR which brings PKA and PKC close to CFTR via NHERF1-erzin-actin complex and NHERF1-RACK1 dimer-tubulin complex, respectively, in addition to the direct interaction of PP2A, PP2C and AMPK to CFTR as described above.

### 1.3.5 R-Region Interactions Induced by Phosphorylation

Several studies have reported phosphorylation-dependent interactions of the R-region with all cytoplasmic parts of CFTR, including the N-terminal lasso motif (Naren et al, 1999), NBD1 (Wang et al, 2002; Baker et al, 2007; Bozoki et al, 2013), NBD2 (Wang et al, 2002; Bozoki et al, 2013), C-terminal tail (Bozoki et al, 2013), and cytoplasmic loops (Wang et al, 2002; Wang, 2010; Wang & Duan,

2012). In addition, interactions with the STAS domain of SLC26A family members (Ko et al, 2004) and with the protein adaptor 14-3-3 (Liang et al, 2012) have also been reported.

Studies using a split CFTR construct, expressing the two CFTR halves and the R-region as three separate polypeptides, have shown that phosphorylation by PKA enhances association of the R-region with both CFTR halves (Chappe et al, 2005), and additional phosphorylation by PKC further enhanced the interactions (Seavilleklein et al, 2008), an indication that phosphorylation regulates CFTR not only by causing its dissociation from an inhibitory site but also by promoting stimulatory R-region interaction with other CFTR domains.

By probing an extensive overlapping peptide library spanning all intracellular regions of CFTR with a recombinant R-region (aa 589-830) peptide, Wang et al (2002) found interactions of the R-region with peptides spanning regions of both NBD1 and NBD2. Recent NMR studies revealed interactions involving several parts of the R-region and both NBDs, and those interaction were mostly eliminated after phosphorylation. Five segments of the unphosphorylated R-region, aa 661-681, 702-718, 748-778, 803-813 and 829-834, that interact with NBD1 were reduced to only three segments, aa 748-778, 805-815, and 829-833, that bound to NBD1 with a four-times weaker strength after phosphorylation. Three segments of the unphosphorylated R-region, aa 661-673, 752-778, and 819-836, also interact with NBD2 and this interaction was reduced to only one weak interacting segment, 802-824, after phosphorylation (Baker et al, 2007; Bozoki et al, 2013). The three first segments interacting with NBD1 as well as the

two first segments interacting with NBD2 contain two PKA phosphorylation sites, one bordering the beginning and another one somewhere in the middle of each interacting segment. Those segments are the ones showing the highest reduction in interactions with the NBDs after phosphorylation. The same study also demonstrated that the putative sites on NBD1 that bind to the R-region are likely located in the NBDs dimer interface (Bozoki et al, 2013). Those results are in accordance to the CFTR structures showing a large EM density ascribed to the R-region located in between the NBDs in the unphosphorylated state, that completely vanished in the phosphorylated state (Liu et al, 2017; Zhang et al, 2018). The observations from NMR studies and cryo-EM structures as well as the fact that phosphorylation promotes ATP hydrolysis (Mense et al, 2006), provide strong evidence for the first mechanism explaining PKA-regulation of CFTR function, described in the previous section, where the R-region modulate channel function by phosphorylation-dependent interference in NBDs dimerization.

Early studies have reported interactions of the R-region with a cluster of acidic residues (D47, E51, E54, D58) localized in the N-terminal lasso motif. Alanine substitution of those residues caused a reduction in both channel function and binding to the R-region. *In vitro* interaction of recombinant R-region and lasso motif peptides showed only a slight increase after phosphorylation (Naren et al, 1999). In addition, a recombinant R-region (aa 589-830) was also found to interact with overlapping peptides comprising the 35 first residues of the lasso motif (Wang et al, 2002). Although in the unphosphorylated CFTR structure no

direct interactions between the lasso motif and the R-region were described, a small helix proposed to be part of the R-region is seen interacting with residues 34-39 of the lasso motif in the phosphorylated human structure. The residues seen interacting with the R-region in the human structure diverge from the ones observed with isolated peptides (Zhang et al, 2018).

Interactions between the R-region and the C-terminal tail (C-tail) of CFTR were only recently described. An isolated peptide comprising residues 1438-1480 was found to interact mostly with one segment (aa 747-771) of the unphosphorylated R-region, with other three segments (663-680, 697-717, and 803-815) showing weaker interactions. After phosphorylation, interactions with the four segments dramatically increased, and one new segment (827-836), mapped at the NEG2 region (aa 817-838), now appeared as a binding partner to the C-tail. The interaction with C-tail, which is also unstructured, promoted a large chemical shift in the R-region, indicating a certain degree of disorder-to-order transition in some parts of the R-region and/or the C-tail (Bozoki et al, 2013). Such disorder-to-order transition could be the explanation for the extra thirteen residues resolved at the C-tail of the phosphorylated human structure, compared to the unphosphorylated structure. Interestingly, those residues form a small helix and are positioned just near one of the R-region densities (Zhang et al, 2018), suggesting a possible interaction with the R-region as the cause for the disorder-to-order transition of this C-tail segment.

In order for phosphorylation to induce channel activity independently of the NBDs motion, as proposed by the second mechanism for PKA activation, interactions

between the R-region and the cytoplasmic loops or directly with the pore region are imperative. A recombinant R-region peptide (aa 589-830) bound to portions of CL1 and CL4, with interaction with the latter reported to be stronger than with the former (Wang et al, 2002).

A series of studies have proposed interactions of some acidic residues within NEG2 with some basic counterparts within CL3, either through a metal ($Fe^{+3}$) bridge or through a complex electrostatic attraction involving an arginine of the S768 PKA consensus site (Wang, 2010, 2011; Wang & Duan, 2012). However, all residues in CL3 reported in those studies (H950, H954 and R946) are located fairly far from the proposed R-region helix (aa 825-836; within NEG2) of the unphosphorylated human CFTR structure, and their side chains are facing away from the helix position (Liu et al, 2017), which in turn, makes it difficult to conceive the feasibility of those interactions. The same crystal structure shows that the R-region helix do interact with CL3, but in residues divergent from the ones proposed in Wang's studies, as well as with CL4 and TM12. In addition, parts of the R-region densities are located nearby to both NBD1-CL1 and NBD1-CL4 interfaces, where it could possibly interfere with the NBD-TMD communication during gating (Liu et al, 2017). In the phosphorylated structure, a stretch of thirteen residues (which could not be assigned) form a helix that is tightly associated with CL4, but at residues distinct from the ones in the unphosphorylated helix (Zhang et al, 2018). The interactions reported in the solved structures as well as the location of the unphosphorylated R-region helix

at the entrance of the intracellular vestibule of the pore provide substantial evidence for a mechanism regulating CFTR activity independent of the NBDs. Phosphorylation also regulates channel activity by promoting intermolecular interactions. Early in this chapter, a functional association between CFTR and members of the SLC 26 family was briefly described. Both CFTR (Wang et al, 1998) and SLC26A transporters (Lamprecht et al, 2002) contain a PDZ motif at their C-terminal ends and through binding to NHERF1, they are co-localized at the apical membrane. In addition, the R-region of CFTR was found to directly interact with the STAS domain of SLC26A3 and A6, in a phosphorylation dependent manner (Ko et al, 2004). CFTR and SLC26A3/A6 are proposed to undergo reciprocal regulation and the R-region and STAS domain play a critical role. First, removal of STAS from SLC26A prevent its binding to and activation of CFTR and the inverse occurs when the R-region is deleted from CFTR in the presence of STAS domain. Second, phosphorylation of the R-region dramatically enhances its association with the STAS domain and consequently, increases reciprocal positive regulation for both membrane translocators, which is facilitated by their PDZ-mediated spatial co-localization (Ko et al, 2004). Phosphorylation not only modulates channel function at the cell surface but also increases the rate of maturation and trafficking of CFTR to the plasma membrane.

14-3-3 proteins are a family of regulatory proteins that typically interact with phosphoserine and phosphothreonine motifs stabilizing the phosphorylated state of proteins in order to regulate several cellular functions. 14-3-3 proteins have

been shown to improve surface localization of several receptors and ion channels, in a posttranslational mechanism (Yuan et al, 2003; Liang et al, 2012). Such mechanism was also reported for CFTR, where the expression levels are enhanced by a mechanism involving PKA phosphorylation and interaction of 14-3-3 proteins with the PKA sites within the R-region (Liang et al, 2012). Two 14-3-3 isoforms, β and ε, have their binding to both immature and mature forms of CFTR increased by phosphorylation. Also, co-expression of 14-3-3β increases biosynthesis and immature-to-mature conversion of CFTR (Liang et al, 2012). NMR studies demonstrated binding of 14-3-3β to five segments of the unphosphorylated R-region and this interaction was increased to eight small segments that bound > 6-times stronger after PKA phosphorylation. Seven out of the eight segments contained at least one phosphoserine (Bozoki et al, 2013). Those results support the idea of a mechanism where phosphorylation promotes CFTR processing by inducing interactions of 14-3-3 proteins with the R-region, which in turn, improve ER exit, maturation and trafficking of CFTR.

### 1.4 Thesis Rationale and Hypotheses

Thirty years after the discovery of the CFTR gene, and even with the recent high-resolution structures of CFTR, a full picture of the molecular events induced by phosphorylation of CFTR is still missing. The majority of phosphorylation sites in CFTR, ten for PKA and seven for PKC, are located in the R-region, a disordered segment that functions as a dynamic hub, proposed to make transient interactions with many partners dependent on its phosphorylation state. While extensive work has been done investigating the role of PKA phosphorylation in modulating channel function and intramolecular interactions, the role of PKC phosphorylation, which is known to be required for and to potentiate PKA responses, has not been investigated to the same extent. Furthermore, the unphosphorylated CFTR structure clearly shows parts of the R-region density situated between the two halves, sterically preventing dimerization, but in the phosphorylated structure the R-region is mostly missing, except for a small helix interacting with residues at CL4 and the lasso motif, hindering the identification of most of the interaction partners of the phosphorylated R-region. A caveat found in previous studies examining PKA modulation of intramolecular interactions in CFTR is that they were done *in vitro*, using isolated polypeptides.

Previous results from our lab showed that deletion of all seven PKC sites within the R-region disturbs channel responses to PKA, prevent the PKC potentiation of PKA responses (PKC enhancing effect), and disrupt R-region intramolecular interactions, indicating that one or more PKC sites are needed for CFTR activation and domain-domain interactions. Moreover, mutation of different

subsets or individual PKC sites were found to disturb channel responses to PKA and PKC differently.

For these reasons, the main goal of my thesis work was to provide novel information about the mechanism underlying the phosphorylation-induced activation of the CFTR channel by means of investigating in detail phosphorylation-dependent R-region interactions and the role of PKC phosphorylation sites in the R-region interactions. The hypotheses were that different states of phosphorylation of the R-region promote different levels of interaction with other parts of CFTR and that the effects of PKC phosphorylation in channel function could be correlated with PKC-driven modulations of the R-region interactions.

To test those hypotheses, I used both *in situ* and *in vitro* approaches to investigate the modulation of R-region interactions by PKA and PKC phosphorylation. For *in situ* analysis, aimed to reflect conditions inside the cell, in the context of the CFTR interactome, a Split-CFTR construct expressing the channel as three separate polypeptides in BHK cells was used, and the interactions of the R-region with the N-terminal and C-terminal halves of CFTR were investigated. By inserting mutations at subsets of PKC sites within the R-region, the effect of PKC phosphorylation in the interactions with the CFTR halves could be analyzed. For in vitro analysis, a recombinant R-region peptide was generated, and the effects of phosphorylation in the interactions of this peptide with six cytoplasmic subdomains of CFTR, three from the N-terminal half (N-tail, CLs 1 and 2) and three from the C-terminal half (CLs 3 and 4 and C-tail),

were investigated. It was expected that those results could be used to propose molecular models for the R-region dynamics induced by phosphorylation and for the mechanism involved in the PKC enhancing effect.

# CHAPTER 2: MATERIALS AND METHODS

## 2.1 CHEMICALS

Monolith NT.115 Capillaries was from NanoTemper (Munich, Germany). IMAC Sepharose™ 6 Fast Flow chromatography medium was from GE Healthcare (Uppsala, Sweden). Ampicillin sodium salt, Chloramphenicol, 2-mercaptoethanol (BME), Isopropyl β-D-1-thiogalactopyranoside (IPTG), Imidazole and Urea were from Bioshop Canada (Burlington, ON). Amicon Ultra-15 Centrifugal Filter Units was from Millipore Sigma (Burlington, MA). cAMP-dependent protein kinase (PKA), catalytic subunit was from New England Biolabs (Ipswich, MA). PKC Lipid Activator, LB broth Miller and LB Agar Miller were from EMD Millipore (Temecula, CA). 10x Tris/Glycine/SDS buffer, 10x Tris/Glycine, Certified™ Molecular biology Agarose, 30% Acrylamide/Bis solution 29:1, Quick Start™ Bradford 1x Dye Reagent and Clarity™ Western ECL chemiluminescence detection kit were from Bio-Rad (Mississauga, ON). Platinum® PCR SuperMix High Fidelity Kit, Ponasterone A (PA), Zeocin and G418 were from Invitrogen (Burlington, ON); 2x Taq FroggaMix was from FroggaBio (Toronto, ON). Methotrexate was from Faulding Inc. (Montreal, QC). GenepHlow™ Gel Extraction Kit and PCR Cleanup Kit was from GeneAid (Taiwan). QIAprep Spin Miniprep Kit was from Qiagen (Mississauga, ON). Quick change II Site-direct mutagenesis kit was from Agilent Technologies (Santa Clara, CA). FuGene® HD Transfection Reagent and Protein Kinase C (PKC) were from Promega (Madison, WI). Penicillin-Streptomycin, Protease inhibitors, Fetal Bovine Serum, DMEM/F12 HEPES medium, BamHI

and SalI restriction enzymes were from ThermoFisher Scientific (Waltham, MA). Vectashield Mounting Medium for Fluorescence was from Vector Laboratories (Burlingame, CA). Duolink *in situ* Proximity Ligation Assay orange Kit, Albumin from bovine serum (BSA), Adenosine 5'-triphosphate magnesium ($Mg^{+2}$-ATP), 8-(4-chlorophenylthio) adenosine 3',5'-cyclic monophosphate sodium salt (cAMP), Forskolin (FSK), DL-Dithiothreitol (DTT), Phorbol 12-myristate 13-acetate (PMA), 3-Isobutyl-1-methylxanthine (IBMX), Tetramethyl ethylenediamine (TEMED) and other chemicals were from Sigma-Aldrich (St. Louis, MO).

### 2.2 ANTIBODIES

A list with the names of CFTR antibodies used during this study as well as the manufacturing company, host, epitopes and dilutions used are shown in Table 1. A list with names of secondary antibodies used during this study as well as the manufacturing company, host and dilutions used are shown in Table 2. All CFTR and secondary antibodies were optimized experimentally by testing specificity, phospho-sensitivity, concentration and incubation times for each technique used.

### 2.3 CFTR POLYPEPTIDES

Polypeptides corresponding to six cytoplasmic regions of CFTR with a N-terminal 5-FAM-tag were synthesized by Proteogenix (Schiltigueim, France). The first three polypeptides are part of our front half construct and corresponded to the sequences of the Lasso motif of CFTR (aa 1-77), the cytoplasmic loop 1

**Table 1. CFTR antibodies Information**

| Name | Company | Host | Target/Epitope | Dilution |
|---|---|---|---|---|
| MM13-4 Monoclonal Antibody | Millipore Sigma (Burlington, MA,USA) | Mouse | Front Half of CFTR. Synthetic peptide (RKGYRQRLELSD) corresponding to residues 25-36 of human (CFTR) | 1:1000 (WB) |
| M3A7 Monoclonal Antibody | Millipore Sigma (Burlington, MA, USA) | Mouse | Back-Half of CFTR. GST-fusion protein corresponding to residues 1197-1480 of human CFTR. The epitope maps within amino acids 1365-1395. | 1:1000 (WB) |
| MAB1660 Monoclonal Antibody | R&D Systems (Minneapolis, MN, USA) | Mouse | R-region of CFTR. Beta-galactosidase-coupled CFTR Cys590-Lys830 (predicted) | 1:1000 (WB)<br>1:500 (IF,PLA) |
| H-182 Polyclonal Antibody | Santa Cruz Biotechnology (Dallas, TX, USA) | Rabbit | Front Half of CFTR. Epitope corresponding to amino acids 1-182 mapping at the N-terminus of human CFTR. | 1:4000 (WB)<br>1:1000 (IF,PLA) |
| C-19 Polyclonal Antibody | Santa Cruz Biotechnology (Dallas, TX, USA) | Goat | Back-Half of CFTR. Epitope mapping near the C-terminus of CFTR of human origin | 1:1000(WB)<br>1:500 (IF,PLA) |

WB: Western Blot
IF: Immunofluorescence
PLA: Proximity Ligation Assay

**Table 2. Secondary Antibodies Information**

| Name | Company | Host | Dilution |
|---|---|---|---|
| Cy3-conjugated anti-mouse IgG | Jackson ImmunoResearch Laboratories (West Grove, PA, USA) | Goat | IF 1:100 |
| Peroxidase-conjugated anti-mouse IgG | Jackson ImmunoResearch Laboratories (West Grove, PA, USA) | Goat | WB 1:10000 |
| Alexa Fluor® 488-conjugated anti-rabbit IgG | Jackson ImmunoResearch Laboratories (West Grove, PA, USA) | Goat | IF 1:200 |
| Peroxidase-conjugated anti-rabbit IgG | Jackson ImmunoResearch Laboratories (West Grove, PA, USA) | Goat | WB 1:5000 |
| Alexa Fluor® 488-conjugated anti-goat IgG | Jackson ImmunoResearch Laboratories (West Grove, PA, USA) | Bovine | IF 1:200 |
| Peroxidase-conjugated anti-goat IgG | Jackson ImmunoResearch Laboratories (West Grove, PA, USA) | Bovine | WB 1:5000 |

WB: Western Blot
IF: Immunofluorescence

comprising the cytoplasmic extensions of TM 2 and 3 (aa 147-195) and the cytoplasmic loop 2 comprising the cytoplasmic extensions of TM 4 and 5 (aa 244-298). The last three polypeptides are part of our back half construct and corresponded to sequences of the cytoplasmic loop 3 comprising the cytoplasmic extensions of TM 8 and 9 (aa 940-990), the cytoplasmic loop 4 comprising the cytoplasmic extensions of TM 10 and 11 (aa 1035-1095) and the C-terminal tail of CFTR (aa 1439-1480). Table 3 shows information and amino acid sequences for each polypeptide. DNA sequences used for polypeptide synthesis were taken from the human CFTR database (UniProt accession #P13569).

### 2.4 Split-ΔR and Split-R cDNAs Construction and transfection into Baby Hamster Kidney Cells

Split-ΔR cDNA ligated into the ecdysone-inducible vector pIND (Split-ΔR), wild-type (R-WT) and mutant R-region cDNAs of R-6CA (S641A/T682A/S707A/ S790A/T791A/S809A), R-S686A and R-S641A/T682A incorporated into the pNUT vector were a generous gift from Dr. John Hanrahan (Department of Physiology, McGill University). For details on the constructs pIND-Split-ΔR and pNUT-R, see Irvine, 2002 and Chappe et al. 2005)

The R-S686D mutant was generated using the R-WT in pNUT (R-WT) vector as a template. First, empty pNUT vector and R-WT containing vector were digested with NCoI restriction enzyme and the presence of an extra band at 862bp in 1% agarose gel confirmed the presence of the R-region insert (two bands of 4774pb and 757pb are expected in the empty pNUT with an extra 862pb present in R-WT

**Table 3. CFTR Polypeptides Information**

| Polypeptide Name | Purity | Amino acid sequence |
|---|---|---|
| CFTR N-terminal<br>(Lasso motif)<br>Amino acids 1-77 | >90% | 5-FAM-MQRSPLEKASVVSKLFFSWTRPILRKGY RQRLELSDIYQIPSVDSADNLSEKLEREWDRELA SKKNPKLINALRRCF-$NH_2$ (77a.a.) |
| CFTR cytoplasmic<br>Loop 1<br>Amino acids 147-195 | >90% | 5-FAM-HIGMQMRIAMFSLIYKKTLKLSSRVLDKI SIGQLVSLLSNNLNKFDEG-$NH_2$ (49a.a.) |
| CFTR cytoplasmic<br>Loop 2<br>Amino acids 244-298 | >90% | 5-FAM-MMKYRDQRAGKISERLVITSEMIENIQSV KAYCWEEAMEKMIENLRQTELKLTRK-$NH_2$ (55a.a.) |
| CFTR cytoplasmic<br>Loop 3<br>Amino acids 940-990 | >90% | 5-FAM-TLITVSKILHHKMLHSVLQAPMSTLNTLK AGGILNRFSKDIAILDDLLPLT-$NH_2$ (51a.a.) |
| CFTR cytoplasmic<br>Loop 4<br>Amino acids 1035-1095 | >90% | 5-FAM-QTSQQLKQLESEGRSPIFTHLVTSLKGL WTLRAFGRQPYFETLFHKALNLHTANWFLYLST-$NH_2$ (61a.a.) |
| CFTR C-terminal tail<br>Amino acids 1439-1480 | >90% | 5-FAM-QAISPSDRVKLFPHRNSSKCKSKPQIAA LKEETEEEVQDTRL-$NH_2$ (42a.a.) |

(Amer, 2010) (Figure 8, lanes 1 and 2). R-WT was then used to transform DH5-α *E. coli* cells and the transformation product was plated in Luria Bertani (LB) plates supplemented with 100mg/ml ampicillin (AMP). A single colony was inoculated in LB+AMP broth overnight at 37ºC and plasmids were isolated using QIAprep Spin Miniprep Kit. Quick change II Site-direct mutagenesis kit was used to generate the R-S686D mutant, using the following primers 5'-TCTCCTGGACA GAAACAAAAAAACAAGATTTTAAACAGACTGGAGAGTTTGG-3' (forward) and 5'-CCAAA CTCTCCAGTCTGTTTAAAATCTTGTTTTTTTGTTTCTGTCCAGGAG A-3' (reverse) (16 cycles: denaturing 95ºC for 30sec, annealing 55ºC for 1 min and extension 68ºC for 6.5min, following manufacturing instructions). Mutagenesis product was used to transform DH5-α *E. coli* cells. Four colonies were selected and inoculated in LB+AMP overnight at 37ºC followed by DNA extraction (QIAprep Spin Miniprep Kit) and products were digested with NCoI to check DNA integrity (Figure 8, lane 3) and R-S686D was confirmed by sequencing.

Plasmid DNA (7.2 µg) from split-ΔR (in pIND vector) alone or in addition to R-WT, R-6CA, R-S686A, R-S686D, R-S641A/T682A (in pNUT vector) was mixed with 22µl of FuGENE® HD reagent in sterile water and incubated for 10 min at room temperature before adding to BHK-21 cells according to manufacturer's instruction. Forty-eight hours post-transfection, adherent cells were harvested and plated at several different dilutions in selective medium that was changed every three days. Stable resistant clones were isolated after 14 days and tested for protein expression using immunoblotting. Successful co-transfection of pIND

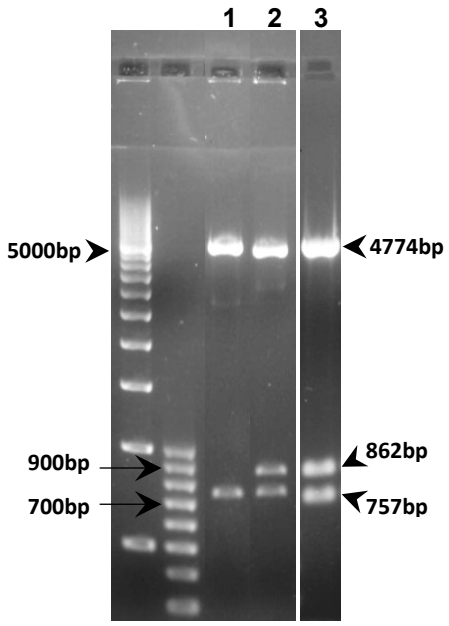


**Figure 8. Preparation of the expression vector pNUT-RDS686D.**

1% agarose gel showing migration of empty pNUT vector (lane 1), pNUT vector containing the wild-type R-region (lane 2) and pNUT vector containing the S686D R-region after site direct mutagenesis (lane 3) after digestion with NCoI, showing an extra fragments at 862bp corresponding to the presence of the R-region (lanes 2 and 3). Visualized by RedSafe staining.

and pNUT vectors into BHK cells induced the expression of three polypeptides: the front half (FH; aa 1-634), and the back half (BH; aa 837-1480) from pIND and the R-region (aa 635-836) from pNUT (see section 3.1 in Results).

### 2.5 Cell Culture

BHK cells were routinely cultured in DMEM/F12 containing 5% fetal bovine serum and 1% penicillin-streptomycin. Medium was replaced twice a week and cells were kept in a humidified incubator at 37°C with 5% CO2. G418 (400 µg/ml) and Zeocin (250 µg/ml) were used to maintain cells stably expressing the split-∆R alone (pIND vector). Cells stably co-expressing split-ΔR and wild-type or mutant R-regions (pIND + pNUT vectors) were selected using the combination of G418 (400 µg/ml), Zeocin (250 µg/ml), and Methotrexate (MTX, 500 µM). MTX is a drug that inhibits folate metabolism and is toxic to cells not expressing pNUT vector which contains a gene encoding a mutated dihydrofolate reductase (resistant to MTX) (Simonsen & Levinson, 1983; Palmiter *et al.* 1987; Chang *et al.* 1993). Expression of the R-region (from pNUT) was constitutive and expression of split-ΔR (from pIND) was induced by Ponasterone A (PA, 10 µM), added to the medium 48 h prior to experiments.

### 2.6 Immunoblotting

Cells stably expressing split-∆R, split-∆R/R-WT (SR-WT), SR-6CA, SR-S686A, SR-S686D and SR-S641A/T682A were cultured in 6-cm dishes until confluency and split-∆R was induced with 10µM PA for 48 h before harvesting. Medium was

removed, and cells were washed three times with ice-cold PBS, harvested by scrapping and subjected to 20 min centrifugation at 13,000 rpm at 4°C. Cell pellets were re-suspended in RIPA buffer (10 mM Tris-Cl, pH 7.5, 1 mM EDTA, 1% Triton X-100, 0.08% deoxycholic acid, 0.1% SDS, 150 mM NaCl) supplemented with a protease inhibitor cocktail (Thermo Fisher) and lysed on ice for 30 min. After centrifugation for 20 min at 4°C, an aliquot of the supernatant (cell lysate) was assayed for protein concentration using the Bradford method (see below). For immunoblotting, 50 µg of extracted proteins was diluted in 2x SDS (sodium dodecyl sulfate) loading buffer (100 mM Tris-HCl pH 6.8, 4% SDS, 0.2% bromophenol blue, 200 mM dithiothreitol (DTT)) and subjected to SDS polyacrylamide gel electrophoresis (SDS-PAGE) for 1.5 hr at 120 V in running buffer (25 mM Tris, 192 mM glycine, 0.1%SDS, pH 8.3). Stacking gels consisted of 5% acrylamide with 125 µM Tris-HCl pH 6.8, 0.1% SDS, 1% ammonium persulfate (APS) and 0.01% Tetramethyl ethylenediamine (TEMED). Resolving gels consisted of 7.5%, 12% or 18% acrylamide, 380 µM Tris-HCl pH 8.8, 0.1% SDS, 0.1% APS and 0.01% TEMED. Separated proteins were transferred to a nitrocellulose membrane for 2 hr at 45 V in transfer buffer (25 mM Tris, 192 mM glycine, 20% methanol, pH 8.3). The membrane was saturated/blocked in Tris-base saline (TBS; 20 mM Tris + 500 mM NaCl, pH 7.5) containing 0.1% tween20 (TBS-T) and 5% skim milk for 1 h at room temperature before incubation with the primary antibody in TBS + 0.2% BSA + 0.01% $NaN_3$ overnight at 4°C with gentle shaking.

The front half (FH) was detected using the MM13-4 monoclonal antibody, the back half was detected using the M3A7 monoclonal antibody and the R-region was detected using the MAB1660 monoclonal antibody (Figure 9). After three 15 min washes in TBS-T followed by one 15 min wash in TBS, membranes were incubated with appropriate peroxidase-conjugated secondary antibody for 2 h at room temperature in TBS + 0.5% skim milk. After five 10 min washes in TBS-T followed by one final 15 min wash in TBS, to remove excess of secondary antibodies, membranes were exposed to Clarity™ Western ECL chemiluminescence detection kit reagents for 2-5 min before exposure on BIOMAX light films (Carestream Health, Rochester, NY, USA). Films were developed in an X-ray processor. Front half and back half of CFTR appeared as a band at 62 kDa and the R-region appeared as a band at 23 kDa on films. After film exposure, membranes were stained for 5 min in amido-black to reveal total protein loaded in each well. Concentration of CFTR proteins expressed in each construct was estimated based on the ratio of the density of the bands in scanned films to the corresponding density of total protein loaded in each well, using the *ImageJ* software (National Institutes of Health; *http://rsb.info.nih.gov/ij/*).

### 2.7 Protein Assay

We used the Bradford method to estimate protein concentration in aliquots of cell lysates or in aliquots of purified recombinant R-region proteins. Concentration standards were prepared by diluting 0, 2, 5, 10 and 15 µg of BSA in dd$H_20$. A standard curve was obtained by plotting the absorbance measured by a

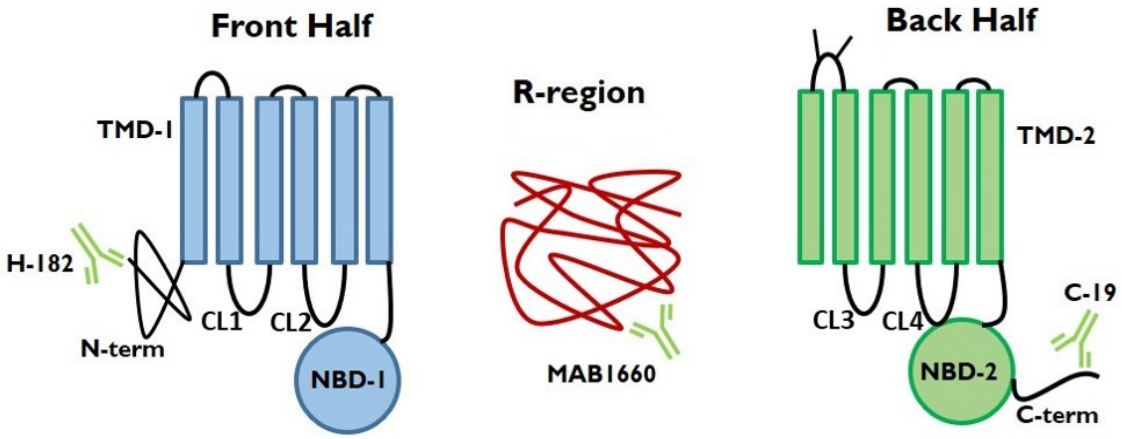


**Figure 9. SplitΔR + R-region construct**.

Cartoon representation of the Front Half, R-region and Back Half polypeptides. Rectangles represent transmembrane (TM) helices of TMD1, in blue, and TMD2, in green. Antibodies recognizing the N-terminal of the front half (H-182), the R-region (MAB1660), and the C-terminal of the back half (C-19) are represented. NBD (nucleotide binding domains), CL (cytoplasmic loops). Epitopes for each antibody are described in *Table 1*.

spectrophotometer at 595 nm for each standard versus their concentration. Extracted proteins (from BHK cells) or purified proteins (from *E. coli*) were first diluted 1/5 in dd$H_20$. 10 µL of the first dilution was diluted in 490 µL dd$H_20$ in duplicates and incubated with Bradford dye for 15 min at room temperature before absorbance measurement at 595 nm. The resulted equation from the standard curve was used to calculate protein concentration of the unknown purified/extracted proteins sample using the Protein/DNA assay software (Copyright by Frederic & Valerie Chappe).

### 2.8 FLUORESCENCE IMMUNOSTAINING

The re-assembly of the 3 CFTR domains and the correct membrane localization for the SR-S686D construct were demonstrated using immunofluorescence assays, as follows: BHK cells stably expressing the SR-S686D, were cultured on glass coverslips at low density inside 35 mm Petri dishes. Expression of the split-∆R was induced by PA (10 µM) for 48 h. The medium was removed, and cells were washed four times with PBS, then fixed with a 2% paraformaldehyde/PBS mixture for 20 min, and then permeabilized with 0.1% TritonX-100/2% BSA in PBS for 45 min at room temperature. After the removal of the permeabilization buffer, the cells were incubated overnight in 600 µl of anti-CFTR antibody (H-182 to detect the FH of CFTR or C-19 to detect the BH of CFTR) diluted in 0.1% TritonX-100/0.2% BSA at 4°C with very gentle shaking. After antibody labeling, the cells were washed three times with PBS/ 0.1% TritonX-100 for 10 min in gentle shaking, and then incubated in 600 µl of Cy3- or Alexa Fluor® 488-

conjugated goat anti-rabbit or bovine anti-goat secondary antibody, diluted in 0.1% TritonX-100/0.2% BSA, for one hour at room temperature, protected from light. Antibody excess was removed by three washes in PBS/ 0.1% TritonX-100 for 10 min each. To detect the co-localization of split-ΔR and R-region, cells were double labeled with a second primary anti-CFTR antibody, targeting the R-region (MAB1660), and a second secondary antibody (Cy3- or Alexa Fluor® 488-conjugated goat anti-mouse or goat anti-rabbit) followed by a final wash. The coverslips were removed from the dishes, then mounted on a glass microscopy slide with mounting buffer, sealed with nail polish and allowed to dry at room temperature before storage at -20°C. Slides were visualized using a Zeiss LSM 510 Confocal Microscope at the Dalhousie Cellular & Digital Imaging Facility of the Faculty of Medicine (https://medicine.dal.ca/ research-dal-med/facilities/cellular-molecular-digital-imaging.html). Negative controls were performed by either immunolabeling non-transfected cells or by omitting primary antibodies.

### 2.9 Iodide Efflux

To determine activity of the reassembled CFTR channels, measurements of iodide efflux from BHK cells were performed as follow. BHK cells were cultured to confluence in 6-well plates. After removing the culture medium and three washes with efflux buffer (136 mM $NaNO_3$, 3 mM $KNO_3$, 2 mM $Ca(NO_3)_2$, 11 mM glucose, and 20 mM HEPES; pH 7.4), the cells were incubated in 2 ml of iodide loading buffer (136 mM NaI, 3 mM $KNO_3$, 2 mM $Ca(NO_3)_2$, 11 mM glucose, and

20 mM HEPES; pH 7.4) at room temperature for 1h. Extracellular iodide was then removed and quickly replaced three times with 2 ml fresh efflux buffer. Afterwards, 1.5 ml efflux buffer was added in each well, collected and replaced with fresh efflux buffer, at 1 min intervals, over 15 min. The three first samples collected were used to establish a stable efflux baseline (time (t)=1 to 3 min). A cocktail composed of 150 µM CPT-cAMP, 1 mM IBMX and 10 µM FSK was added to the efflux buffer from t =4 min to t =15 min to stimulate CFTR. When also tested for PKC stimulation, cells were exposed to 20 nM PMA for 2 h prior to the assay (first hour PMA was added to cell culture medium; second hour PMA was added to iodide loading buffer). Control cells (basal) received efflux buffer free of stimulators during the whole assay. Iodide concentration (in nmol/ml/min) in each sample collected (t=1 min to 15 min) was measured by a computer-controlled iodide-sensitive electrode (Thermo Electron) based on a standard curve generated from known iodide concentrations and plotted versus time (Efflux Analysis Software, copyright to F. Chappe & V. Chappe). From these plots, the iodide efflux rate constant $k$ ($min^{-1}$) was calculated based on Becq et al. (2003; European working group on CFTR expression) for every minute interval. Iodide efflux peaks (maximum efflux rate obtained during stimulation) were compared after subtraction of the efflux rate measured under basal conditions of the same efflux time.

## 2.10 *IN SITU* PROXIMITY LIGATION ASSAY (PLA)

The proximity ligation assay (PLA) depends on the concurrent and specific identification of two target molecules by a pair of affinity probes each linked to a DNA aptamer, that are able to hybridize to a DNA connector and serve as template for a fluorescence-detectable rolling-circle amplification reaction, only if the two target molecules are in close proximity (≤40 nm). This way, a specific mechanism of simultaneous recognition of two different molecules is translated to amplifiable circular DNA sequences, which are easily visualized due to the hybridization of complementary fluorescence-labeled oligonucleotides (Fredriksson et al. 2002; Gullberg et al.2004; Soderberg et al. 2006) (Figure 10).

In the PLA experiments, using Duolink® PLA reagents (Sigma) following the manufacturer's instructions, interactions between the R-region and either the front or back halves of CFTR were investigated *in situ*, preserving the cytoplasmic environment for optimal interaction. BHK cells were cultured on glass coverslips at low density. The cells were then induced by PA for 48 h, and stimulated (or not), at 37°C for 2 h prior to the assay, either with a cAMP cocktail (150 μM CPT-cAMP, 1 mM IBMX and 10 μM FSK) to activate PKA, or with 20 nM PMA to activate PKC, or with a combination of PKA and PKC stimulators to activate both kinases. The culture medium was removed; then cells were washed three times with PBS and fixed with 2% paraformaldehyde for 20 min at room temperature, followed by permeabilization/ blocking in a PBS solution containing 0.1% TritonX-100/2% BSA for 45 min at room temperature.

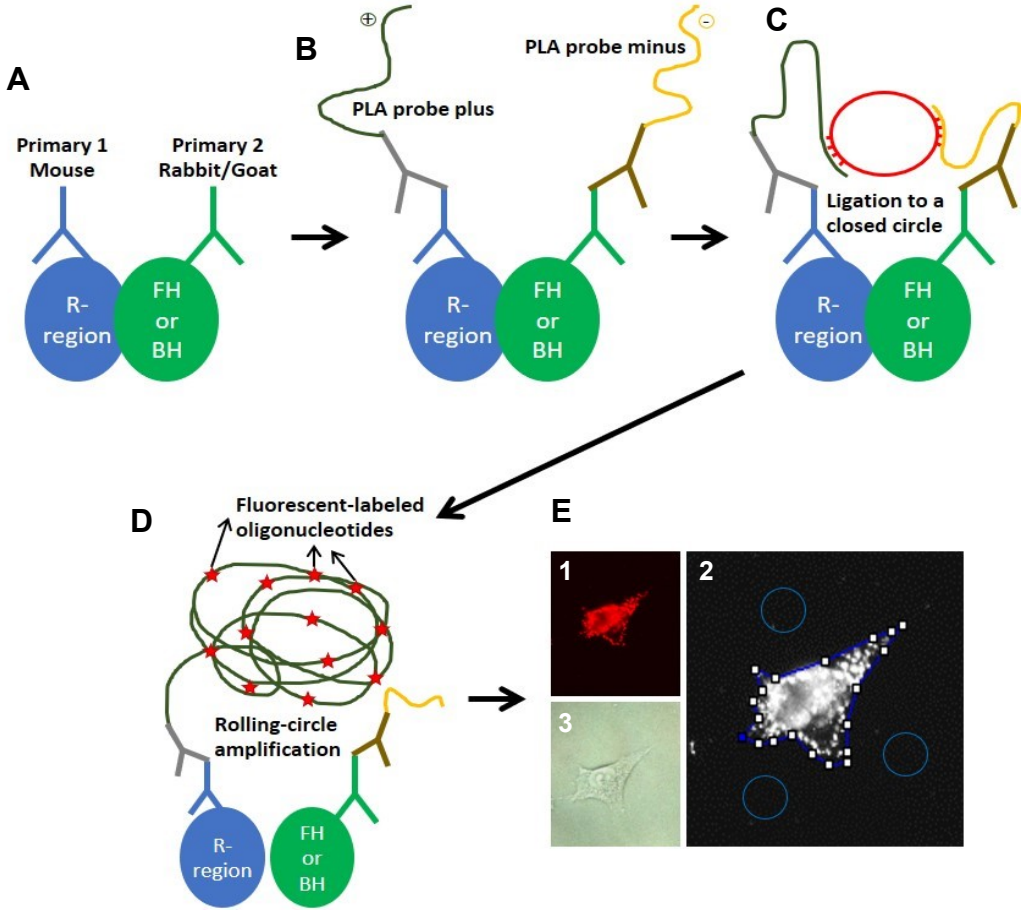


**Figure 10. Principle of the in situ proximity ligation assay.**

**A,** Samples are incubated with primary antibodies targeting the two proteins of interest. **B,** species-specific secondary antibodies conjugated to oligonucleotides (PLA probes plus and minus) are added to the reaction. **C,** a ligation solution containing oligonucleotides and ligase are added to the reaction. The oligonucleotides will hybridize with the PLA probes and form a closed circle only if the two proteins of interest are in close proximity. **D,** an amplification solution containing nucleotides and fluorescent oligonucleotides and polymerase are added to the reaction. One of the PLA probes function as a primer for a rolling-circle amplification and the ligated circular oligonucleotide from **C** serve as a template. The fluorescent oligonucleotides hybridize to the amplification product creating the PLA signal. **E,** (1) the PLA signal is easily visible as a fluorescent red spot by fluorescence microscopy. The images are converted to a gray scale and a line is drawn following the cell membrane (2) guided by the brightfield image of each cell (3), using the ImageJ software (National Institutes of Health; http://rsb.info.nih.gov/ij/)

The cells were incubated at 4°C overnight with the two primary antibodies simultaneously in PBS/0.1% Triton X-100/0.2% BSA. In PLA, the primary antibodies targeting the two proteins investigated must be raised in different host species; here, the front half was detected by the rabbit polyclonal H-182 antibody, the back half by the goat polyclonal C-19 antibody and the R-region by the mouse monoclonal MAB1660. Assays either used H-182 + MAB1660 to investigated FH-R interactions or C-19 + MAB1660 to investigated BH-R interactions. After removing the primary antibodies, the cells were washed three times with PBS/0.1% Triton X-100/0.2% BSA for 10 min, and then incubated with two PLA probes (oligonucleotide-tagged secondary antibodies) diluted 1:5 in PBS/0.1% Triton X-100/0.2% BSA for 60 min at 37°C. Each PLA probe, containing a PLUS or MINUS version of the oligonucleotide tag, recognizes a different species of primary antibody: anti-rabbit PLUS (for H-182), anti-mouse MINUS (for MAB1660) or anti-goat PLUS (for C-19). The cells were then washed twice with PLA wash buffer A and incubated with the ligation mixture for 30 min in water bath at 37°C, washed again with PLA wash buffer A, and incubated with the amplification mixture (containing fluorophore-tagged oligonucleotides that hybridize to the amplification product) for 100 min in water bath at 37°C, protected from light. After two final 10 min washes in PLA wash buffer B, the cells were mounted on a glass microscopy slide using the Duolink *in situ* mounting medium with DAPI, sealed and dried. Slides were visualized using filters 365/420 nm and 546/590 nm for DAPI and PLA orange fluorophore

visualization, respectively, in a Zeiss Axiovert II MOT Fluorescence Microscope (Dalhousie Cellular & Digital Imaging Facility of the Faculty of Medicine).
For each condition tested, a total of 110-230 cells distributed in a minimum of 8 different microscopic fields were measured in at least three independent experiments (three different cell passages) using 400x total magnification. Cell fluorescence (PLA signal) was calculated as corrected total cell fluorescence (CTFC), based on the signal intensity and the area of each cell. CTFC is used to normalize the distribution of the signal (fluorescence) inside the cell Every cell was delineated at the cell membrane, and the area,integrated density (the product of Area and Mean Gray Value) as well as three measurements of the background around each cell ) were calculated using the *ImageJ* software (National Institutes of Health; http://rsb.info.nih.gov/ij/) (Figure 10 E, image 2). CTCF was calculated as follows: CTCF = Integrated Density - (Area of selected cell x Mean fluorescence of background) (Gavet & Pines 2010; McCloy et al. 2014).

### 2.11 Generation of Recombinant R-region

The DNA sequence encoding the wild-type R-region of CFTR (aa 635-836) was synthesized and incorporated into stock pUC57-Amp vectors using BamHI 5' end and SalI 3' end cloning sites by Bio Basic (Markham, Ontario). pUC57-R-region vectors were digested with BamHI and SalI restriction enzymes for 45min at 37°C, and the fragment corresponding to the R-region (~600pb), visualized in 1% agarose gels (Figure 11 A), was extracted and purified using the GenepHlow™

Gel Extraction Kit. The R-region fragment was ligated (Ligation: 16ºC for 15min, 22ºC for 30min; using T4 DNA Ligase from New England Biolabs) into a modified version of a pET21 plasmid (pET-21(+) DNA - Novagen), containing a hexahistidine tag and the sequence encoding the B1 domain of *Streptococcal* protein G (GB1) incorporated into the multiple cloning site (kindly provided by Dr. David Langelaan, Dept. of Biochemistry & Molecular Biology, Dalhousie University) (Figure 12). GB1 is a 56-residue highly soluble and stable protein. It enhances expression levels, stability and refolding of fusion proteins and, because of its small size, it does not affect the structure of the target protein (Gronenborg & Clore, 1996; Zhou et al, 2001; Cheng & Patel, 2004). Ligation product was used to transform chemically competent DH5-α *E. coli* cells (New England Biolabs) which were plated in LB + AMP plates and left overnight at 37°C. Ten colonies were selected for PCR (initial denaturing at 94ºC for 5 min followed by 30 cycles of denaturing at 94ºC for 30s, annealing at 57°C for 30s and extension at 72°C for 1min, followed by a final extension of 7min at 72°C; using 2x Taq FroggaMix) using T7 promoter forward (TAATACGACTCA CTATAGGG) and T7 terminator reverse (GCTAGTTATTGCTCAGCGG) primers and then visualized in 1% agarose gels (Figure 11 B). Colonies showing a band at ~950 pb (~600 pb from the R-region and ~350 pb from the vector) were inoculated in LB broth + AMP overnight at 37ºC. Plasmid DNA was isolated using QIAprep Spin Miniprep Kit and DNA sequences were confirmed by sequencing. pHis-GB1-R-region (HGB1-R) vectors were transfected into Rosetta BL21(DE3) competent cells (Novagen), which contains an extra chloramphenicol-resistant

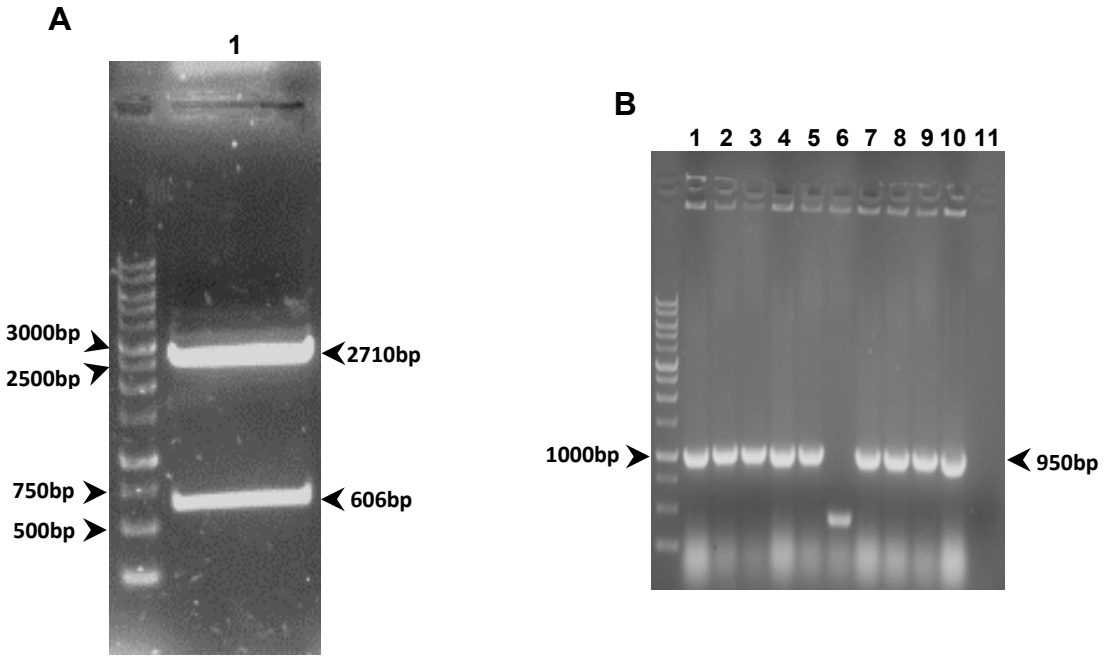


**Figure 11. Preparation of pHis-GB1-R-region vector.**

**A,** Preparation of the R-region insert. 1% agarose gel showing migration of pUC57-R-region vector, loaded in lane 1, after double digestion with BamHI and SalI, resulting in fragments at 2710bp and 606bp. The fragment at 606bp, corresponding to the R-region, was cut out of the gel and used for gel extraction and purification for subsequent ligation into pHis-GB1 vector. **B,** Ligation of R-region insert into pHis-GB1 vector. After R-region insert (from **A**) ligation into pHis-GB1 vector and transformation of DH5-α E. coli cells with the ligation product, ten colonies were selected for colony PCR and DNA amplicons from each colony were loaded in lanes 1-10 of a 1% agarose gel. Migration resulting in a fragment at ~950bp indicates the ligation of the R-region insert (606bp) into the pHis-GB1 vector (~350bp). Lane 11 was loaded with PCR mix without DH5-α cells. Visualized by RedSafe staining

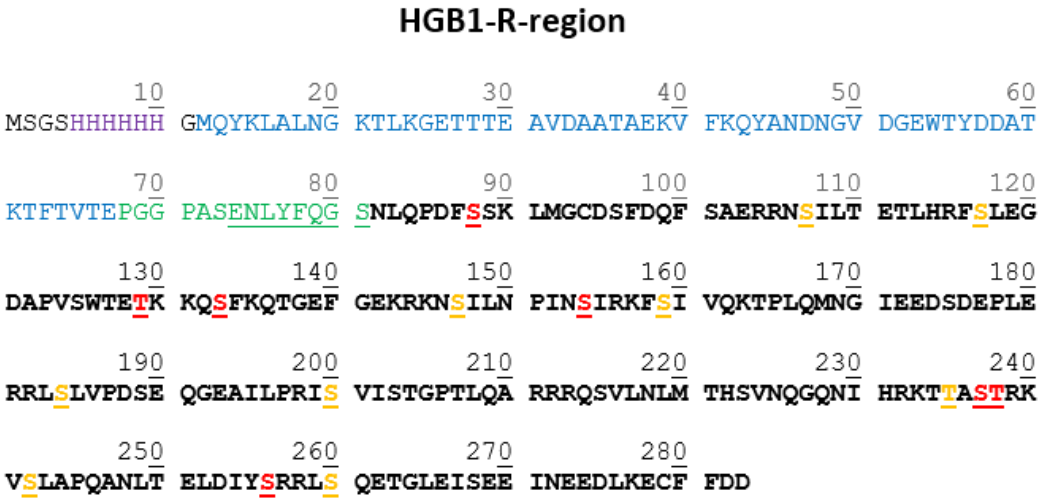


**Figure 12. Amino acid sequence of the modified pET21 plasmid.**

A pET21 b(+) plasmid (Novagen) was modified by the insertion of a hexahistidine tag (in purple), a GB1 protein (in blue), and a linker (in green) containing the TEV protease restriction site (underlined). The sequence of the R-region (aa 635-836 from the human CFTR sequence; in bold) was inserted into the plasmid multiple cloning site. PKC and PKA sites within the R-region are underlined and coloured in red and gold, respectively.

plasmid encoding extra tRNA that enhance the expression of eukaryotic proteins, and platted in LB+AMP+CAM.

### 2.12 Expression and Purification of Recombinant R-region

A single colony of Rosetta BL21 (DE3) strain harboring HGB1-R vector was used to grow a 5 ml starter culture (LB + AMP + CAM) overnight and then used to inoculate 1 L of LB + AMP + CAM). Cells were grown in a shaker (200 rpm) at 37°C until an absorbance of 0.6-0.8 (at 600 nm) was attained, followed by 4 h induction with 0.5 mM IPTG under same conditions. Bacteria were pelleted by 20 min centrifugation at 4,000 rpm and resuspended in 20 ml of denaturing lysis buffer (20 mM Tris-HCl pH 8.0, 250 mM NaCl, 8 M urea). After sonication, bacteria were centrifuged at 14,500 rpm for 20 min and the supernatant was loaded into a column containing 5 ml of immobilized metal affinity chromatography (IMAC) medium (GE healthcare) that was pre-charged with $Ni^{2+}$ ions and pre-equilibrated with lysis buffer. The column was then washed with lysis buffer containing 5 mM imidazole and the fusion protein was eluted by lysis buffer containing 300 mM imidazole and 5 mM BME. The choice for denaturing conditions during purification was due to the poor yield of fusion protein when native buffers (without the addition of 8 M urea) were used. Protein expression and purification yield were verified by 12% SDS-PAGE stained with Coomassie brilliant blue. Unfolding of the R-region fusion protein was performed by overnight dialysis against a 10 mM HCl solution containing 5 mM BME. Dialysis product was concentrated using AMICON centrifugal filters (MWCO 10 kDa) to a final

volume of 1 mL. 2 mM of DTT was added to the concentrated protein before the pH was adjusted to 7.5-8.0 using tris-base pH 11.0. Protein concentration was measured using the Bradford method.

An empty HGB1 vector was expressed in BL21 cells and purified using the same protocol as the fusion R-region protein with the difference being the use of native buffers (without 8 M urea). Protein expression and purification yield of the empty vector was verified by 18% SDS-PAGE stained with Coomassie brilliant blue. This construct was used as a negative control for protein-protein interaction experiments (see below).

### 2.13 Phosphorylation of recombinant R-region

Phosphorylation of the concentrated purified fusion R-region was performed by adding 100 nM PKA + 2 mM $Mg^{+2}$-ATP, for PKA phosphorylation; by adding 2 mM $Mg^{+2}$-ATP + 5 nM PKC + PKC lipid activator for PKC phosphorylation; or by adding 100 nM PKA + 2 mM $Mg^{+2}$-ATP + 5 nM PKC + PKC lipid activator for PKA + PKC phosphorylation, followed by 2 h incubation at 30°C. To verify the phosphorylation status of the R-region, aliquots (1.25 µg) were loaded into 12% SDS-PAGE and stained with Coomassie brilliant blue or Pro-Q diamond phosphoprotein gel stain. For Coomassie stain, gels were incubated in 0.1% Coomassie brilliant blue + 50% methanol + 10% glacial acetic acid for 40 min and destained overnight in 40% methanol + 10% glacial acetic acid. For the selective phosphoprotein gel stain, gels were fix in 50% methanol + 10% glacial acetic acid for 1 h, followed by three washes in ultrapure water for 10 min each

before incubation in Pro-Q diamond phosphoprotein gel stain for 90 min protected from light. Gels were then destained in 20% acetonitrile + 50 mM sodium acetate, pH 4.0 followed by two washes of 5 min in ultrapure water. Bands were imaged using the VersaDoc 4000 MP system with Quantity one software using the Cy3 filter and quantified using the ImageJ software (National Institutes of Health; *http://rsb.info.nih.gov/ij/*).

### 2.14 Proteomic Analysis of HGB1-R-region

To verify the phosphorylation status of the R-region, aliquots of purified fusion R-region that were left untreated or after PKA, PKC, PKA + PKC treatment were separated in 12% SDS-PAGE and stained with Coomassie brilliant blue and bands corresponding to the R-region fusion protein were sent to the Dalhousie Biological Mass Spectrometry Core Facility of the Faculty of Medicine.
The excised gel slices, stained with Coomassie brilliant blue, were processed for LC-MS/MS as previously described (Shevchenko et al., 2007), with minor modifications. Briefly, gel slices were rinsed for two hours in water and then cut into ~1 mm cubes and rinsed twice with 200 µL of $dH_2O$. Gel cubes were reduced with 10 mM dithiothreitol (DTT) at 56°C for 30 minutes, alkylated with 55 mM iodoacetamide for 30 minutes at room temperature in the dark, and dehydrated with 200 µL ACN. Dried gel cubes were saturated with 20 µg/mL of trypsin protease (Pierce Thermo Scientific) for 2 hours, then 20 µL of 50 mM ammonium bicarbonate was added and the samples were incubated overnight at 37°C. Digested peptides were extracted from the gel cubes on a gentle vortex

shaker using 100 µL of 50% ACN in 5% formic acid. The samples were finally dried to a pellet in a vacuum centrifuge and subsequently resuspended in 20 µL of a 3% ACN, 0.5% formic acid solution. The samples were transferred to a 300 µL HPLC vial and subject to analysis by LC-MS/MS on a VelosPRO orbitrap mass spectrometer (ThermoFisher Scientific) equipped with an UltiMate 3000 Nano-LC system (ThermoFisher Scientific). Chromatographic separation of the digests was performed on PicoFRIT C18 self-packed 75 µM x 60 cm capillary column (New Objective, Woburn, MA) at a flow rate of 300 nl/min. MS and MS/MS data was acquired using a data-dependent acquisition method in which a full scan was obtained at a resolution of 30,000, followed by ten consecutive MS/MS spectra in both higher-energy collisional dissociation (HCD) and collision-induced dissociation (CID) mode (normalized collision energy 36%). Internal calibration was performed using the ion signal of polysiloxane at m/z 445.120025 as a lock mass. Raw MS data were analyzed using Proteome Discoverer 2.2 (ThermoFisher Scientific). Peak lists were searched against the human CFTR database (UniProtKB - P13569) as well as the E. coli BL21 database and cRAP database of common contaminants (Global Proteome Machine Organization). Cysteine carbamidomethylation was set as a fixed modification, while methionine (Met) oxidation, N-terminal Met loss, and phosphorylation on serine, threonine, and tyrosine were included as variable modifications. A mass accuracy tolerance of 5 ppm was used for precursor ions, while 0.02 Da for HCD fragmentation or 0.6 Da for CID fragmentation was used for product ions. Percolator was used to determine confident peptide identifications using a 0.1% false discovery rate

(FDR). Site-specific determination of phosphorylated amino acids was confirmed using PhosphoRS (ThermoFisher Scientific) (Taus et al, 2011).

### 2.15 MICROSCALE THERMOPHORESIS (MST)

Thermophoresis is the directed movement of molecules induced by thermal gradients. This physical phenomenon strongly depends on molecular properties such as size, charge, hydration shell and conformation. After interaction of two molecules, one or more of those parameters is altered, modifying the movement of the molecule through the thermal gradient. In MST experiments an infrared laser creates the thermal gradient and the molecules movement through the gradient are detected and quantified by fluorophores attached to one of the binding partners (Seidel et al. 2013; Jerabek-Willemsen et al. 2014; Schubert & Längst, 2015) (Figure 13).

In our MST experiments we used six 5-carboxyfluorescein (5-FAM)-fluorescent-tagged CFTR polypeptides (N-terminal lasso motif, cytoplasmic loops 1-4 and C-terminal tail; see table 3) to measure protein-protein interaction with the recombinant R-region. CFTR polypeptides were diluted in MST buffer (50 mM Tris-HCl pH 7.4, 150 mM NaCl, 10 mM $MgCl_2$, 0.05% Tween-20) to a stock concentration of 2μM. Purified fusion R-region was phosphorylated by PKA or PKA + PKC or left untreated (basal control). A 350 μM stock concentration of purified fusion R-region (basal, PKA or PKA + PKC) was titrated 3/1 into 12 tubes using 50 mM Tris-HCl pH 8 + 2 mM DTT. 5-FAM-CFTR polypeptides were added to each tube to a final concentration of 150 nM followed by a 10 min incubation at

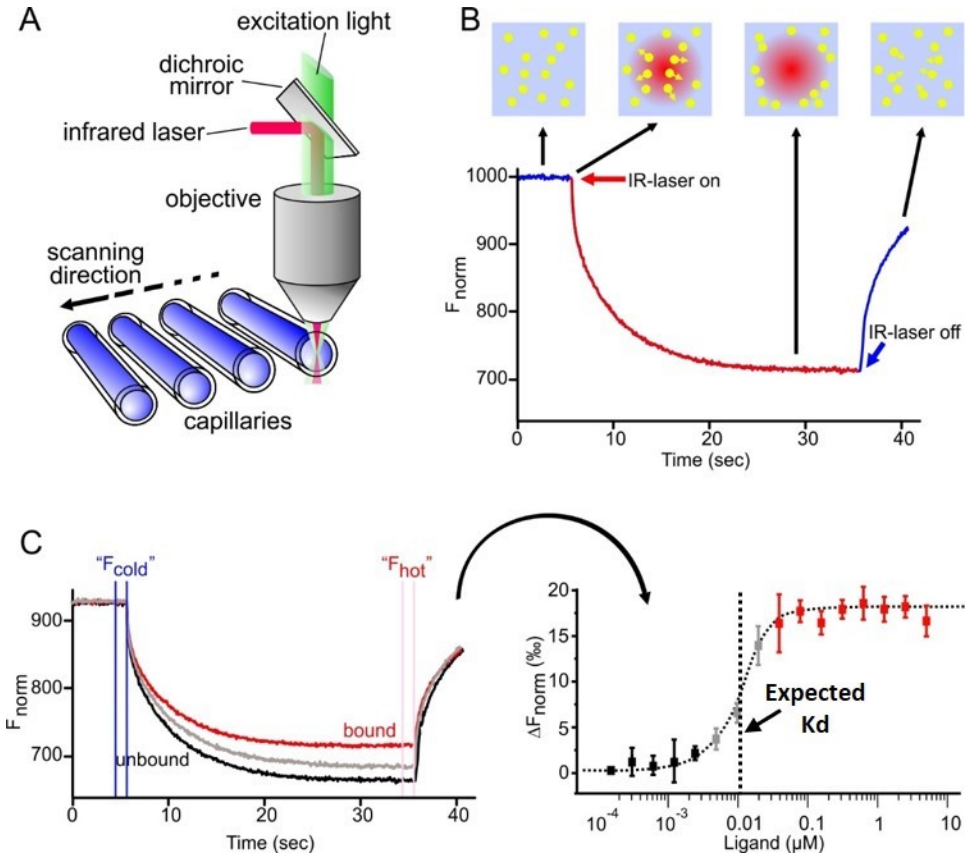


**Figure 13. Microscale Thermophoresis technical setup.**

(**A**) In thin glass capillaries, the movement of the optically visible interaction partner through temperature gradients, induced by an infrared laser, is monitored by optically focusing the centre of the capillary. (**B**) MST time trace - a profile depicting the movement of molecules in a temperature gradient. After 5 sec of cold phase (laser off), the laser is switched on and establishes the temperature gradient. After the initial T-Jump phase, in which heat induction results in the decrease of fluorescent dye signal yield, the thermophoretic movement takes place. The laser is turned off again after 30 sec and the molecules diffuse back into the observation window. (**C**) Results of a typical MST experiment: 12-16 capillaries containing a low nanomolar concentration of a fluorescent interaction partner and increasing concentrations of an unlabelled ligand. The MST profiles are recorded over time (three of the MST traces are shown in the graph on the left side). The normalized fluorescence of all MST traces is plotted against the concentration of the ligand (graph on the right). Data points were fitted to obtain binding parameters such as the binding affinity (black - unbound; grey - partially bound; red - fully bound state). Reproduced from Studying epigenetic interactions using MicroScale Thermophoresis (MST) by Schubert T & Langst G (2015), licensed under CC BY 4.0. Minor modifications made.

room temperature protected from light and loaded into monolith NT.115 standard capillaries. MST experiments were performed in a Monolith NT.115 system using the MO.Control software (NanoTemper Technologies).

Samples were exposed to an infra-red laser at 'high' power and excited with a green LED-filter (at 60% power) and thermophoresis of fluorescent signals measured during 20 sec. Affinity curves with dissociation constant (Kd) values were obtained by plotting MST raw data into the MO.Affinity Analysis software (NanoTemper Technologies). The Kd values were derived from monitoring the target's (CFTR polypeptides) MST signals over a dilution series of the ligand (R-region). The ligand concentration where 50% of the target is bound is the Kd value. Because the GB1 was used as a fusion partner to compensate for solubility issues of the R-region, MST experiments following the same conditions as described above, were performed using the GB1 protein (expressed from empty HGB1 vector) as the binding partner to the six CFTR polypeptides to verify for any unspecific interaction.

### 2.16 STATISTICAL ANALYSIS

Results are reported as the mean ± SEM with N=number of independent experiments. When comparing multiple values, differences were assessed using one-way ANOVA, followed by Dunnett's or Tukey's post test corrections for multiple comparisons. When comparing two groups, differences were assessed using Student's *t* test. For all comparisons, a value of $p<0.05$ was considered significant.

# CHAPTER 3: RESULTS

## 3.1 Co-expression and Co-localization of Split-ΔR and wild-type or mutant R-regions

Previous works have used split-CFTR constructs for biochemical and functional studies. Several studies have tested the functional and physical association of split-CFTR channels and demonstrated that such channels display the typical features of full-length CFTR, which includes phosphorylation and ATP-dependence for gating, slow channel conductance, and open-locked state by use of non-hydrolysable AMP analogs (Ostedgaard et al. 1997; Chan et al. 2000; Csanady et al. 2000; Chappe et al. 2005; Seavilleklein et al. 2008). Our lab has previously demonstrated that split-ΔR constructs lacking the R-region (aa 1-634 + aa 837-1480) form constitutively active channels that acquire the ability to respond to PKA when co-expressed with the R-region (aa 635-836). Moreover, PKA was shown to increase the interaction of the phosphorylated R-region to both halves of split-ΔR CFTR (Chappe et al. 2005). For my thesis work, I used the same split-CFTR constructs, expressing the CFTR protein as 3 separated polypeptides (front half (FH), back half (BH), and R-region) to pursue further insights on the phosphorylation-induced inter-domain interactions within CFTR, with focus on the R-region dynamics.

Because a mutant R-region construct lacking all seven PKC consensus phosphorylation sites (R-7CA) had its ability to interact with split-ΔR after phosphorylation dramatically reduced (Seavilleklein et al. 2008), here, I decided

to use four R-region constructs (R-6CA, R-S641A/T682A, R-S686A and R-S686D) containing different combinations of PKC site mutations to investigate the roles of specific PKC consensus sites in phosphorylation-dependent R-region interactions with other parts of the channel. The selection of PKC sites for this study was based on the functional effects of mutations at PKC sites revealed by patch-clamp studies of full-length CFTR (Chappe et al. 2004). Mutations S641A and T682A generated highly responsive channels, hence identifying them as inhibitory sites or gain-of-function mutations. Conversely, mutation S686A generated low responsive channels, hence identifying it as a stimulatory site or a loss-of-function mutation (Chappe et al. 2004). In order to further explore the role of the PKC site S686, a construct where S686 is the only active PKC site (R-6CA) and a construct where a phosphomimetic substitution at S686 was applied (R-S686D) were used in my analysis.

Expression of the three CFTR fragments was determined by immunoblotting of cell lysates stably co-expressing split-ΔR with either WT (split-ΔR/R-WT; hereafter SR-WT) or mutated R-regions (R-6CA, R-S641A/T682A, R-S686A or R-S686D) using antibodies recognizing each of the three polypeptides. Front and back halves of CFTR were detected in blotting membranes as a ~62kDa band by MM13-4 and M3A7 antibodies, respectively. A ~23kDa band was observed when membranes were exposed to the R-region specific antibody MAB1660.

All antibodies used to detect the expression of the front and back halves or R-region of CFTR were tested in lysates of non-transfected BHK cells (BHK-21) (Figure 14 A, far right row in each blot) for specificity. MAB1660, the antibody

detecting the R-region of CFTR is not phospho-sensitive as it was able to recognize the unphosphorylated and phosphorylated versions of the R-region similarly (Seavilleklein et al, 2008)

Although expression of mutant R-regions was similar to the WT polypeptide, the FH expression in SR-S641A/T682A was lower (69% of WT; $p<0.05$) (Figure 14 B).

Following proof of expression of the three polypeptides in BHK cells, the next step was to determine if split-ΔR and R-region can reassemble and co-localize at the cell periphery. Detection of the wild-type and mutant R-regions (SR-6CA, SR-S641A/T682A and SR-S686A) in BHK cells as well as their co-localization with the split-ΔR were previously demonstrated using fluorescence immunolabelling with specific monoclonal antibodies followed by confocal microscopy visualization (Chappe et al, 2005; Amer, 2010). Here, a similar approach was used, immunolabelling the 3 CFTR polypeptides to demonstrate the successful re-assembly in the SR-S686D construct. This was confirmed by double labeling the R-region + FH (using H-182 antibody for the FH and MAB1660 antibody for the R-region) or the R-region + BH (using C-19 antibody for the BH and MAB1660 antibody for the R-region) followed by visualization of overlapping signals near the cell surface by confocal microscopy. Probing non-transfected BHK cells or omitting the two primary antibodies in SR-S686D showed no signal, confirming labeling specificity (Figure 15).

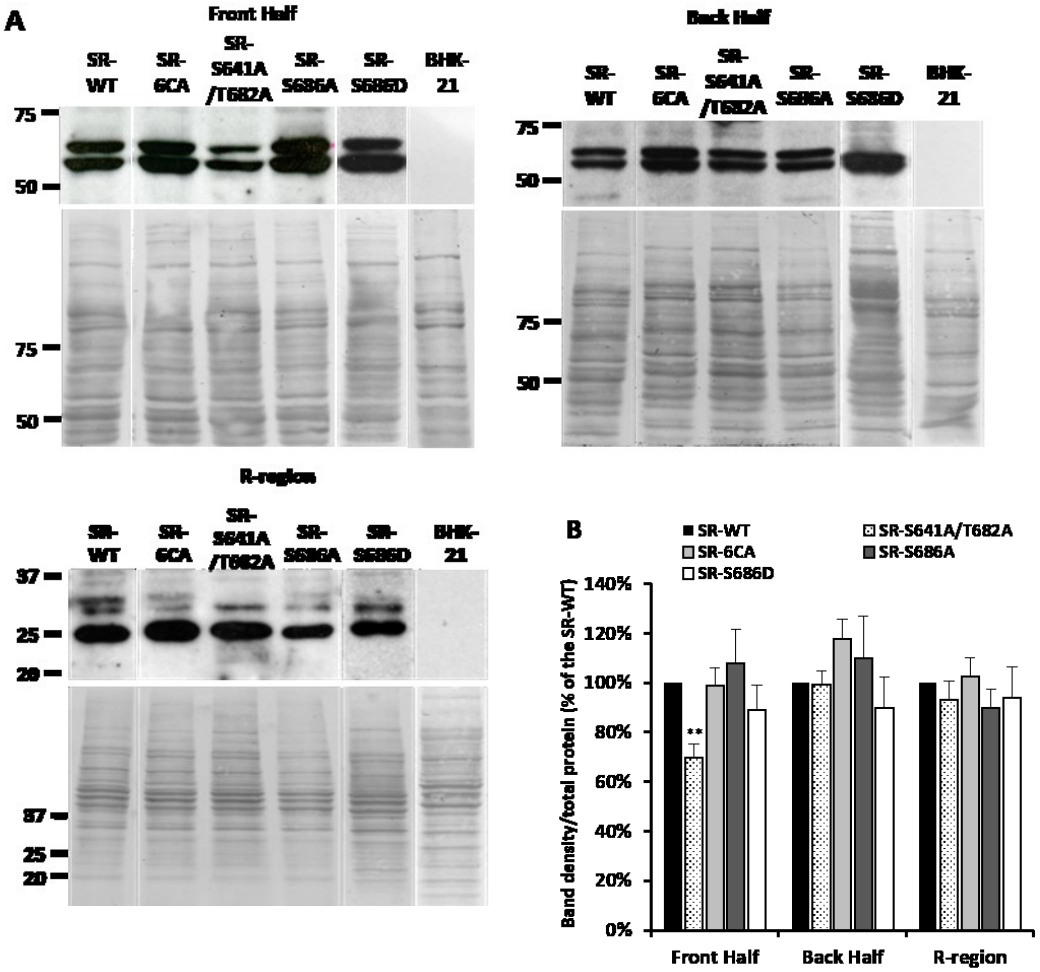


**Figure 14. Expression of the Split-CFTR front half, back half and R-region Polypeptides in BHK cells.**

**A,** Representative Western blots showing Split-CFTR front half (FH), back half (BH) and R-region in cells expressing SR-WT, SR-6CA, SR-S641A/T682A, SR-S686A and SR-S686D, detected with MM13-4 (FH), M3A7 (BH), or MAB1660 (R-region) monoclonal antibodies. Non-transfected BHK cells (BKH-21) probed with each of the antibodies are shown in the far right for each blot. ***B,*** Histogram representing averages of expression levels measured by band density. Band densities were normalized based on the total protein loaded in each well, measured after membrane staining with amido-black (shown below each blot). All densities were measured using the ImageJ software (National Institutes of Health; http://rsb.info.nih.gov/ij/). Levels for each mutant construct are expressed as a percentage of that for the wild-type. Values are means ± SEM for 3 independent experiments; *p<0.05.

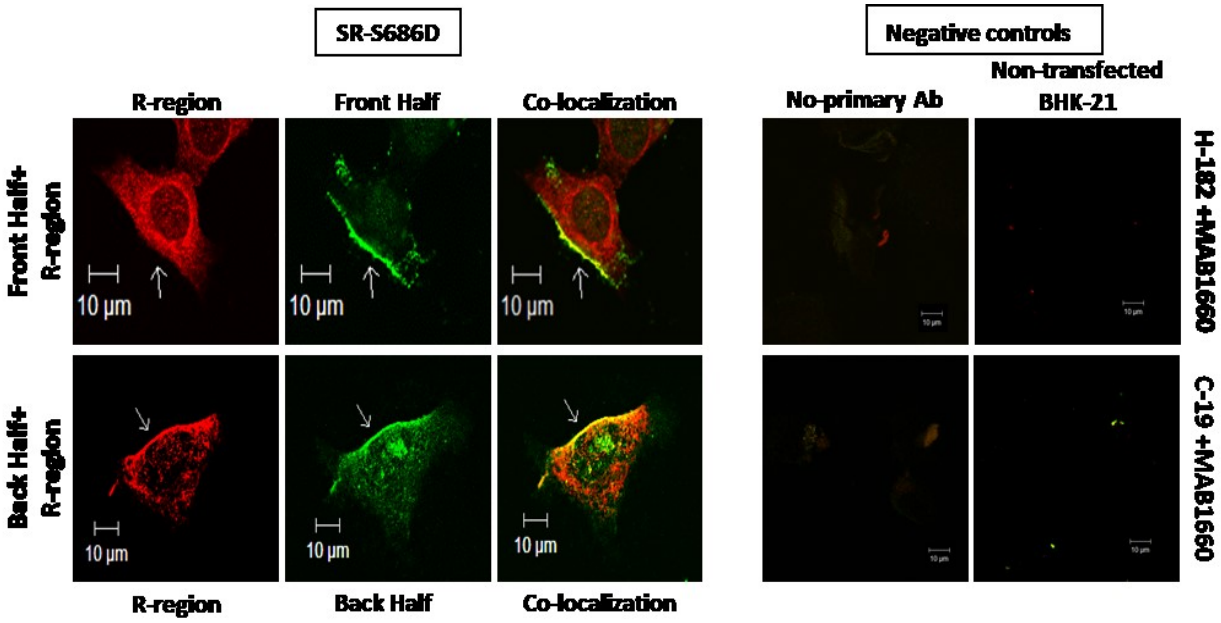


**Figure 15. Co-localization of Split-CFTR FH, BH and R-region Polypeptides in BHK cells expressing SR-S686D.**

Left panel, representative confocal microscopy images of BHK cells co-expressing the split-CFTR front half (FH) or back half (BH) in green and the S686D-R-region in red. Upper row shows FH and R-region labeling and bottom row show BH and R-region labeling, with membrane co-localization, in yellow, indicated by arrows. FH, BH and R-region were detected by H-182 (1:1000), C-19 (1:500) and MAB1660 (1:500) antibodies, respectively. Right panel, negative controls images where primary antibodies were omitted or where non-transfected BHK cells were probed.

### 3.2 Co-expressed Split-ΔR and Mutant R-regions Produce Active Channels

After confirmation of expression and membrane localization of the two halves plus the R-region polypeptides in BHK cells, I investigated the activity of re-assembled CFTR channels by performing iodide efflux assays using confluent monolayers of BHK cells that stably express WT or mutant constructs. The use of nonradioactive iodide efflux assays to measure ion flow from CFTR channels is a fast and convenient method to access real time ion movement from large groups of cells and has the ability to sense the effect of channel modulators (Hyde et al. 1993; Chang et al, 1993; Long & Walsh, 1997). Thus, this assay is suitable to test the functional viability of the split-CFTR channel constructs studied here. Iodide ions serve as a tracer for chloride and are easily detected by an iodide-specific electrode. In my assay, iodide ions flowing outside the cells were traced for 15 minutes with aliquots collected every minute for iodide concentration measurement (*see section 2.9 in Materials and Methods*).

Iodide efflux traces for SR-WT are shown in Figure 15 B with iodide efflux peaks induced by PKA and PKC + PKA stimulation indicated by arrows. As expected, because of the presence of the R-region, an increase in the iodide efflux rate was measured after cAMP cocktail stimulation (PKA agonists) and a further increase was observed when cells were pre-treated with PMA (PKC agonist) 2 h prior to cAMP stimulation ($0.33 \pm 0.03$ to $0.60 \pm 0.10$ $min^{-1}$, $p<0.01$). Iodide efflux rate peaks in response to PKA and PKC + PKA in SR-WT were used to compare with the ones observed in mutant constructs. To confirm that responses to PKA and PKC agonists are dependent on the presence of the R-region, I performed iodide

effluxes using the same conditions as used for SR-WT in split-ΔR cells, which lack the R-region, and responses to PKA or PKC + PKA phosphorylation were abolished (Figure 16 A). Iodide efflux traces for each mutant at basal or after PKA or PKC + PKA stimulations are shown in Figures 16 C-F. No significant peaks were observed in any of the mutants at basal conditions. However, baseline levels of iodide release from SR-S686D were significantly higher than any other construct (0.23 ± 0.03 $min^{-1}$ for SR-S686D compared to 0.11 ± 0.01 $min^{-1}$ for SR-WT; 0.10 ± 0.01 $min^{-1}$ for SR-6CA; 0.13 ± 0.01 $min^{-1}$ for SR-S641A/T682A; 0.09 ± 0.02 $min^{-1}$ for SR-S686A, $p<0.001$ for all constructs), indicating that this mutation disturbs the inhibitory role of the unphosphorylated R-region, creating a constitutive activity for this mutant channel (Figure 17 A and B).

As described in section 2.9 in Material and Methods, in order to reflect only the effect of phosphorylation on CFTR channels' activity, the basal values shown above for each construct were subtracted from the values obtained after cAMP and PMA + cAMP stimulations, which are discussed next.

All mutant constructs were functional with respect to stimulation by the cAMP cocktail (Figure 16 G). SR-6CA, SR- S641A/T682A and SR-S686A displayed iodide efflux peaks similar to SR-WT. SR-S686D peak was two-fold higher than other constructs (0.60 ± 0.17 for SR-S686D compared to 0.33 ± 0.03 $min^{-1}$ for SR-WT, $p<0.01$; 0.40 ± 0.04 $min^{-1}$ for SR-6CA, $p<0.05$; 0.26 ± 0.05 $min^{-1}$ for SR-S641A/T682A, $p<0.05$; 0.26 ± 0.04 $min^{-1}$ for SR-S686A, $p<0.01$). These results

indicate that none of the mutated sites are essential for PKA-dependent activation of CFTR (Figure 16 C-F and white bars at Figure 16 G).

In cells pre-treated with PMA before cAMP stimulation, a further increase in iodide efflux peaks was observed in SR-6CA (0.40±0.04 $min^{-1}$ for cAMP to 0.53±0.04 $min^{-1}$ for PMA + cAMP, $p<0.05$) (Figure 16 C and 16 G) and SR-S641A/T682A (0.26 ± 0.05 $min^{-1}$ for cAMP to 0.41 ± 0.07 $min^{-1}$ for PMA + cAMP, $p<0.05$) (Figure 16 D and 16 G). SR-S686A did not respond to PMA pre-treatment, indicating that the PKC enhancing effect is lost in the absence of serine 686 (0.26 ± 0.04 $min^{-1}$ for cAMP to 0.25 ± 0.03 $min^{-1}$ for PMA + cAMP; $p>0.4$) (Figure 16 E and 16 G). Cells expressing SR-S686D also did not respond to PMA pre-treatment (0.60 ± 0.17 $min^{-1}$ for cAMP to 0.69 ± 0.22 $min^{-1}$ for PMA + cAMP) (Figure 16 F and 16 G). However, because stimulation with cAMP alone induced very high iodide efflux peaks in SR-S686D, which were equivalent to those observed in SR-WT cells after PMA + cAMP treatment (0.60 ± 0.17 $min^{-1}$ for S686D after cAMP and 0.60 ± 0.10 $min^{-1}$ for SR-WT after PMA + cAMP; $p>0.5$) (Figure 16 G), The conclusion is that the phosphomimetic mutation introduced at this site yields a constitutive enhancing effect where maximal efflux levels are achieved without the need of PKC as well as a mild basal (i.e. constitutive) activity of CFTR.

Taken together these data indicate that all re-assembled SR-CFTR channels are functional (responsive to PKA) and consensus PKC site S686 is required for the enhancing effect of PKC, further confirming the critical role of S686 in the

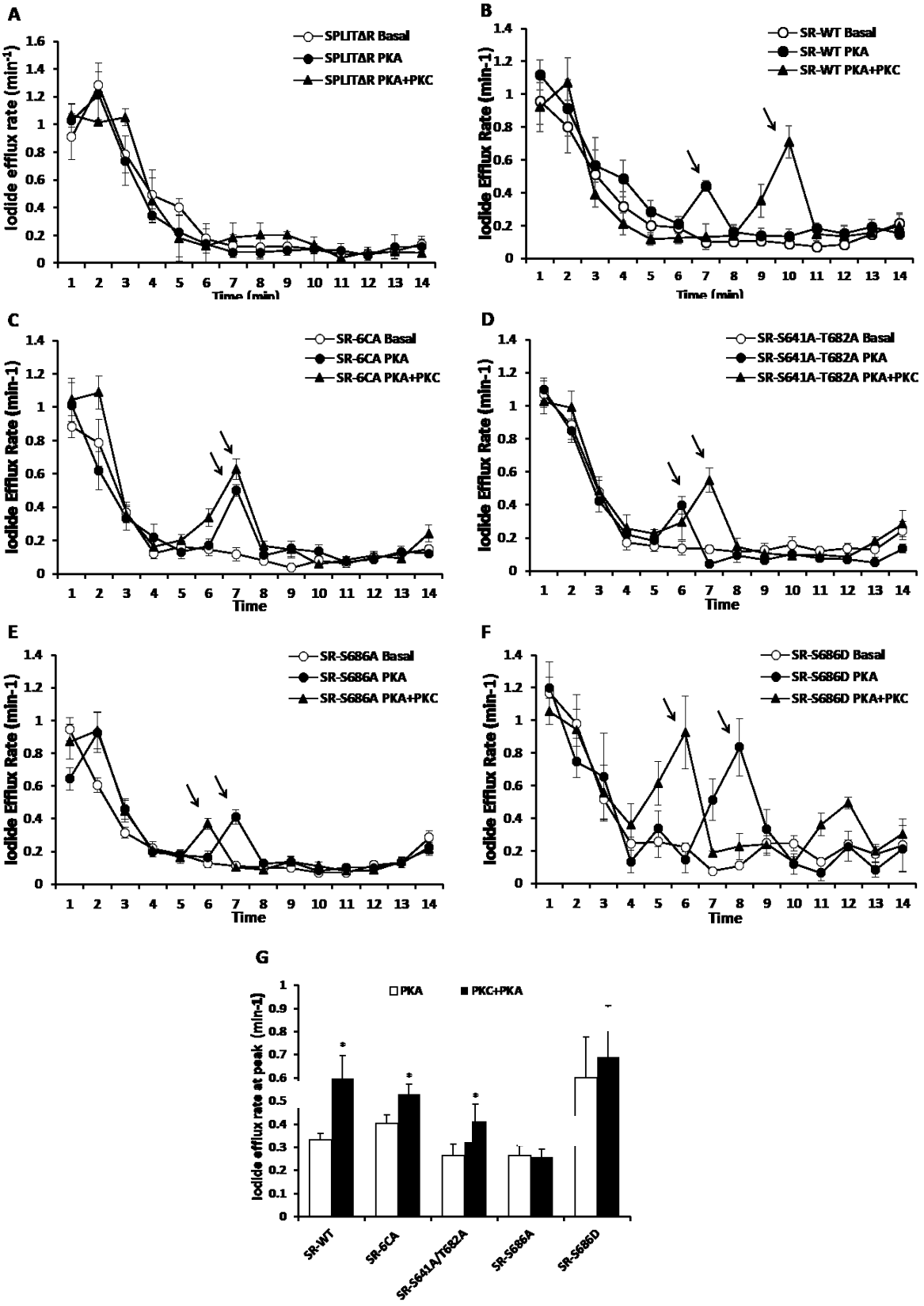
A
SPLITΔR Basal
SPLITΔR PKA
SPLITΔR PKA+PKC
Iodide efflux rate (min-1)
Time (min)
B
SR-WT Basal
SR-WT PKA
SR-WT PKA+PKC
Iodide Efflux Rate (min-1)
Time (min)
C
SR-6CA Basal
SR-6CA PKA
SR-6CA PKA+PKC
Iodide Efflux Rate (min-1)
Time
D
SR-S641A-T682A Basal
SR-S641A-T682A PKA
SR-S641A-T682A PKA+PKC
Iodide Efflux Rate (min-1)
Time
E
SR-S686A Basal
SR-S686A PKA
SR-S686A PKA+PKC
Iodide Efflux Rate (min-1)
Time
F
SR-S686D Basal
SR-S686D PKA
SR-S686D PKA+PKC
Iodide Efflux Rate (min-1)
Time
G
PKA
PKC+PKA
Iodide efflux rate at peak (min-1)
SR-WT
SR-6CA
SR-S641A/T682A
SR-S686A
SR-S686D

**Figure 16. Basal and phosphorylation-induced activity of SplitΔR/R constructs.**

Iodide effluxes were measured from BHK cell monolayers induced with 10μM ponasterone A (PA) for 48h. **A,** Iodide efflux from cells expressing SplitΔR in the absence of the R-region. No peaks were observed after addition of PKA (150μM CPT-cAMP, 1mM IBMX and 10μM FSK, dark circles) or PKA+PKC (150μM CPT-cAMP, 1mM IBMX ,10μM FSK and 20nM PMA, dark triangles) stimulants starting at time t=4min. Peaks indicating the effect of PKA stimulation (dark circles) or PKC+PKA stimulation (dark triangles) added from time t=4min on iodide effluxes from cells expressing SR-WT (**B**), SR-6CA (**C**), SR-S641A/T682A (**D**), SR-S686A (**E**) and SR-S686D (**F**) are indicated by arrows. No peak was observed in cells left untreated (basal activity, open circles). **G**, average iodide efflux rates at peak (efflux rate at peak - efflux rate at basal at the time of the peak; *see section 2.9 in materials and methods*) after PKA (white bars) and PKC + PKA (black bars) stimulations for each of the constructs displayed in A-F**.** Significance (*$p<0.05$) was calculated between PKC + PKA and PKA stimulations for each construct. Values are means ± SEM of a minimum of 4 independent experiments performed in duplicate.

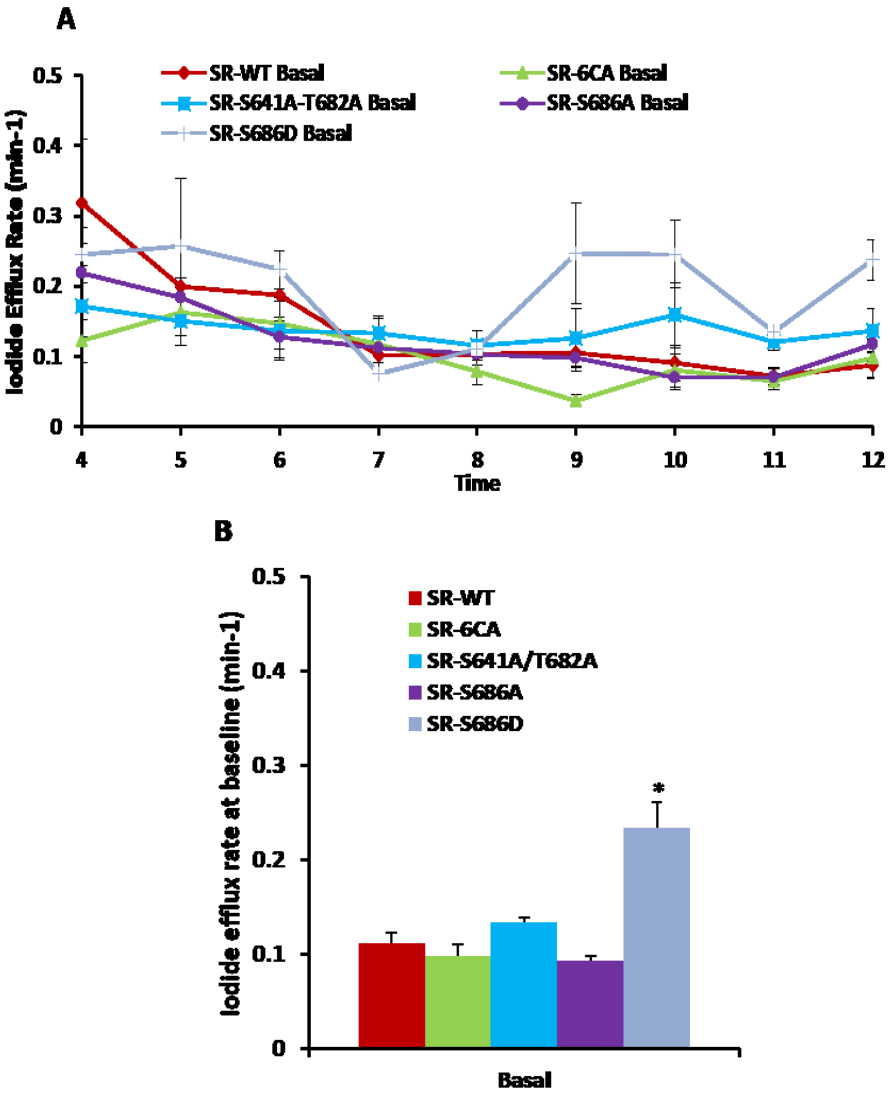


**Figure 17. Iodide efflux rates at basal conditions.**

Iodide effluxes were measured from BHK cell monolayers, after induction with 10μM ponasterone A (PA) for 48h, at 1 min intervals**. A,** iodide efflux traces from unstimulated cells (basal conditions) expressing SR-WT, or SR-6CA, or SR-S641A/T682A, or SR-S686A or SR-S686D. **B**, Histogram representing the average of iodide efflux rates measured from time t=4min (after stable baseline was achieved) to t=12min (before cells start to rupture) for each of the constructs displayed in **A.** Significance (*p<0.001) was calculated in relation to values measured in SR-WT. Values are means ± SEM of a minimum of 4 independent experiments performed in duplicate.

channel regulation as reported previously with full-length CFTR channels (Chappe et al. 2004).

### 3.3 Phosphorylation Changes R-region Association with Both Halves of CFTR

After confirming that all mutant constructs can assemble into functional CFTR channels at the cell membrane, interaction of the R-region with both CFTR halves was assessed by *in situ* proximity ligation assay (PLA). For each assay, two primary antibodies, raised in different species, either targeting FH+R-region or BH+R-region must recognize their specific target simultaneously. If targets recognized by the two primary antibodies are localized within 40 nm distance (close proximity), two unique complementary DNA strands attached to the secondary antibodies will be able to hybridize, circularize and serve as primers for a rolling circle amplification (PCR reaction) that uses fluorophore-tagged oligonucleotides which generate the PLA signal. This way, concurrent binding of two antibodies to two very close epitopes can be translated to an amplified fluorescence signal that can be easily visualized by fluorescence microscopy. Fluorescence can be semi-quantified using ImageJ software (*see section 2.10 in Material & Methods for details*). Antibodies H-182 and C-19 detected the front and back halves of CFTR at the cell surface of BHK cells expressing SR-WT. No signal was observed in the absence of primary antibodies or in non-transfected BHK cells (BHK-21), showing their specificity (Figure 18 E and F). Detection of front and back halves by H-182 and C-19 was not affected by phosphorylation (Figure 18 A - D).

First, PLA signals were imaged in BHK cells stably expressing SR-WT stimulated with either cAMP cocktail, or PMA, or PMA + cAMP cocktail or left untreated (basal conditions) (Figure 19 A, B). At basal conditions, the unphosphorylated R-region showed the same level of interaction, measured by corrected total cell fluorescence (CTCF), with both CFTR halves. The R-region interaction with the FH (FH-R) significantly increased by 45% from basal conditions after cell stimulation with cAMP cocktail (CTCF = 3.90 ± 0.18 at basal and 5.67 ± 0.55 after cAMP; $p<0.01$) and further increased to 7.91 ± 0.21 ($p<0.0001$) after PMA + cAMP cocktail stimulation. Stimulation with PMA alone did not affect FH-R interaction, which remained similar to basal conditions (Figure 19 A, C). The R-region interaction with the BH (BH-R) was enhanced by 42% when the cells were stimulated by the cAMP cocktail (CTCF = 3.41 ± 0.20 at basal and 4.82 ± 0.39 after cAMP stimulation; $p<0.01$). No changes in BH-R interaction was observed after PMA or PMA + cAMP cocktail treatments (Figure 19 B, C).

These results indicate that PKA phosphorylation, which supports CFTR function, induces stronger interactions of the R-region with both halves of the CFTR channel. Interestingly, maximal activation of CFTR, which is induced by PKC + PKA stimulation, promotes a very strong interaction of the R-region with the front half of CFTR only.

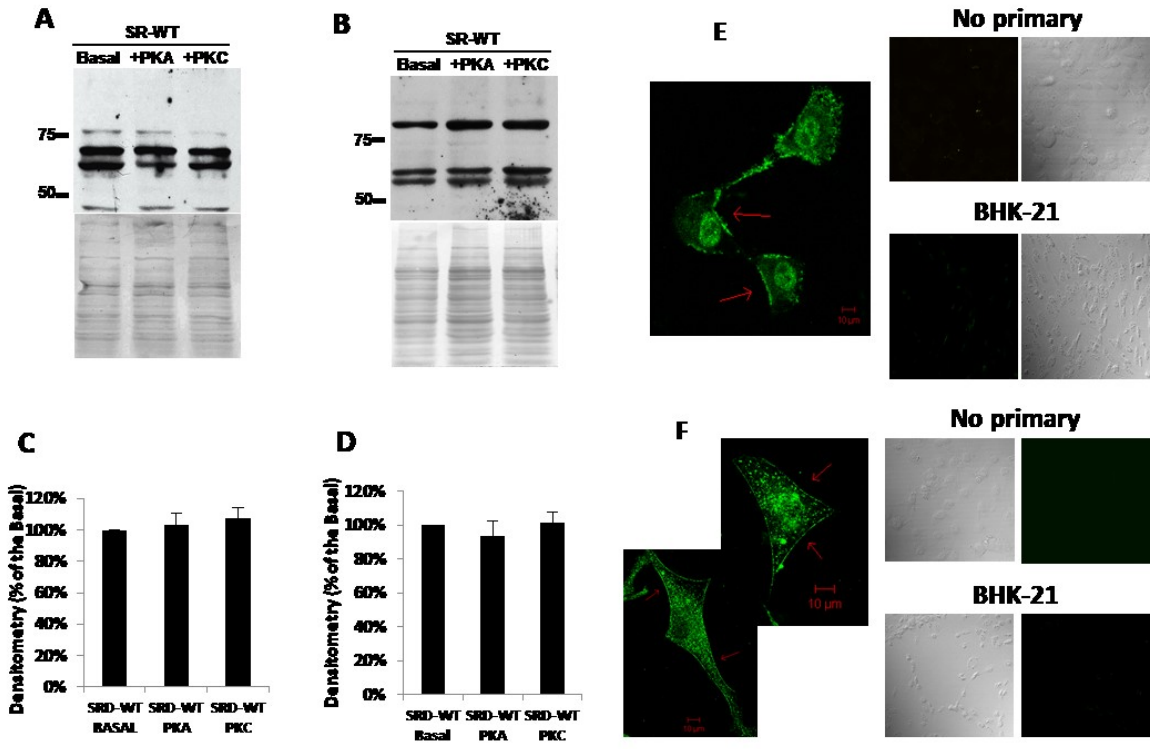


**Figure 18. Specificity and phospho-sensitivity tests for CFTR antibodies used in proximity ligation assays.**

BHK cells expressing SR-WT were PKA-stimulated with cAMP cocktail (150 µM CPT-cAMP, 1 mM IBMX and 10 µM FSK) or PKC-stimulated with 20 nM PMA for 2 h or left untreated (basal). Cell lysates were probed with CFTR antibody H-182, targeting the front half (**A**), or CFTR antibody C-19, targeting the back half (**B**) showing bands at ~62 kDa. Detection was not affected by phosphorylation of the R-region as shown in the histograms representing the bands for H-182 (**C**) and C-19 (**D**) antibodies. Band densities were normalized based on the total protein loaded in each well, measured after membrane staining with amido-black (showed bellow each blot). All densities were measured using the ImageJ software (National Institutes of Health; http://rsb.info.nih.gov/ij/). Values for PKA or PKC phosphorylation are expressed as a percentage of that for basal conditions (unphosphorylated). Values are means ± SEM for 3 independent experiments. Confocal microscopy images of BHK cells expressing SR-WT showing detection of the front (**E**) and back (**F**) halves at the cell surface using H-182 and C-19 antibodies. Negative control images where primary antibodies were omitted or where non-transfected BHK cells were used are shown as indicated.

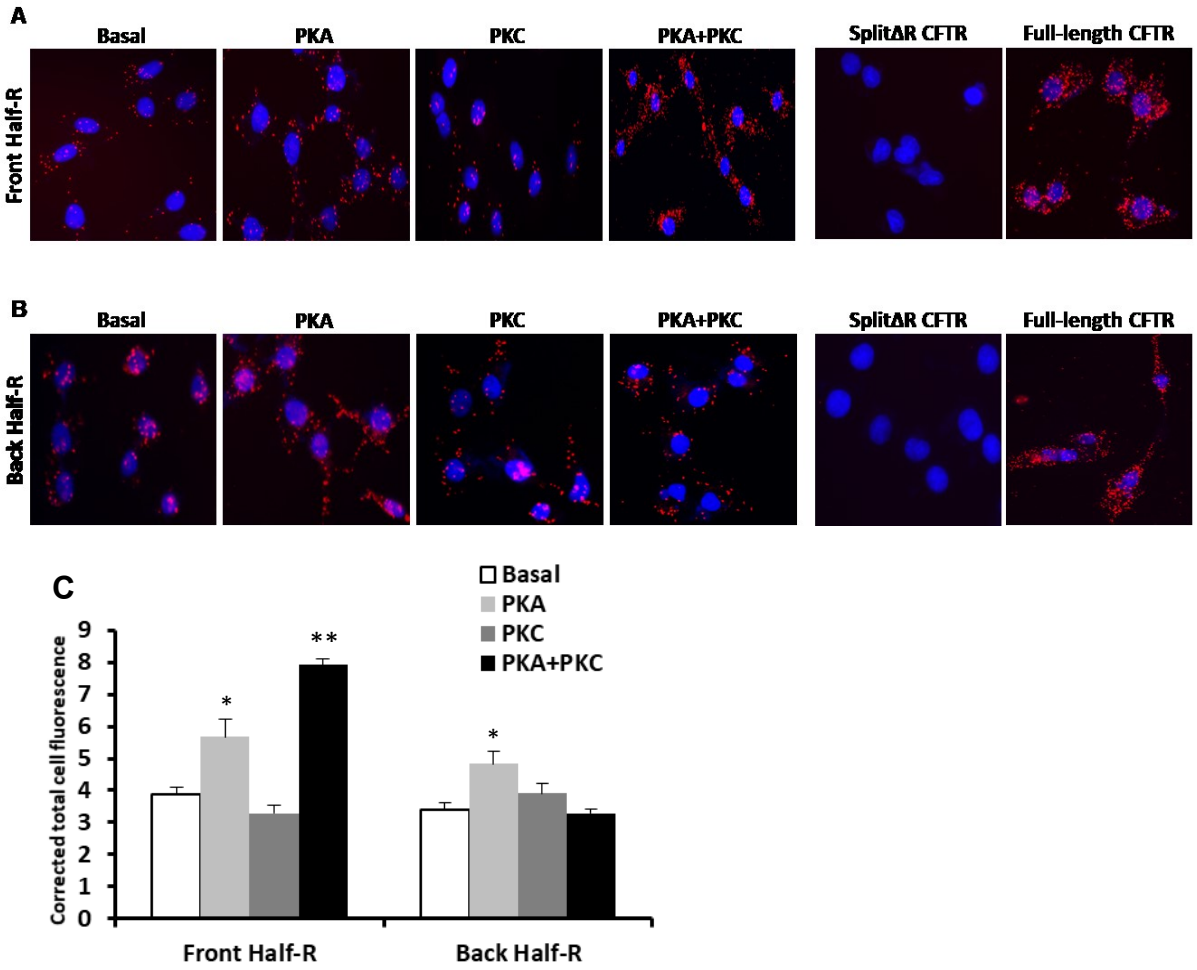


**Figure 19. R-region Interaction with the FH and the BH of CFTR.**

Representative fluorescence microscopy images from *in situ* PLA experiments showing FH-R (**A**), and BH-R (**B**) interactions (red dots). SR-WT cells were either left untreated (Basal), or PKA stimulated with 150μM CPT-cAMP+1mM IBMX+10μM FSK, or PKC stimulated with 20nM PMA, or PKA+PKC stimulated with 150μM CPT-cAMP+1mM IBMX+10μM FSK+20nM PMA. Cells expressing SplitΔR CFTR (with no R-region) and full-length CFTR were used as negative and positive controls, respectively. Cell nuclei were stained with DAPI (blue). FH, BH and R-region were detected by H-182, C-19 and MAB1660 antibodies, respectively. Assays either used H-182+MAB1660 to investigate FH-R interactions or C-19+MAB1660 to investigate BH-R interactions. **C,** Histogram representing averages of the corrected total cell fluorescence (CTCF) for the FH-R and BH-R interactions, measured in BHK cells in each condition displayed in A and B (*see section 2.10 in materials & methods for CTCF calculation*). Statistical significance (*$p<0.01$; **$p<0.0001$) was calculated in relation to basal values for each half. Values are means ± SEM for a minimum of 5 independent experiments

### 3.4 MUTATIONS AT CONSENSUS PKC SITES DISTURB R-REGION INTERACTION WITH CFTR HALVES

After establishing how the wild-type R-region interactions with both halves of CFTR change depending on its phosphorylation status, I asked whether mutations at important PKC sites (S641A/T682A, S686A, S686D, and 6CA) modify the R-region dynamic interactions (Figure 20 A-D), since mutations at PKC sites are known to affect channel function (Chappe et al, 2004).

In cells expressing the SR-CFTR with the two inhibitory PKC sites inactivated (SR-S641A/T682A; Figure 20 A), the R-region interaction with the BH was 3.5-fold higher than that measured with SR-WT under basal conditions (CTCF = 11.8 ± 0.91 compared to 3.41 ± 0.20, respectively; $p < 0.0001$), whereas the FH-R interaction was reduced by 2.5-fold compared to SR-WT (CTCF = 1.45 ± 0.27 in SR-S641A/T682A and 3.90 ± 0.18 in SR-WT; $p < 0.0001$) (Figure 20 E, F). This reduction was too extensive to be explained only by the lower expression of the FH in SR-S641A/T682A (see Figure 14 B). The basal weak FH-R interactions, nonetheless, were gradually increased to very high levels by stimulation of PKA, PKC, and PKC + PKA in this highly functional channel. From basal (CTCF = 1.45 ± 0.28) to PKA stimulation (CTCF = 4.24 ± 0.65; $p < 0.01$), a ~3-fold increase was observed. After PKC stimulation, a ~6-fold increase from basal occurred (CFTC = 9.26 ± 0.64; $p < 0.0001$), and the highest measured interaction (9-fold increase from basal) was obtained following PKC + PKA stimulation (CTCF = 13.01 ± 1.11; $p < 0.0001$). PKA stimulation in SR-S641A/T682A brings FH-R interactions back to the level of SR-WT (CTCF = 4.24 ± 0.65 and 5.67 ± 0.55

respectively; p>0.1), whereas PKC and PKC + PKA stimulations induced FH-R interactions 3-fold and 1.5-fold stronger than observed in SR-WT (PKC: 3.30 ± 0.55 for WT and 9.26 ± 0.64 for SR-S641A/T682A; PKC + PKA: 7.91 ± 0.21 for WT and 13.01 ± 1.11; p<0.0001 for both comparisons) (Figure 20 A, E). On the other hand, BH-R interaction was back to the WT levels after PKA stimulation and remained even at all phosphorylation conditions (Figure 20 A, F). These results suggest that when the R-region is unphosphorylated, S641 and T682 are important for interactions with both halves; however, when phosphorylated, those sites are only involved in FH-R interactions. Since full-length channels with S641A and T682A mutations display larger functional responses to PKA and PKC phosphorylation than WT CFTR (Chappe et al. 2004), the conclusion is that the increased interaction of the phosphorylated R-region with the FH, as measured here, plays a key role in CFTR functional response to phosphorylation. In full-length CFTR with the S686A mutation, the functional response to PKA was reduced and the enhancing effect of PKC was lost (Chappe et al. 2004). In the present study, alanine substitution in Ser686 (SR-S686A) strongly reduced the basal BH-R interaction compared to the WT (> 50% decrease; CTCF = 3.41 ± 0.20 in WT to 1.56 ± 0.14 in S686A; p < 0.001) (Figure 20 B, F) and shifted the R-region towards the FH, increasing the FH-R interaction by 25% under basal conditions (CTCF for WT was 3.90 ± 0.18 and 4.86 ± 0.35 for S686A; p<0.05) (Figure 20 B, E). Levels of BH-R interaction remained lower after PKA and PKC + PKA stimulations, compared to SR-WT (PKA: CTCF = 1.51 ± 0.20 for S686A and 4.82 ± 0.39 for WT; p<0.0001and PKC + PKA: 1.82 ± 0.19 for S686A and

3.28 ± 0.15; p<0.02) (Figure 20 B, F). Interestingly, but not unexpectedly, FH-R interaction after PKC stimulation was abolished (CTCF = 0.51 ± 0.14 for S686A compared to 3.29 ± 0.24 for WT; p<0.0001) and FH-R interaction after PKC + PKA stimulation was dramatically reduced in this construct (CTCF = 3.49 ± 0.13 for S686A and 7.91 ± 0.21 for WT; p<0.0001) (Figure 20 B, E). In SR-S686A, PKC + PKA phosphorylation induced a reduction (~45%) rather than a further enhancement in FH-R interactions when compared to PKA phosphorylation alone (CTCF = 6.15 ± 0.17 for PKA and 3.49 ± 0.13 for PKC + PKA; p<0.0001), suggesting that serine 686 plays a key role in the PKC further enhancement in FH-R interactions as observed in SR-WT (Figure 20 C).

In cells expressing the phosphomimetic mutation S686D, the functional opposite mutation of S686A, it was expected to see contrasting results and this was partially achieved. Unlike SR-S686A, R-region interactions with both halves resembled those of SR-WT under basal conditions, restoring proper basal interaction with the BH (Figure 20 C, F). R-region interaction with the FH after PKC stimulation was re-established to levels even higher than the WT (CTCF = 4.54 ± 0.46 for S686D and 3.29 ± 0.24 for WT; p<0.05), and after PKA + PKC stimulation, was recovered to the WT levels (CTCF = 6.16 ± 0.38 for S686D and 7.91 ± 0.21 for WT; p>0.05).. FH-R interactions induced by PKA alone seem not to be affected by S686 (CTCF = 5.67 ± 0.55 for WT, 6.15 ± 0.18 for S686A; p>0.9, and 6.75 ± 0.33 for S686D; p>0.2) (Figure 20 C, E). In this construct BH-R interactions remained lower compared to SR-WT in all phosphorylation conditions (Figure 20 F).

All together, these results indicate that basal interaction of the R-region with the BH plays a permissive role for the phosphorylation-dependent increase in FH-R interaction that is thought, based on our data, to induce the CFTR functional response to PKA and PKC + PKA stimulation.

The SR-6CA construct was developed with the idea to investigate the behaviour of channels where S686 is the only active PKC site. This channel is still able to respond to PKA or PKC + PKA stimulations similar to the SR-WT despite lacking 6 PKC sites, as measured in iodide efflux assays (Figure 16 C and G). PLA experiments showed that the unphosphorylated R-region almost completely dissociated from the FH (<10% of the SR-WT; CTCF = 0.33 ± 0.07 for 6CA and 3.90 ± 0.18 for WT; $p<0.0001$) while no changes were observed in basal BH-R interaction (Figure 20 D). Note that the findings for the SR-S686A mutant at basal conditions were the opposite of the ones observed in SR-S641A/T682A and SR-6CA. Also, in SR-6CA and SR-S641A/T682A, the reduced FH-R interaction at basal conditions did not impact the channel response to the PKC effect, unlike reduced BH-R interaction observed in SR-S686A which abolish such response, as demonstrated in iodide efflux assays and previous studies (Chappe et al. 2004). Although still very low compared to the WT, I measured an increase from basal conditions in the FH-R interaction after PKA stimulation in SR-6CA, as expected for a functional channel (CTCF = 0.33 ± 0.07 at basal and 1.40 ± 0.27 after PKA; $p<0.01$). Stimulation for PKC and PKC + PKA strongly increased the FH-R interaction compared to basal conditions (CTCF = 5.54 ± 0.31 for PKC and 5.28 ± 0.68 for PKC + PKA, $p < 0.0001$) (Figure 20 D, E).

Two main conclusions emerge from these results. First, a phosphorylation-dependent increase in the FH-R interaction is related to channel activation. This increase can be achieved either by inducing new R-region interactions with the front half or by making stronger the FH-R interactions already present in the unphosphorylated R-region. Second, interactions of the unphosphorylated R-region with the BH seems to play a permissive role to the PKC enhancing effect observed in CFTR function. That is, if the unphosphorylated R-region is displaced from the BH, PKC phosphorylation is not able to play its synergic role with PKA to enhance FH-R interactions and therefore, channel function. PKC site S686 seems to be central in this mechanism. Based on these findings, a schematic model describing the effect of phosphorylation in the R-region dynamics was developed and it is illustrated in Figure 21.

### 3.5 Phosphorylation-induced Changes in R-region Interaction with Cytoplasmic CFTR Polypeptides.

In the previous section, I established a new molecular model for the effect of phosphorylation (by PKA and PKC) in the profile for R-region interactions with the two halves of CFTR. Although novel and illustrative, this model does not show what regions within the front half and back half are interacting with the R-region in each phosphorylation condition.

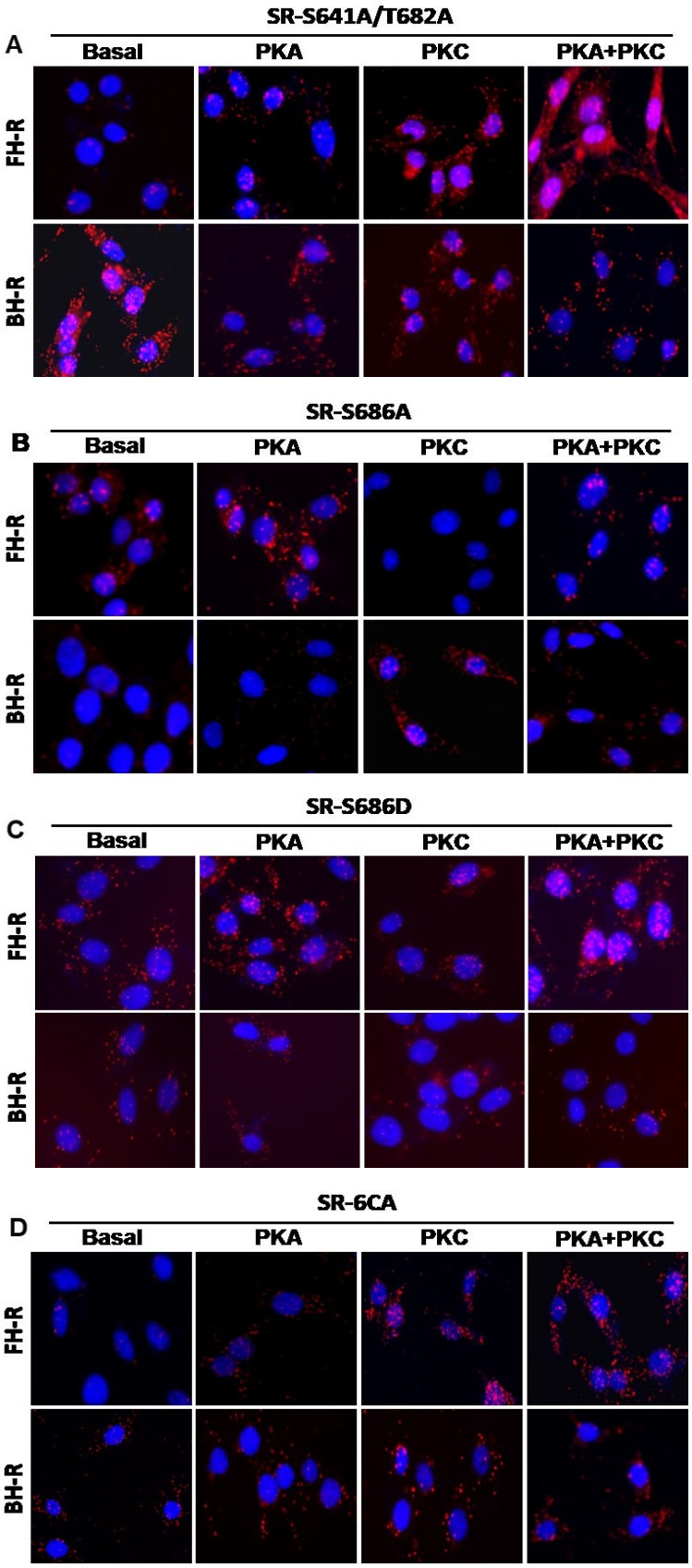
A
SR-S641A/T682A
Basal
PKA
PKC
PKA+PKC
FH-R
BH-R
B
SR-S686A
Basal
PKA
PKC
PKA+PKC
FH-R
BH-R
C
SR-S686D
Basal
PKA
PKC
PKA+PKC
FH-R
BH-R
D
SR-6CA
Basal
PKA
PKC
PKA+PKC
FH-R
BH-R

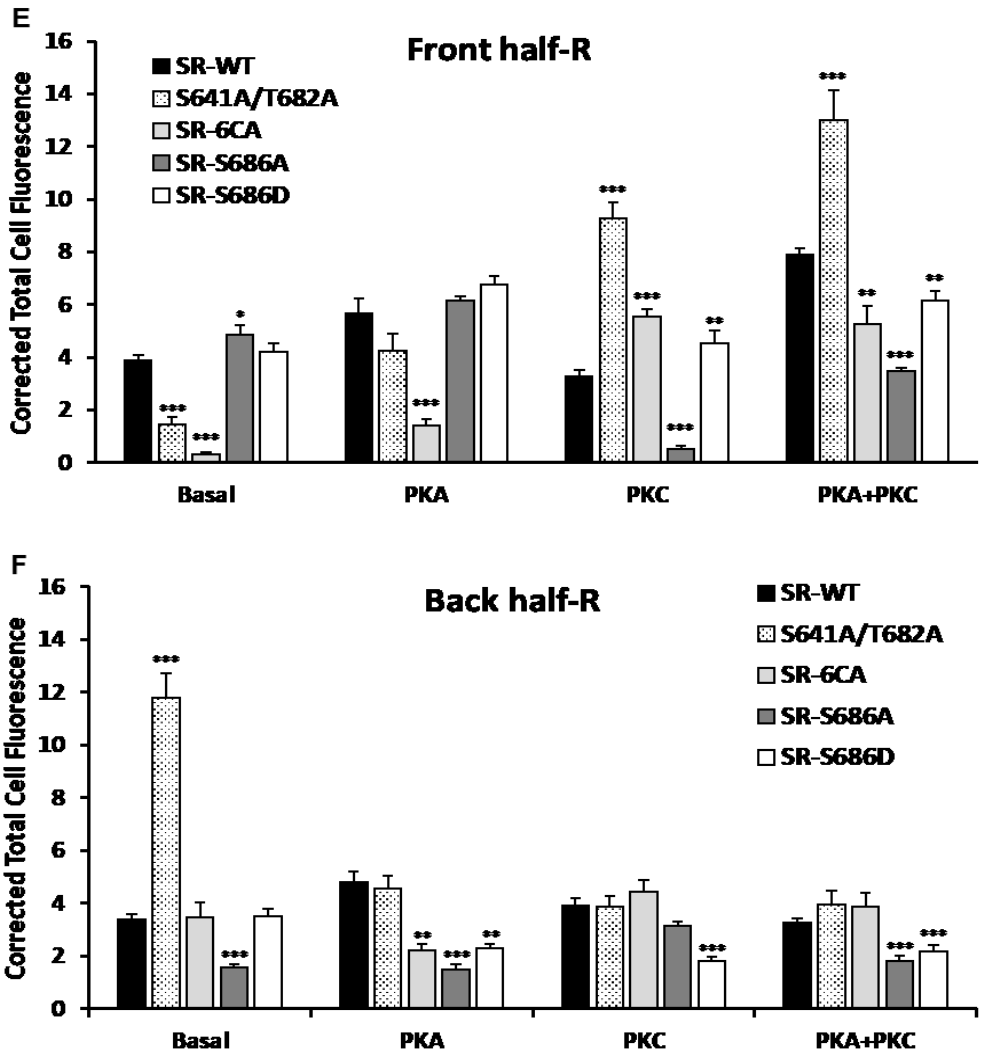


**Figure 20. Mutant R-region interactions with the FH and the BH of CFTR.**

Representative fluorescence microscopy images from *in situ* PLA experiments showing FH-R (upper row) and BH-R (lower row) interactions (red dots) for mutant constructs SR-S641A/T682A **(A)**, SR-S686A **(B)** SR-S686D **(C)** and SR-6CA **(D)** at basal or after PKA or PKA+PKC stimulation as described in figure 6. Cell nuclei were stained with DAPI (blue). FH, BH and R-region were detected by H-182, C-19 and MAB1660 antibodies, respectively. Assays either used H-182+MAB1660 to investigated FH-R interactions or C-19+MAB1660 to investigated BH-R interactions. Histograms representing the average of corrected total cell fluorescence for FH-R (**E**) and BH-R (**F**) interactions measured in BHK cells from **A-D**. Statistical significance (*p<0.05; **p<0.01; ***p<0.001) was calculated in relation to values for SR-WT in each phosphorylation condition. Values are means ± SEM for a minimum of 3 independent experiments

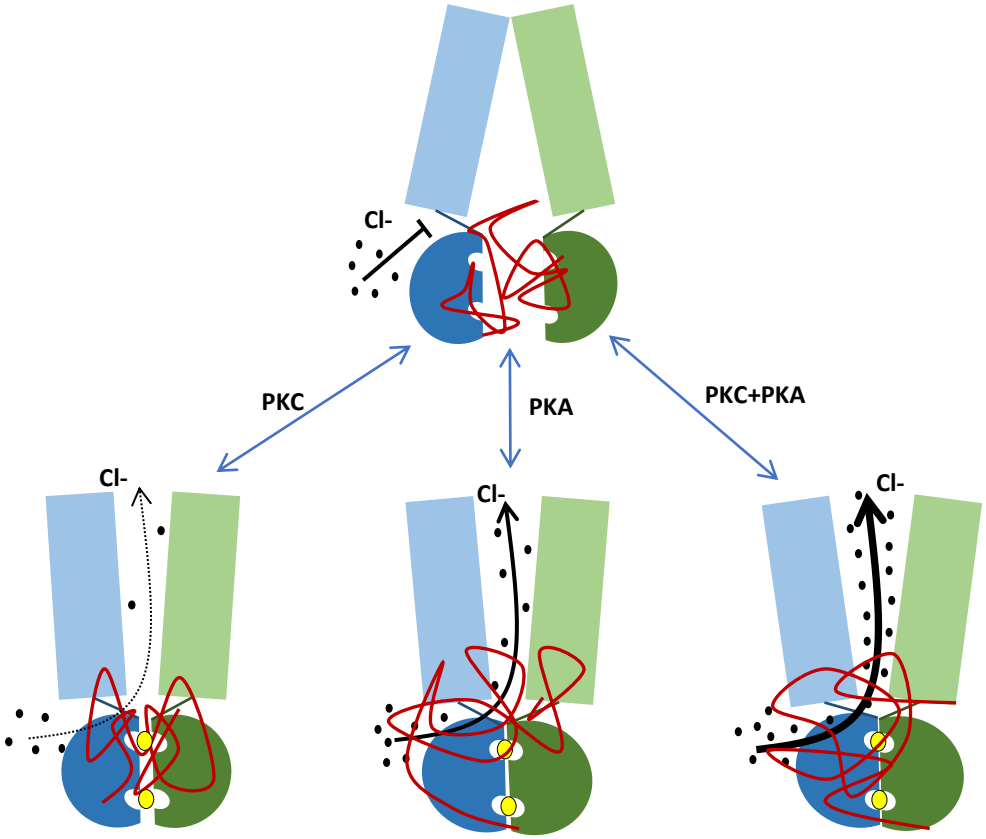


**Figure 21. Schematic model of the R-region dynamic interactions with the split CFTR.**

When the channel is closed, under basal conditions, the unphosphorylated R-region interacts equally with both half of the split CFTR, preventing NBD dimerization. Following PKC phosphorylation, the R-region interaction strength remains unchanged but now in a new permissive location, allowing NBD dimerization and ATP binding, making the split CFTR channel competent for gating with minimal activity. After PKA phosphorylation, the R-region interaction increases, with both FH and BH, allowing normal gating and activity of the channel. In presence of both PKA and PKC phosphorylation, the strongest FH-R interaction is measured, while a basal BH-R interaction enables the enhancing effect of PKC. FH: TMD1 (light blue) + NBD1 (dark blue); BH: TMD2 (light green) + NBD2 (dark green); red ribbon: R-region; ATP (yellow circles) binds to NBDs in the open states; black dots: chloride ions; black arrows: chloride flow.

I then decided to investigate the association of the R-region with polypeptides designed based on six cytoplasmic subdomains of CFTR, three from the front half and three from the back half. From the front half, I used the N-terminal lasso motif (aa 1-77), the cytoplasmic loop 1 (aa 147-195) and the cytoplasmic loop 2 (aa 244-298). From the back half, I used the cytoplasmic loop 3 (aa 940-990), cytoplasmic loop 4 (aa 1035-1095) and the C-terminal tail (aa 1439-1480). The subdomains' boundaries and amino acids sequences used for polypeptide synthesis were taken from the human CFTR database (UniProt accession #P13569) which are based on the human unphosphorylated CFTR structure (Liu et al, 2017). All polypeptides were synthesized with a 5-FAM tag incorporated at the N-terminal end, to a purity level of >90% by Proteogenix (Schiltigueim, France) (see Table 3 for polypeptides sequences).

To analyze interactions with those polypeptides, the DNA sequence encoding the same amino acid sequence of the R-region used in PLA assays described in the first section (aa 635-836) was incorporated into a pET21 vector containing a 6x-histidine tag, for binding to $Ni^{+2}$ columns and the sequence encoding the B1 domain of *Streptococcal* protein G (GB1), for solubilization purposes, and expressed this recombinant R-region in E. coli cells followed by purification using $Ni^{+2}$ column affinity chromatography (*see section 2.11 in Material and Methods for details*). Addition of the GB1 motif rendered a ~5-fold increase in the solubility of the final renatured R-region fusion protein.

As many eukaryotic proteins, the R-region DNA sequence has several codons rarely used in the E. coli machinery, including arginine, isoleucine, leucine and

proline codons. To achieve good expression of the R-region, I used the Rosetta™ BL21 E. coli strain which contains an extra plasmid encoding tRNAs that enhance the expression of such eukaryotic proteins.

Even with the addition of GB1 in our construct, the R-region was highly insoluble in native buffers usually used for purification, so I used an 8 M urea denaturing purification. Expression of the R-region induced by IPTG in Rosetta BL21 cells, and purification in denaturing conditions showed a very good protein yield in the elution fraction (Figure 22 A). This high amount of fusion protein, however, was mostly precipitated after overnight dialysis against a variety of buffers in the pH range of 7-8, which are suitable for the subsequent phosphorylation steps. The maximum concentration achieved in those buffers was ~75 μM, which was found to be insufficient for microscale thermophoresis (MST) measurements. During the extensive solubilization tests, the R-region was found to be more soluble in pure water, shifting the water pH to acidic levels of 4-5. The R-region fusion protein was then dialyzed against a 10 mM HCl solution containing 5 mM BME and precipitation was avoided. After centrifugal concentration, the pH was adjusted to 7.5-8 (in the optimal range for PKA and PKC phosphorylation) by adding Tris-base pH 11 to a final concentration of 60-80 mM. This procedure rendered a maximum of 350 μM of stable soluble fusion protein, now in sufficient amount for MST measurements. Expression and purification of the GB1 protein followed a similar protocol as used for the recombinant R-region with the difference of the use of BL21 cells (no rare codons for E. coli are found in GB1) and native buffers (GB1 is highly soluble in aqueous buffers). The high amount of

protein that was obtained in the elution fraction (Figure 22 B) was diluted to 350 µM, the same as obtained for the recombinant R-region, to be used as a negative control for protein-protein interaction experiments. Purified fusion R-region was then phosphorylated by PKA (100 nM PKA + 2 mM $Mg^{+2}$-ATP) and PKA + PKC (100 nM PKA + 2 mM $Mg^{+2}$-ATP + 5 nM PKC + PKC lipid activator) for 2 h at 30°C or left untreated (basal control). Attempts to phosphorylate the R-region only with PKC by adding 5 nM PKC + 2 mM $Mg^{+2}$-ATP + PKC lipid activator caused most of the protein to precipitate and it could not be re-solubilized. For this reason, PKC-phosphorylated R-region proteins were not tested for protein-protein interactions with the cytoplasmic CFTR polypeptides. Phosphorylation of the R-region was verified by selective staining of phosphoproteins by the use of Pro-Q diamond stain and by the change in the electrophoretic mobility on SDS-PAGE (Figure 23), as reported in previous studies (Picciotto et al. 1992; Ostedgaard et al. 2000). When the R-region protein was treated with PKA and PKA + PKC, the electrophoretic shift was observed after Coomassie brilliant blue staining (Figure 23 A, upper lanes 1 to 3) and strong bands were detected after 8.5 seconds of exposure using a Cy3 filter in a VersaDoc MP 4000 system, compared to the untreated protein (Figure 23 A, bottom lanes 1 to 3), although no significant difference was observed between the two phosphorylation conditions after measuring the density of the bands (Figure 23 B).

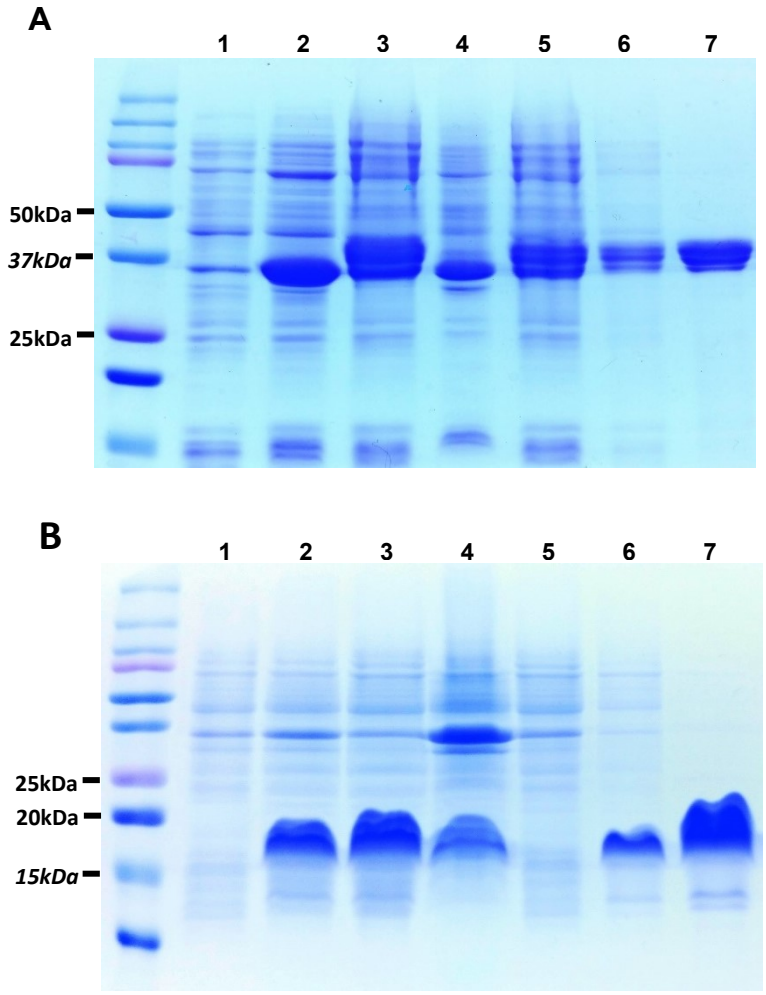


**Figure 22. Expression and purification of recombinant R-region and HGB1 proteins.**

12% (**A**) and 18% SDS polyacrylamide gels (**B**) after Coomassie blue staining representing expression and purification steps of the wild type recombinant R-region (**A**) and HGB1-empty vector (**B**). Expression of both proteins after induction by 4h incubation with 0.5mM IPTG was detected in lane 2 as a band at ~35kDa (R-region, **A**) and ~18kDa (HGB1, **B**), compared to lane 1 (before IPTG induction). Total bacteria lysate was subjected to centrifugation and after separation of soluble (lane 3) and insoluble (lane 4) fractions, the soluble fraction was loaded into a $Ni^{+2}$ affinity column. Unbound proteins are observed at the column flow through (lane 5). After column wash (lane 6) using 5-10mM imidazole to remove undesired entrapped proteins, purified recombinant R-region (**A**) and HGB1 (**B**) proteins were eluted from column using 300mM imidazole (lane 7).

To demonstrate R-region phosphorylation by PKC, an aliquot of the R-region that remained soluble after PKC treatment was exposed to the selective phosphoprotein stain and a band was detected only after a long exposure of 60 s (7-fold longer than the one used to detect PKA phosphorylation) using the same filter and imaging system described above (Figure 23 A, bottom lanes 4 and 5). The difference observed in phosphorylation levels after PKA and PKC treatment may explain why a difference between PKA and PKA + PKC phosphorylation was not visible under the Pro-Q phosphoprotein staining technique.

As an alternative to verify the phosphorylation state of the R-region, samples of the R-region after PKA, PKC and PKA + PKC treatments were sent for proteomic analysis by mass spectrometry. Each sample was digested by trypsin protease, generating a population of peptides that were analyzed by mass spectrometry. All ten PKA sites within the R-region (S660, S670, S700, S712, S737, S753, S768, T788, S795, S813) and four out of seven PKC sites within the R-region (S686, S707, S790, T791) were found to be phosphorylated in the analysis. The majority of phosphorylation sites (S660, S670, S686, S700, S707, S712, S737, S753, S768, S795, S813) were identified with nearly 100% accuracy, that is, in nearly 100% of the phosphorylated peptides bearing those sites, site-specific determination (PhosphoRS algorithm; Taus et al, 2011) identified phosphorylation modifications at those residues. In the phosphorylated peptides bearing T788, S790 and T791, PhosphoRS could not identify the specific residue modified by phosphorylation, probably because the quality of fragmentation in the mass spectra was not sufficient to unequivocally identify the phosphorylation

sites, what could be explained by the close proximity of those phosphorylation sites. PhosphoRS was able, however, to calculate site probabilities for those phosphorylation sites. In the peptide “TTASTR” (aa 234-239 in the HGB1 sequence at Figure 12), the probability of phosphorylation of S790 was higher (50-90%) compared to T791 (50%). Phosphorylation of T788 was found in the peptide “KTTASTR” (aa 233-239 in Figure 12) with probabilities varying from 50-99%.

R-region interaction with each of the polypeptides was assessed by MST, which identifies protein-protein interactions in solution by detecting changes in the movement, induced by a thermal gradient, of one of the binding partners before and after a binding event.

To confirm that the interactions described below were attributed to the R-region and no interference was caused by the fusion partner GB1, we tested the interaction of each CFTR polypeptide with GB1 with the same buffers, concentrations and conditions applied to the R-region fusion protein. No significant changes in MST curves were found and no Kd values could be calculated from the MST curves after addition of GB1 alone to any of the CFTR polypeptides tested indicating that GB1 does not bind the polypeptides tested in this study (Figure 24). To improve our understanding of the FH-R interactions observed in PLA, I addressed the interaction of the recombinant R-region peptide with the lasso motif, and cytoplasmic loops 1 and 2, parts of the front half.

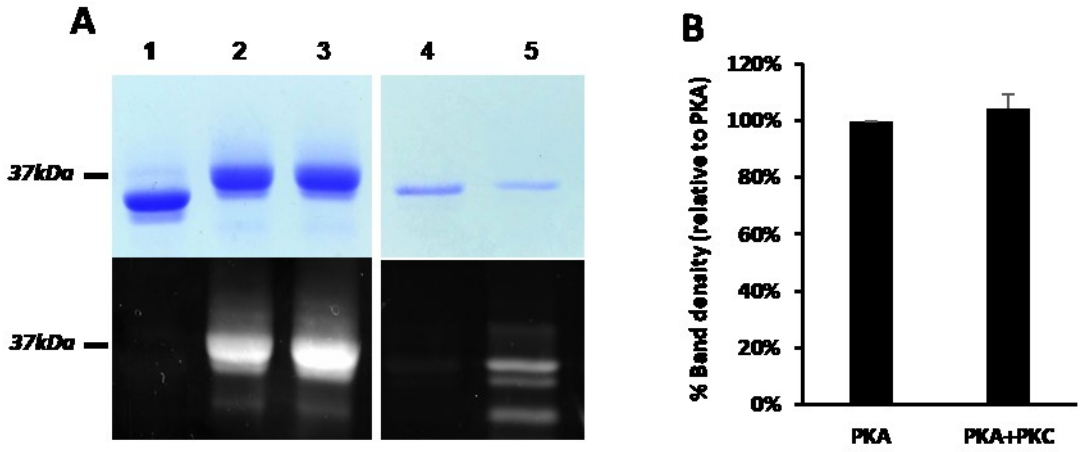


**Figure 23. Analysis of the phosphorylation state of purified R-region.**

**A,** 12% SDS polyacrylamide gels after Coomassie blue staining (upper) and after Pro-Q diamond phosphoprotein gel stain (lower) showing phosphorylation of the R-region after treatment with PKA + $Mg^{+2}$-ATP (lane 2), PKA + PKC + $Mg^{+2}$-ATP + PKC lipid activator (lane 3) and PKC + $Mg^{+2}$-ATP + PKC lipid activator (lane 5) for 2 h at 30°C, compared to the unphosphorylated R-region (lanes 1 and 4). Note the mobility shift in the recombinant R-region migration after PKA phosphorylation (lanes 2 and 3). Phosphoprotein stained gels were imaged on a VersaDoc 4000 MP with Quantity One software using the Cy3 filter and exposed for 8.5 seconds (lanes 1-3) and 60 seconds (lanes 4 and 5). **B,** Histogram showing band density averages of PKA and PKA + PKC phosphorylated R-regions (lanes 2 and 3) measured using the ImageJ software (National Institutes of Health; http://rsb.info.nih.gov/ij/). Values for PKA + PKC are expressed as a percentage of that for PKA. Values are means ± SEM for 5 independent experiments.

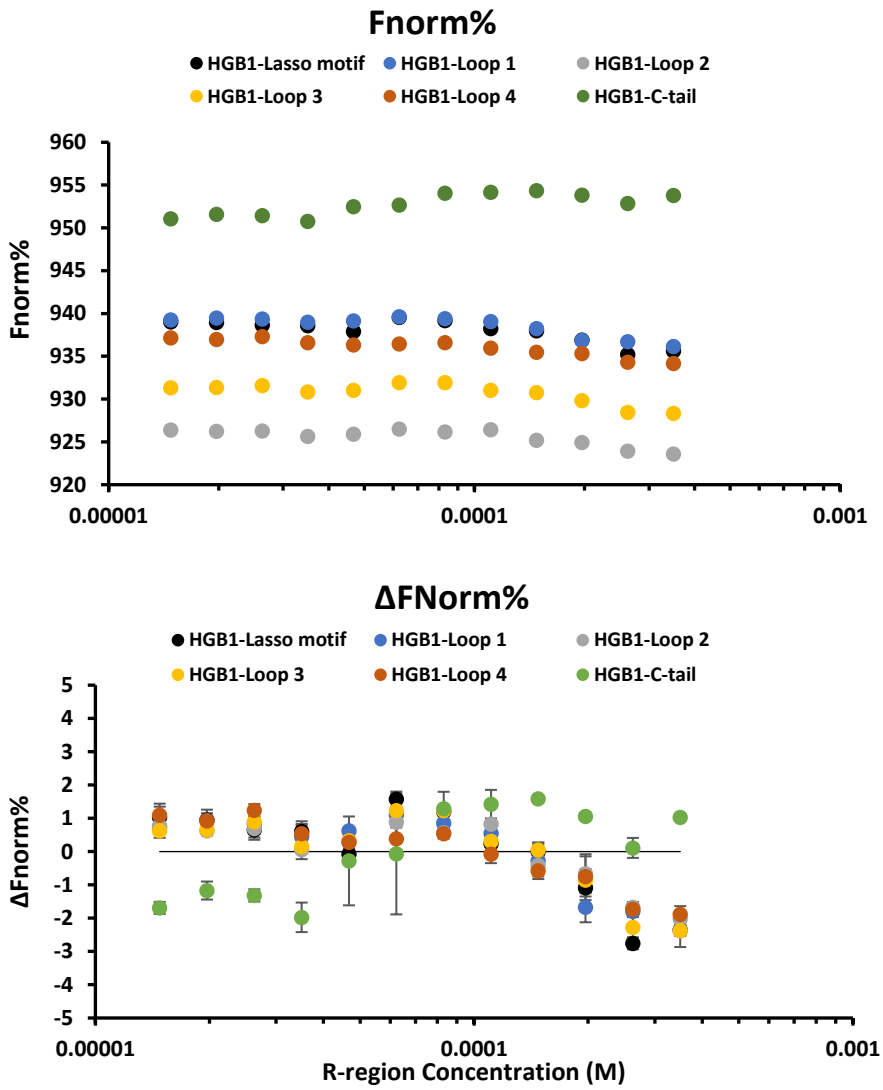


**Figure 24. Interaction of His-GB1 with CFTR polypeptides**

MST experiments where the concentration of the 5-FAM-labeled N-terminal lasso motif, cytoplasmic loop 1-4 and the C-terminal tail was kept constant (150nM), while the non-labeled His-GB1(HGB1) protein was serial diluted (3:1) starting at 350μM, similarly to the R-region in figures 18 and 19. Reactions were performed as described in figure 17 and no Kd was derived from any reaction indicating the absence of interaction between peptides. **A,** normalized fluorescence (Fnorm%) and **B,** baseline corrected normalized fluorescence (ΔFnorm%) showing no significant change in the MST signal at different concentrations of HGB1 (N=3 independent measurements, error bars represent the standard error).

Interaction of the unphosphorylated R-region (resembling the basal conditions found in PLA) with the N-terminal lasso motif was ~2.5-fold weaker than observed after PKA phosphorylation with dissociation constants (Kd) of 316 ± 26.3 μM for basal and 118.8 ± 2.4 μM for PKA phosphorylated peptides ($p<0.0001$). Additional PKC phosphorylation did not alter the binding affinity of the R-region to the lasso motif compared to PKA alone (Kd =118.8 ± 2.4 μM for PKA and 128.4 ± 11.6 μM for PKA + PKC $p>0.9$) (Figure 25 A). MST measurements for the R-region interaction with the first and second cytoplasmic loops showed that the basal interaction found for both polypeptides was not significantly altered by phosphorylation. Dissociation constants for the R-region interaction with cytoplasmic loop 1 at basal (Kd = 111.3 ± 7.7 μM) remained constant after PKA (Kd = 131.7 ± 2.9 μM; $p>0.1$) and PKA + PKC phosphorylation (Kd=119.3 ± 9.2 μM; $p>0.7$) (Figure 25 B). Similar results were found for the R-region interaction with the cytoplasmic loop 2 (Kd =106.8 ± 8.4 μM for basal; 137.6 ± 12.0 μM for PKA; $p>0.1$ and 107.0 ± 11.3 μM for PKA + PKC; $p>0.9$) (Figure 25 C). These results demonstrate that the increase in FH-R interactions found in PLA experiments after PKA stimulation is due to new interactions with the lasso motif.

The BH-R interactions found in PLA were further studied by testing the effects of phosphorylation on the recombinant R-region interaction with the third and forth cytoplasmic loops as well as with the C-terminal tail. Interactions of the unphosphorylated R-region with the cytoplasmic loop 3 remained similar after

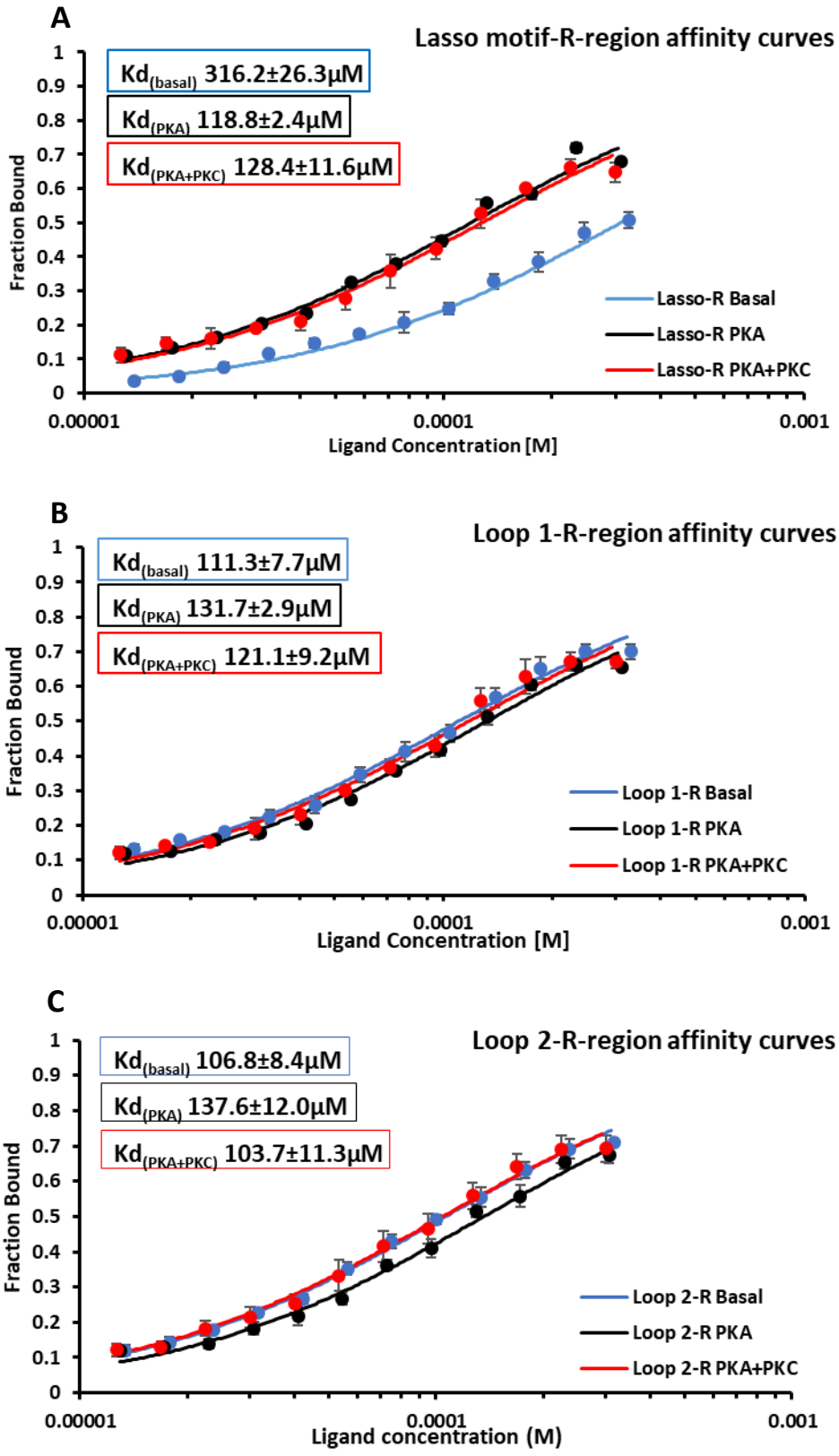
A
Lasso motif-R-region affinity curves
Kd(basal) 316.2±26.3µM
Kd(PKA) 118.8±2.4µM
Kd(PKA+PKC) 128.4±11.6µM
Fraction Bound
Ligand Concentration [M]
Lasso-R Basal
Lasso-R PKA
Lasso-R PKA+PKC
B
Loop 1-R-region affinity curves
Kd(basal) 111.3±7.7µM
Kd(PKA) 131.7±2.9µM
Kd(PKA+PKC) 121.1±9.2µM
Fraction Bound
Ligand Concentration [M]
Loop 1-R Basal
Loop 1-R PKA
Loop 1-R PKA+PKC
C
Loop 2-R-region affinity curves
Kd(basal) 106.8±8.4µM
Kd(PKA) 137.6±12.0µM
Kd(PKA+PKC) 103.7±11.3µM
Fraction Bound
Ligand concentration (M)
Loop 2-R Basal
Loop 2-R PKA
Loop 2-R PKA+PKC

**Figure 25. Affinity curves for the interaction of the R-region with polypeptides comprised into the front half of CFTR.**

Affinity curves obtained in MST experiments where the concentration of the 5-FAM-labeled N-terminal lasso motif **(A)**, cytoplasmic loop 1 **(B)** and cytoplasmic loop 2 **(C)** was kept constant (150 nM), while the non-labeled unphosphorylated (blue), or PKA (black) or PKA + PKC (red) phosphorylated R-region was serial diluted (3:1) starting at 350 μM. After a 10 min incubation the samples were loaded into Monolith NT.115 Standard Treated Capillaries and the MST measurement was performed using the Monolith NT.115. An MST-on time of 20 s was used for analysis, and the Kd derived from each interaction is shown at the top left boxes color coded as the curves (N>3 independent measurements, error bars represent the standard error).

PKA phosphorylation (Kd = 80.8 ± 9.9 μM for basal and 95.9 ± 7.5 μM after PKA; $p>0.4$). Dual PKA + PKC phosphorylation, however, reduced significantly the binding affinity to this loop (Kd = 136.4 ± 7.9 μM), compared to basal ($p<0.01$) and to PKA phosphorylation only ($p<0.05$) (Figure 26 A). In the case of R-region interactions with the cytoplasmic loop 4, only PKA phosphorylation caused a reduction in the association to this loop(Kd = 80.0 ± 3.9 μM for basal and 120.6 ± 10.1 μM after PKA; $p<0.01$) while PKA + PKC did not induce significant changes in the interactions (Kd = 104.5 ± 9.9 μM; $p>0.1$) (Figure 26 B). Although phosphorylation in general weaken R-region binding affinity to both loops in the BH, this displacement seems to happen differently for each loop. While PKA phosphorylation affects the interaction with the loop 4, PKA + PKC phosphorylation affects the interaction with loop 3. Finally, the interaction of the recombinant R-region with the C-terminal tail of CFTR exhibited a strong modulation by PKA and PKC. Phosphorylation promoted a strong association (~2.3-fold higher) of the R-region to this final segment of CFTR, with no difference observed between PKA and PKA + PKC stimuli (Kd = 136.1 ± 7.5 μM for basal, 64.3 ± 3.9 μM after PKA and 55.1 ± 3.8 μM after PKA + PKC; $p<0.0001$ for both comparisons) (Figure 26 C). These results demonstrate that phosphorylated-induced changes in BH-R interactions found with the PLA method are due to a coordinated shift of the R-region from loops 3 and 4 to the C-terminal tail. After PKA, the increase in BH-R interactions found in PLA experiments could be explained by the stronger increase in interactions with the C-tail compared to a weaker displacement from loop 4. The displacement from

loop 3 with no further interaction with the C-tail after PKA + PKC would explain the BH-R interaction levels in found with PLA at the same condition.

After analyzing the effect of phosphorylation in association of the R-region with each polypeptide individually, we took a different perspective of our MST studies, and analyzed binding affinities found with all of the six polypeptides in each phosphorylation condition to have an insight of the R-region dynamics throughout the CFTR protein. Figure 27 A shows affinity curves for the unphosphorylated R-region interactions with the lasso motif, cytoplasmic loops 1 to 4 and the C-terminal tail of CFTR. It is clearly visible the weaker association of the unphosphorylated R-region with the lasso motif (Kd Lasso-R = 316.2 ± 26.3 μM) and the stronger association with both cytoplasmic loops 3 and 4 (Kd Loop 3-R = 77.8 ± 17.0 μM and Loop 4-R = 80.0 ± 3.9 μM; $p<0.0001$ for both compared to Lasso-R). Interactions with the CFTR C-tail were weaker than interactions with loops 3 and 4 (Kd C-tail-R = 136.1 ± 7.5 μM; $p<0.03$ to both loops), but much stronger compared to interactions with the lasso motif ($p<0.0001$). This analysis shows that besides the interactions reported with the NBDs (Baker et al, 2007; Bozoki et al. 2013), the unphosphorylated R-region is also in contact (with different affinities) with all cytoplasmic subdomains of CFTR.

A

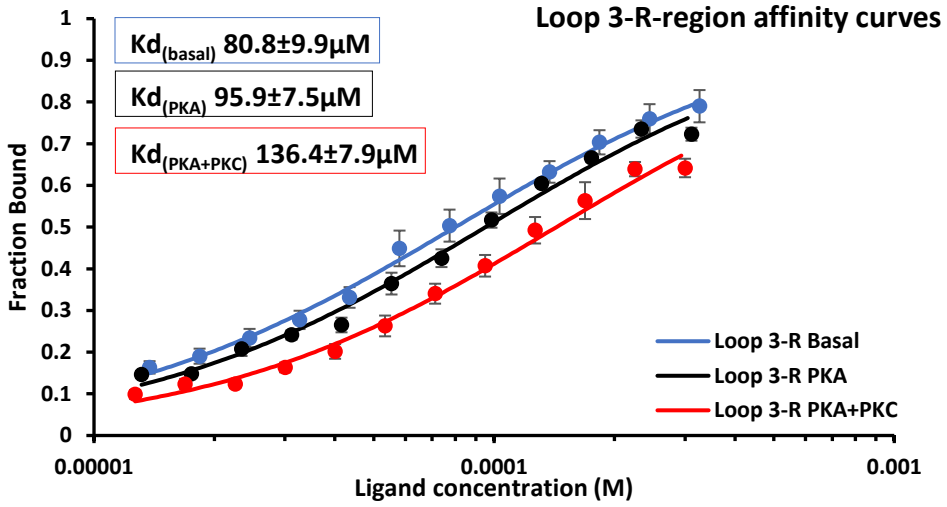
Loop 3-R-region affinity curves
Kd(basal) 80.8±9.9μM
Kd(PKA) 95.9±7.5μM
Kd(PKA+PKC) 136.4±7.9μM
Fraction Bound
Ligand concentration (M)
0.00001
0.0001
0.001
Loop 3-R Basal
Loop 3-R PKA
Loop 3-R PKA+PKC

B

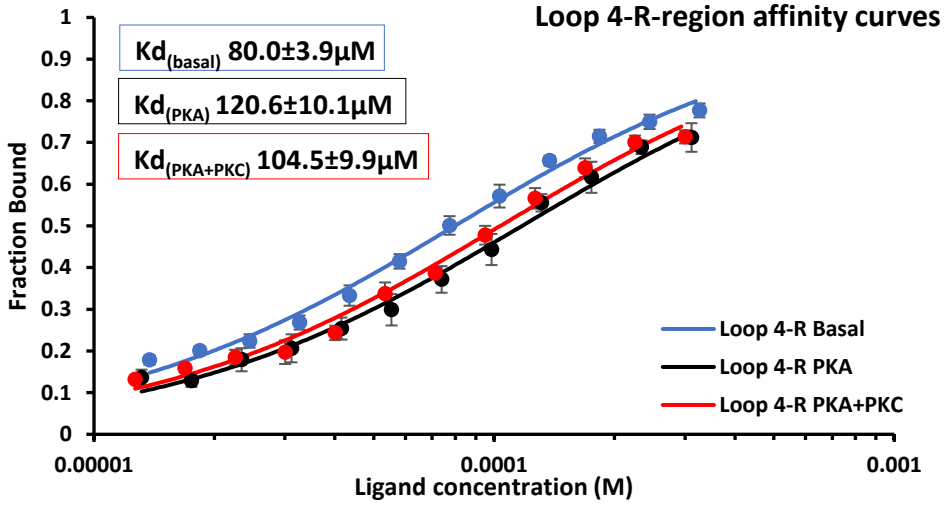
Loop 4-R-region affinity curves
Kd(basal) 80.0±3.9μM
Kd(PKA) 120.6±10.1μM
Kd(PKA+PKC) 104.5±9.9μM
Fraction Bound
Ligand concentration (M)
0.00001
0.0001
0.001
Loop 4-R Basal
Loop 4-R PKA
Loop 4-R PKA+PKC

C

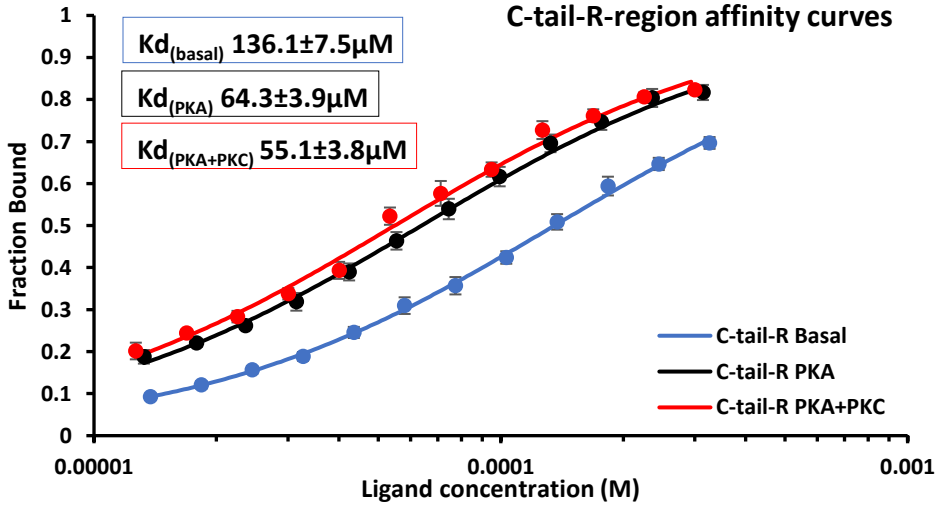
C-tail-R-region affinity curves
Kd(basal) 136.1±7.5μM
Kd(PKA) 64.3±3.9μM
Kd(PKA+PKC) 55.1±3.8μM
Fraction Bound
Ligand concentration (M)
0.00001
0.0001
0.001
C-tail-R Basal
C-tail-R PKA
C-tail-R PKA+PKC

**Figure 26. Affinity curves for the interaction of the R-region with polypeptides comprised into the back half of CFTR.**

Affinity curves obtained in MST experiments where the concentration of the 5-FAM-labeled N-terminal lasso motif **(A)**, cytoplasmic loop 1 **(B)** and cytoplasmic loop 2 **(C)** was kept constant (150 nM), while the non-labeled unphosphorylated (blue), or PKA (black) or PKA + PKC (red) phosphorylated R-region was serial diluted (3:1) starting at 350 μM. Reactions were performed as described in figure 17 and the Kd derived from each interaction is shown at the top left boxes color coded as the curves (N>3 independent measurements, error bars represent the standard error).

Figure 27 B shows affinity curves of the PKA-phosphorylated R-region. Interactions with the C-tail peptide becomes prevalent compared to all other CFTR regions tested after PKA phosphorylation. Moderate interaction was observed with the cytoplasmic loop 3 (Kd C-tail-R = 64.3 ± 3.9 μM and Kd Loop 3-R = 95.9 ± 7.5 μM; $p<0.03$) and the weakest interactions were observed with cytoplasmic loops 1 and 2 (Kd Loop 1-R = 131.7 ± 2.9 μM; $p<0.02$ and Kd Loop 2-R = 137.6 ± 12.0 μM; $p<0.01$) compared to Loop 3-R. Interactions with the lasso motif and cytoplasmic loop 4 were neither significantly different from Loop 3-R nor from Loop 1-R and Loop 2-R.

Dual phosphorylation of the R-region with PKA and PKC promoted a significant reduction in the R-region association with the cytoplasmic loop 3 compared to PKA phosphorylation alone (Kd = 95.9 ± 7.5 μM after PKA and 136.4 ± 7.9 μM for PKA + PKC; $p<0.05$) while maintaining strong interactions with both lasso motif and C-tail polypeptides. Interactions with the C-tail remained the most prevalent compared to interactions with all other CFTR polypeptides ($p<0.03$) (Figure 27 C). In general, the R-region is displaced from the central area of the protein where it prevents NBDs dimerization to interact strongly with new partners in both amino and carboxyl ends of the protein. Interactions with the cytoplasmic loop 4 must be disrupted in order to permit the channel activation by PKA just as interactions with the cytoplasmic loop 3 must be disturbed for PKC to promote its enhancing effect. A schematic model illustrating the effect of phosphorylation in the R-region dynamics in respect to the six CFTR polypeptides described above is shown in Figure 28.

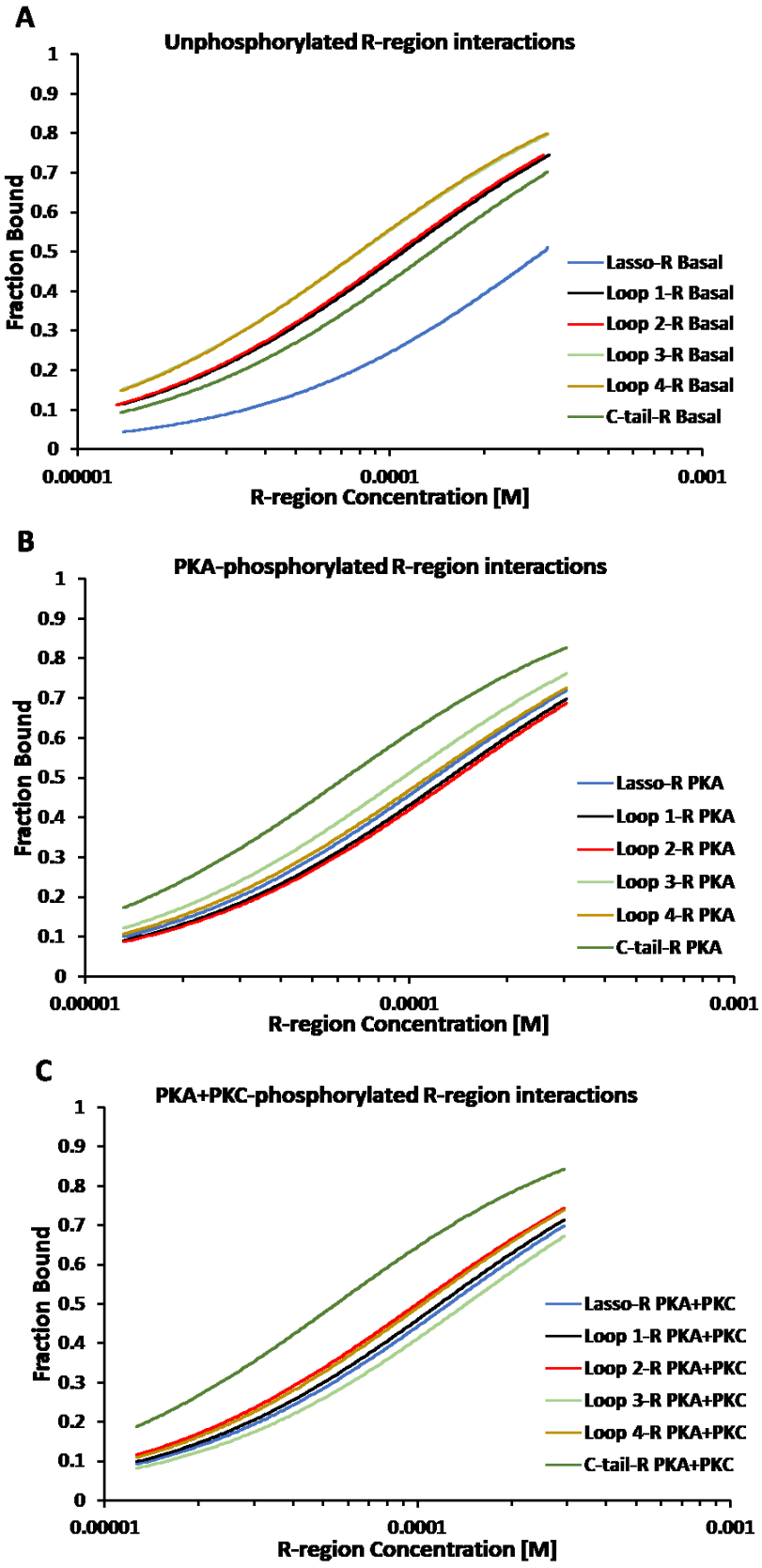
A
Unphosphorylated R-region interactions
Fraction Bound
R-region Concentration [M]
0.00001
0.0001
0.001
Lasso-R Basal
Loop 1-R Basal
Loop 2-R Basal
Loop 3-R Basal
Loop 4-R Basal
C-tail-R Basal
B
PKA-phosphorylated R-region interactions
Fraction Bound
R-region Concentration [M]
Lasso-R PKA
Loop 1-R PKA
Loop 2-R PKA
Loop 3-R PKA
Loop 4-R PKA
C-tail-R PKA
C
PKA+PKC-phosphorylated R-region interactions
Fraction Bound
R-region Concentration [M]
Lasso-R PKA+PKC
Loop 1-R PKA+PKC
Loop 2-R PKA+PKC
Loop 3-R PKA+PKC
Loop 4-R PKA+PKC
C-tail-R PKA+PKC

**Figure 27. Phosphorylation effects on the interaction of the R-region with CFTR polypeptides.**

Affinity curves from figures 17 and 18 were re-organized per phosphorylation condition showing interaction of the N-terminal lasso motif (blue), cytoplasmic loop 1 (black), cytoplasmic loop 2 (red), cytoplasmic loop 3 (light green), cytoplasmic loop 4 (gold) and C-terminal tail (dark green) with the unphosphorylated **(A)**, or PKA-phosphorylated **(B)**, or PKA + PKC-phosphorylated **(C)** R-regions.

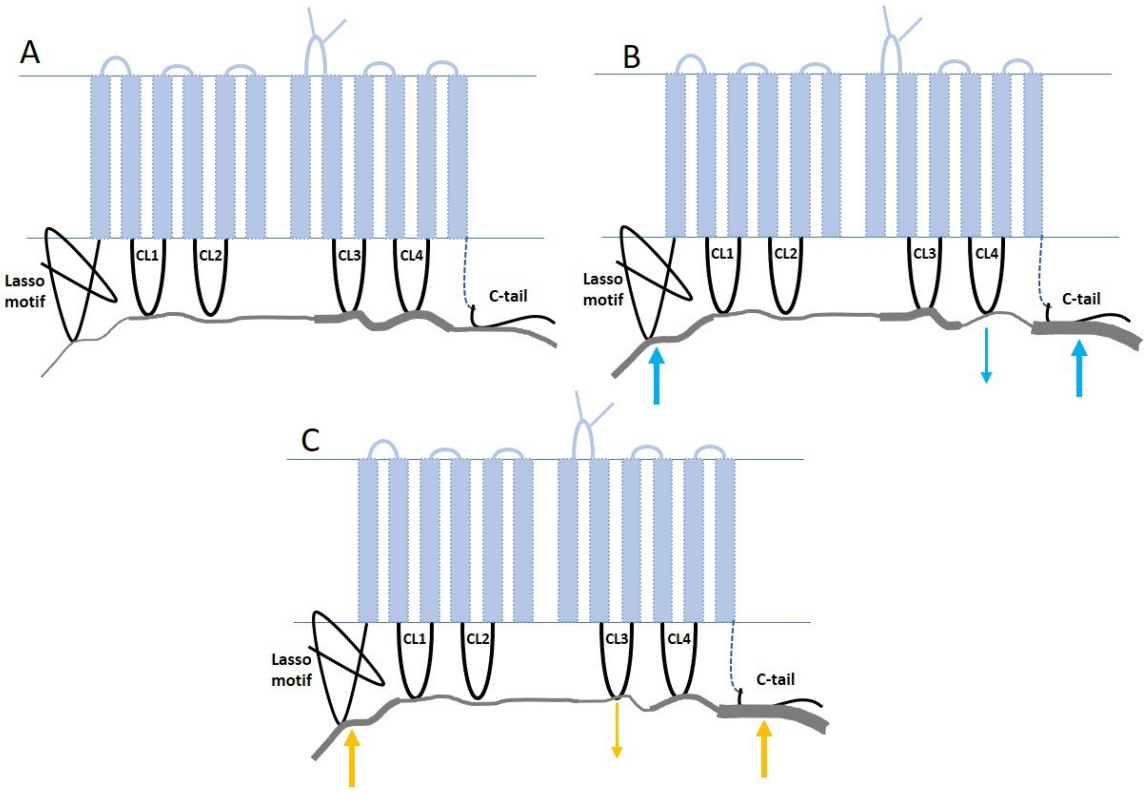


**Figure 28. Schematic model of the R-region interaction with the CFTR polypeptides.**

Interaction of the R-region with six CFTR cytoplasmic polypeptides was tested *in vitro* and the corresponding localization of each polypeptide in the full length CFTR protein is shown as black ribbons. Effect of R-region phosphorylation by PKA or PKA + PKC on those interactions are shown as cyan or gold arrows, respectively. R-region is represented by a gray ribbon. **A,** the unphosphorylated R region binds weakly with the lasso motif, strongly with cytoplasmic loops (CLs) 3 and 4 and moderately with the CLs 1 and 2 and the C-tail. **B,** PKA phosphorylation increased the association of the R-region to both lasso motif and C-tail while reducing the interaction with the CL 4. **C,** Additional PKC phosphorylation (PKA + PKC) maintain the strong association of the R-region with the lasso motif and C-tail while reducing interaction with CL 3. R-region interaction with CL 1 and 2 was not affected by phosphorylation. Light blue bars represent transmembrane helices and blue lines represent the plasma membrane. NBDs were omitted for better visualization.

# CHAPTER 4: DISCUSSION

The fact that phosphorylation of the R-region is responsible for the activation of CFTR is a well-established concept, but its mechanism of action remains to be elucidated. The current data point to a mechanism where the R-region regulates channel function through interactions with multiple partners coordinated by phosphorylation of several consensus sites. Removal of individual or groups of PKA sites showed different effects in channel activity, with none of the ten PKA sites found in the R-region being specifically required for regulation, and demonstrated that these sites typically function in an additive way (Cheng et al, 1991; Rich et al, 1993; Chang et al, 1993), where most sites are stimulatory and two sites, S737 and S768, are inhibitory (Wilkinson et al, 1997). Deletion of the R-region generates channels that open spontaneously in the presence of ATP, with no need of phosphorylation (Rich et al, 1991; Ma et al, 1997, Chappe et al., 2005). Addition of exogenous unphosphorylated R-region restored inhibition while addition of exogenous phosphorylated R-region stimulates activity of those channels (Winter & Welsh, 1997, Ma et al, 1997, Ostedgaard et al, 2000, Chappe et al, 2005). Two segments of the R-region, aa 760-783 and 817-838 have been found to be important to prevent spontaneous activity, with the latter also being critical for channel response to PKA (Baldursson et al, 2000; Xie et al, 2002). All together, those studies demonstrate that the R-region orchestrate a complex regulatory mechanism for CFTR activity, where multiple interactions of the unphosphorylated R-region play inhibitory roles, keeping the channel closed and

phosphorylation relieves inhibitory interactions, potentially also promoting stimulatory interactions that activate the channel.

In order to conceptualize such a complex regulation, we must consider that the R-region is an intrinsically disordered region (IDR) of CFTR that behaves as an intrinsically disorder protein (IDP). Rather than forming stable well-folded structure, IDPs alternate between several flexible interchangeable conformations in physiological conditions (Wright & Dyson, 1999). Besides this flexibility, IDPs have other features such as a low complex and biased primary sequence, with a low rate of hydrophobic and a high rate of hydrophilic amino acids, the presence of multiple accessible sites for post-translational modification (i.e. phosphorylation sites), short linear binding motifs, and the capacity of binding with high specificity but moderate affinity. Those features are implied to grant advantages to IDPs in signalling and regulatory processes where multiple quick-reversible interactions with several binding partners are all-important. During those processes, several interactions are formed and IDPs can engage in multiple complexes, binding to distinct partners transiently and dynamically through multiple, often overlapping binding sites, while still accessible to a delicate control by cellular signals and post-translational modifications, allowing them to function as ‘switches’ (on-off signals) or ‘rheostats’ (gradation of signals) and in some cases providing a link between two related processes (Dyson & Wright, 2005; Wright & Dyson, 2015).

As an IDR of CFTR (Baker et al, 2007; Bozoki et al, 2013), the R-region probably exerts its regulation on CFTR function by local conformational shifts induced by

phosphorylation which change the number and strength of interactions with distinct parts of the channel. Several partners for intramolecular interactions with the R-region, including all other CFTR subdomains, have been described (Naren et al, 1999; Wang et al, 2002; Baker et al, 2007; Wang & Duan, 2012; Bozoki et al, 2013). Because the R-region is unique to CFTR and there is no other related protein in all kingdoms of life (Sebastian et al, 2013) that can be used as a template, homology modeling of the R-region is impossible. This and the fact that attempts to predict R-region structure using computational methods have generated conflicting results (Hegedus et al, 2008; Mornon et al, 2009), hindering the comprehension of how the R-region is arranged in the context of the full-length protein and how it activates CFTR when phosphorylated.

Recently, electron cryo-microscopy structures of the full-length CFTR from zebrafish and human, in both unphosphorylated and phosphorylated states were determined (Zhang & Chen, 2016; Liu et al, 2017; Zhang et al, 2017; Zhang et al, 2018). The two orthologs share 55% residues identity, and were found to be very similar, displaying a mostly disordered R-region positioned between the NBDs and the cytoplasmic loops. In both structures, the R-region has multiples contacts with both halves of the molecule, consistent with the model proposed here. In the phosphorylated state, the R-region was displaced from between the NBDs and becomes even more unstructured and not visible in cryo-EM maps, except for a small helix and a couple of small amorphous densities. Because of the unstructured nature of the R-region, the novel full-length CFTR structures were unable to provide significant insights into the interacting partners of the

phosphorylated R-region. Therefore, the data presented here, showing the R-region dynamic interactions *in situ* and *in vitro* in response to PKA and PKC stimulations, contribute with novel findings for the understanding of how the R-region regulates channel activity. Moreover, it proposes a model that explains PKC enhancing effect which was described functionally but not structurally.

### 4.1 Split-CFTR Channels Bearing PKC Mutations are Functionally Reassembled at the Cell Surface

All split-CFTR constructs used in the present study were successfully expressed in BHK cells, consistent with the variable structural organization of core domains in ABC transporters and previous studies (Chappe et al, 2005; Seavilleklein et al, 2008). In previous studies, although no mature complex glycosylated form of the wild type split-CFTR construct was detected after expression in BHK cells, functional reassembly of the core glycosylated isoform of CFTR at the plasma membrane was confirmed by cell surface biotinylation, immunofluorescence localization, iodide efflux assays, and patch clamping (Chappe et al, 2005). It was thus demonstrated that complex glycosylation is not a definite determinant for CFTR targeting to the apical membrane or for its activity as a chloride channel (Morris et al, 1993). Also, a portion of immature CFTR can be trafficked to the membrane through a nonconventional pathway (Yoo et al, 2002).

Insertion of mutations in the R region did not prevent the expression and functional re-assembly of the 3 domains at the cell surface. Expression of split-ΔR was less efficient compared to full length CFTR, but enough for detection of

substantial activity by both iodide efflux and patch clamp assays (Irvine, 2002; Chappe et al, 2005). Similar to SR-WT (Chappe et al, 2005), SR-7CA (Seavilleklein et al, 2008), SR-6CA, SR-S641A/T682A and SR-S686A (Amer, 2010), the three polypeptides of the new SR-S686D construct introduced in this work reassembled and co-localized at the cell surface as visualized in immunolabeling assays using specific antibodies for each polypeptide (Figure 15).

SR-S686D responses to PKA were amplified compared to SR-WT, reaching levels equivalent to responses observed only when SR-WT channels were pre-treated with PKC before PKA stimulation. Serine-to-aspartate mutations to mimic the effect of addition of negatively charged phosphates groups were previously tested in several proteins including CFTR. In another study, substitution of no less than six serine residues within PKA sites for aspartate generated a mild constitutive activity that was enhanced by cAMP treatment (Rich et al, 1993). Interestingly, this constitutive activity was only observed after S686 (which was thought to be a PKA site in that study) was included in the list of sites mutated in that study, consistent with the mild increase found in basal (constitutive) activity of the SR-S686D in the present study.

Expression of S686A channels in oocytes and BHK cells showed contrasting results in previous works. In oocytes, whole-cell measurements after IBMX and FSK stimulation did not show any alteration in channel response (Wilkinson et al, 1997). In contrast, single channel measurements in BHK cells showed a dramatic reduction in responses to PKA and abolition of the PKC enhancing effect

(Chappe et al, 2004). In the present work, SR-S686A responses to PKA, measured by iodide efflux, were comparable to SR-WT but this channel was insensitive to PKC, abolishing the enhancing effect (Figure 16 G). The considerable differences found in responses to PKA or PKC + PKA of SR-S686D and SR-S686A suggests that modifications at this specific site disturb significantly the sensitivity of CFTR to kinases.

### 4.2 Modulation of the Wild Type R-region Interactions with the CFTR Halves by Phosphorylation

*In situ* PLA data showing the dynamics of interactions between the R-region and both front and back halves of CFTR, under different stimulation conditions, allowed us to consider the channel structure/function relationship in its native cell environment and to investigate the molecular mechanism by which phosphorylation regulates CFTR activity. I found that the unphosphorylated R-region (basal conditions) interacts similarly with both halves of the channel, consistent with several other studies (Wang et al, 2002; Baker et al, 2007; Wang, 2010; Wang & Duan, 2012; Bozoki et al, 2013; Zhang & Chen, 2016; Liu et al, 2017). This basal level of interaction is thought to keep the channel in the closed state, most probably by preventing the NBDs interaction, as demonstrated by NMR data (Bozoki et al, 2013) and by the R-region densities that were found to be located between the two NBDs in the unphosphorylated CFTR structures (Zhang & Chen, 2016; Liu et al, 2017). Here, *in situ* PLA data confirmed that phosphorylation of the R-region by PKA significantly enhances its interaction with

other parts of the channel, as previously reported (Chappe et al, 2005; Seavilleklein et al, 2008). Moreover, I found that FH-R interactions are particularly increased by PKA and further increased by additional PKC phosphorylation (Figure 19 C). Although *in vitro* interactions of the R-region with the NBD1 domain (part of the FH construct) alone was reported to be considerably reduced after PKA phosphorylation (Baker et al, 2007; Bozoki et al, 2013), a well conserved, highly charged segment comprising the second helix of the lasso motif (aa 46-60) was shown to interact with the R-region after PKA phosphorylation (Naren et al, 1999). Successive elimination of negatively charged residues within the second lasso motif helix was shown to gradually reduce both channel activity and binding to the R-region, therefore pointing this segment as a good candidate binding partner of the PKA-phosphorylated R-region. Indeed, the recent human CFTR crystal structure in the phosphorylated state shows a helix which is proposed to be part of the R-region interacting with residues 34-39 of the lasso motif (Zhang et al, 2018). Data obtained in the present study with *in vitro* MST assays, show a great increase in the R-region interaction with the peptide containing the lasso motif after PKA phosphorylation (Figure 24 A). In the human structure (Zhang et al, 2018), phosphorylation did not completely displace the R-region from NBD1, instead, it seems to create additional binding sites with areas away from the NBD dimer surface. Newly formed interactions may contribute to the channel activation through favoring NBDs dimer formation, ATP binding and hydrolysis or the NBDs-TMDs communication, as suggested previously (Ma et al, 1997). I propose that these

newly formed interactions contribute to the increased FH-R interactions found in situ by PLA in the present work.

In this study, the FH of the channel was found to be the major recipient area for the phosphorylated R-region, which supports CFTR function. Consistent with this, phosphorylation by both PKC and PKA, which increase channel responses to PKA by 2-fold (Jia et al, 1997; Chappe et al, 2003), induced the strongest binding of the R-region to the front half, yet leaving binding to the back half unaltered, indicating that more interactions were formed, rather than a relocation of the R-region. This further enhancement in FH-R interactions was then proposed to be related to the PKC enhancing effect.

Phosphorylation by PKC alone is known to elicit only minor CFTR activity and in this study, it did not cause any significant change in the R-region interaction profile. This pattern differs from previous immunoprecipitation experiments that showed an increased R-region binding to both halves of CFTR after stimulation by PKC alone (Seavilleklein et al, 2008). Co-immunoprecipitation experiments used in previous studies require cell lysis and protein purification which significantly impacts proteins organization and interactions which are later probed in non-native, lipid-free environment. The PLA experiments used in the present study analyze protein interactions *in situ* (i.e. in intact cells) preserving the membrane environment and all cytosolic interacting partners that could be competing for binding to the R-region. Also, it is a more sensitive and specific technique (*see section 2.10 in Material and Methods*) to evaluate transient and fast interactions made by disordered proteins like the R-region. For instance, the

unphosphorylated R-region was not found in pull downs with the two CFTR halves (Seavilleklein et al, 2008), although substantial interactions of unphosphorylated R-region with both NBDs have been described (Baker et al, 2007; Bozoki et al, 2013). Those interactions were now detected in the *in situ* PLA experiments.

*In situ* BH-R interactions were significantly increased after PKA stimulation (Figure 19 C). Moreover, phosphorylation enhanced the *in vitro* association of the R-region with the C-tail peptide designed for the present study (Figure 25 C). Previously, PKA phosphorylation was shown to reduce R-region interactions with NBD2 (part of the BH construct), but also to induce a strong interaction with the C-terminal tail of CFTR (aa 1438-1480) (Bozoki et al, 2013).

### 4.3 PKC SITE S686 IS KEY FOR R-REGION INTERACTIONS INVOLVED IN THE PKC ENHANCING EFFECT

Removal of PKC sites was previously shown to modify CFTR responses to phosphorylation by PKA and PKC, in both full-length and half-CFTR channels (Chappe et al, 2004; Seavilleklein et al, 2008), indicating an important functional role for these sites. Thus, it raised the question to whether disabling these PKC sites would also impact the R-region interacting profile. Indeed, *in vitro* interaction of the R-region was lost in immunoprecipitation experiments using a R-region lacking all seven PKC sites (Seavilleklein et al, 2008). I thus investigated the effect of mutations at PKC sites in the R-region interaction, *in situ,* to refine our model and better understand the regulation of CFTR activity by PKC. All PKC

mutant constructs studied here displayed alterations, to different degrees, in the R-region interactions to the CFTR halves and some striking changes could be fairly associated with functional impairments. The R-region, as a disordered segment, can make transient connections, where multiple segments can bind and detach dynamically from a variety of interaction partners, as indicated in NMR studies (Baker et al, 2007, Bozoki et al, 2013). In our model, the unphosphorylated R-region binds to both halves equally. PKC phosphorylation alone did not change the pattern observed at basal conditions, consistent with CD spectra data showing that PKC phosphorylation do not induce the conformational changes observed with PKA phosphorylation (Dulhanty & Riordan, 1994). This is also consistent with functional studies that show very minor current after PKC phosphorylation alone (Tabcharani et al, 1991; Berger et al, 1993, Chappe et al, 2003). However, PKC phosphorylation induced a marked increase of R-region interaction with the FH over PKA alone, consistent with the PKC enhancing effect on CFTR activity. Among the mutant constructs studied here, SR-S686D and SR-S641A/T682A can be classified as ‘gain of function’ while SR-S686A as a ‘loss of function’ mutant. Reduced FH-R interactions at basal conditions were observed in SR-S641A/T682A channels but that did not prevent their response to phosphorylation. A construct where the only functional PKC site is S686 (SR-6CA) showed even weaker FH-R interactions, but still responded to phosphorylation similarly to SR-WT in iodide efflux measurements. In contrast, reduced binding of the R-region to the BH at basal conditions, as observed in S686A channels, was associated with the inability of this mutant to

strongly increase R-region interactions with the FH in response to PKC + PKA phosphorylation, thus abolishing the PKC enhancing effect. The opposite mutation, S686D, on the other hand, displayed normal basal BH-R and FH-R interactions and was overresponsive to phosphorylation. Furthermore, SR-6CA, that had similar basal BH-R interactions as SR-WT was able to increase FH-R interactions after PKC + PKA phosphorylation and SR-S641A/T682A, that displayed a 3.5-fold increase in basal BH-R compared to SR-WT, had its FH-R interaction after PKC + PKA increased by a similar level (~3-fold). These results demonstrate that interactions of the unphosphorylated R-region with the BH are crucial for the phosphorylation-induced increased interactions of the R region with the FH, resulting in channel activation. These data also suggest a mechanism where strong anchoring of the unphosphorylated R-region to unidentified regions in the BH is critical for the R-region phosphorylation-dependent interaction with the FH which regulates CFTR activity.

### 4.4 Phosphorylation Induces R-region Interactions with the N- and C-Terminal Domains of CFTR

In order to improve the model derived from *in situ* PLA data, I used MST experiments to investigate R-region interactions with the cytoplasmic loops within each half of CFTR as well as with the amino and carboxyl ends of the protein. Acquisition of sufficient amounts of soluble recombinant R-region peptides for protein-protein assays has been proved challenging and, in the literature, only a few studies, have reported successful purifications of the whole R region. A 124-

residues peptide (aa 708-831) was purified to ~400 μM (Ostedgaard et al, 2000), while a longer peptide of 185 residues (aa 654-838), carrying a F833L polymorphism (Baker et al, 2007; Bozoki et al, 2013) was purified to ~500 μM. Other studies have used a purified 190-residues peptide (aa 645-834) but maximal concentrations were not reported (Picciotto et al, 1992; Winter & Welsh, 1997).

The R-region used in the present study was slightly longer (202 residues; aa 635-836) to contain the consensus PKC site at position 641. The N-terminal of this construct differs from the two previous long constructs reported by the addition of the final residues of helix H8 and the whole helix H9 described in the mouse and human NBD1 structures (Lewis et al, 2004; 2005). Here, even with the use of GB1 domain as a solubilizing tag partner, the presence of the N-terminal helical segment may explain the low yield of ~350 μM of soluble R-region at the maximum. Even trying to include the F833L polymorphism as used by others (Baker et al, 2007) did not improve significantly the solubility of the R-region.

The MST technique requires only small amounts of soluble protein for probing protein-protein interactions (<50μL of R-region was used for each experiment) and for that reason this method was chosen to test *in vitro* R-region interactions with the cytoplasmic regions of CFTR.

My result show that the R-region interacts with all peptides tested with moderate affinities (in the micromolar range), consistent the expected behaviour of an intrinsically disordered protein (Dyson & Wright, 2005; Wright & Dyson, 2015).

Previous data also demonstrated this promiscuous behaviour with multiple segments of the R-region interacting with different partners (Bozoki et al, 2013). In addition, EM densities attributed to the R-region in the unphosphorylated structures of CFTR show interactions with several areas of the protein (Zhang & Chen, 2016; Liu et al, 2017).

Phosphorylation strongly enhanced interactions of the R-region with the lasso motif and the C-tail by 2.5-fold and 2.3-fold respectively, while only a smaller but significant reduction in the interaction with CLs 3 and 4 was observed (Figure 27). Deletion of the C-tail was shown to reduce by half the open probability of CFTR in epithelial cells (Ostedgaard et al, 2003) and phosphorylation-induced interactions with the C-tail were previously suggested to be involved in stimulation of NBDs dimerization and channel function (Bozoki et al, 2013). The latter study also showed that interactions between the R-region and C-tail, which is also disordered, caused a certain degree of ordering, at least in part, of those segments, an outcome not common in R-region interactions with other parts of CFTR tested in the study (Bozoki et al, 2013).

The disordered C-tail segment is not visible in the unphosphorylated structures of CFTR, but it becomes partially ordered in the phosphorylated structures. Interestingly, the extra thirteen residues resolved at the C-tail in the phosphorylated human structure form a small helix that is positioned just near one of the R-region densities (Zhang et al, 2018), providing further support for a possible disorder-to-order transition involved in this interaction.

R-region interactions with the lasso motif were also previously reported, but their association with phosphorylation was not very clear (Naren et al, 1999). In the present study, I demonstrate for the first time an association with the lasso motif that is strongly dependent on phosphorylation.

Because interactions with CLs 1 and 2 were not affected by phosphorylation, the increased interaction with the FH observed *in situ* (in cells) with PLA can be attributed to the lasso motif. Consequently, I propose that the Lasso-R interactions are responsible at least in part for the channel activation induced by PKA phosphorylation, probably in combination with interactions with the C-tail.

With MST *in vitro* experiments, I could not reproduce the dramatic increase in FH-R interactions observed after PKC + PKA stimulation *in situ* compared to PKA alone stimulation. A possible explanation for this is that inside the cells multiple other partners are interacting with the R-region and the lasso motif, for instance syntaxin 1A (Naren et al, 1997; Naren et al, 2000), and in the absence of optimal physiological conditions where CFTR engages in several complexes with scaffold proteins, this interaction may not be formed.

In addition, my data suggests that R-region displacement from CLs 3 and 4 also support the channel function. Missense mutations in both CLs 3 and 4 have been found in patients with CF, with some of them reported to disturb channel gating, altering the open probability of the channel and to promote a small change in channel conductance (Seibert et al, 1996a; 1996b). Also, mutation of a well conserved residue in CL 3, K978, leads to ATP-independent channel activity (Wang et al, 2010). The involvement of those loops in channel gating and

conductance suggest that, perhaps, small adjustments in those channel properties underlie the mechanism by which R-region interactions with those loops regulate channel function. In fact, MST data showed that R-region release from those loops was fine-tuned with its phosphorylation state with partial displacement of the R-region from the CL 4 after PKA phosphorylation suggested to aid in CFTR activation by PKA, and partial displacement from the CL 3 after dual phosphorylation suggested to be involved in the mechanism for the PKC enhancing effect.

In summary, the results reported here complement previous data on the R-region interactions (Bozoki et al, 2013) and suggest a model where phosphorylation controls R-region dynamic interactions with all cytoplasmic domains of CFTR. When in resting conditions strong interactions with the NBDs and cytoplasmic loops 3 and 4 keep the channel closed. Phosphorylation does not only decrease inhibitory interactions with those central areas of the protein but also stimulates new interactions with peripheral areas, the N- and C-terminus, which facilitate channel activation.

### 4.5 Conclusion and Importance of the Study

The present study provides new insights on the understanding of the R-region dynamics, analyzing *in situ* interactions with the front and back halves of CFTR as well as *in vitro* interactions with six cytoplasmic subdomains in three different phosphorylation conditions (PKA, PKC and PKC + PKA). Together with previous results reported by our group (Chappe et al, 2004; Chappe et al, 2005;

Seavilleklein et al. 2008), the present findings reinforce the importance of PKC sites in CFTR function and domains interaction. They show that R-region dynamics change considerably with different phosphorylation states which may reflect the mechanisms used by different kinases to regulate CFTR activity. The molecular model proposed here shows that R-region interactions within the front half, especially with the lasso motif, are important to regulate phosphorylation-dependent activation of the channel. Interactions with the C-terminal tail, part of the back half, also support function. Moreover, I propose that PKC enhancing effect is mediated by a permissive interaction of the R-region with the back half of CFTR, with PKC site S686 being crucial in this mechanism. Future experiments investigating interactions of recombinant R-regions carrying S686A or S686D mutations with the cytoplasmic subdomains of CFTR may provide more information about this mechanism.

Unfortunately, at the moment, with the technology available, we still do not have enough data to predict what is the actual conformation of the R-region in the whole protein. As the R-region controls channel function, a lot is missing on the molecular mechanism of channel activation. The R-region is physically present in between the two halves but, is it interfering directly with ATP binding or hydrolysis? Or is it exerting its inhibition by just sterically blocking NBDs dimerization? Do the interactions with the cytoplasmic loops affect directly the pore properties? How the phosphorylated R-region stimulates channel function? Those are few out of many questions that still remain to be answered.

The disordered nature of the R-region has prevented the resolution of most of its sequence in all crystal structures currently available, with the two helices and some patches of densities ascribed to be parts of the R-region combined with extensive biochemical and functional data nurturing the speculations about its mechanism of action. The specific interaction sites in each of the CFTR halves that are involved in both inhibitory and stimulatory functions of the R-region still need to be discovered; however, the comprehension of how phosphorylation changes the R-region dynamics in the context of the full CFTR protein, in its native membrane environment, like it was demonstrated in this study, is of fundamental importance to understand the mechanism by which phosphorylation regulates CFTR activation. Also, the finding that interactions with the lasso motif and CL 3 and 4 are modulated by phosphorylation contribute for building up a more complete model for this complex regulatory mechanism.

A better understanding of the mechanism underlying the 2-fold increase in PKA-activated CFTR currents elicited by PKC as well as the identification of the inhibitory and stimulatory interactions of the R-region may facilitate the design of therapeutic drugs (potentiators) that either compete with the unphosphorylated R-region and (partially) release its inhibition or mimic the R-region stimulation on CFTR gating to treat patients that have mutant forms of classes III, IV or V, that escape from the ERQC machinery, reach the cell surface but are incapable of generate ion currents.

# REFERENCES


1. The Clinical and Functional Translation of CFTR (CFTR2). Retrieved from https://cftr2.org/ (accessed April 2, 2019).
2. Cystic Fibrosis Mutation Database. Retrieved from http://www.genet.sickkids.on.ca (accessed April 2, 2019). Last updated 25 Apr 2011.
3. Cystic Fibrosis Foundation – Sweat test. Retrieved from https://www.cff.org/What-is-CF/Testing/Sweat-Test/ (accessed June 28, 2019)
4. Aleksandrov L, Aleksandrov AA, Chang XB, Riordan JR. The First Nucleotide Binding Domain of Cystic Fibrosis Transmembrane Conductance Regulator Is a Site of Stable Nucleotide Interaction, whereas the Second Is a Site of Rapid Turnover. Journal of Biological Chemistry 2002;277(18):15419-15425.
5. Alshafie W, Chappe FG, Li M, Anini Y, Chappe VM. VIP regulates CFTR membrane expression and function in Calu-3 cells by increasing its interaction with NHERF1 and P-ERM in a VPAC1-and PKCε-dependent manner. American Journal of Physiology-Cell Physiology 2014;307(1):C107-C119.
6. Amer, Noha (2010). Serine 686 is critical for PKA association of the R Domain with other regions of CFTR. Master Thesis. Dalhousie University, Halifax, Canada.
7. Andersen DH. Cystic fibrosis of the pancreas and its relation to celiac disease: a clinical and pathologic study. American journal of Diseases of Children 1938;56(2):344-399.
8. Andersen DH, Hodges RG. Celiac syndrome: V. genetics of cystic fibrosis of the pancreas with a consideration of etiology. American journal of diseases of children 1946;72(1):62-80.
9. Anderson MP, Berger HA, Rich DP, Gregory RJ, Smith AE, Welsh MJ. Nucleoside triphosphates are required to open the CFTR chloride channel. Cell 1991;67(4):775-784.
10. Armstrong DS, Hook SM, Jamsen KM, Nixon GM, Carzino R, Carlin JB, et al. Lower airway inflammation in infants with cystic fibrosis detected by newborn screening. Pediatric Pulmonology 2005;40(6):500-510.

11. Auerbach M, Liedtke CM. Role of the scaffold protein RACK1 in apical expression of the cystic fibrosis transmembrane regulator (CFTR). American Journal of Physiology-Cell Physiology 2007;293(1):C294-C304.

12. Bai Y, Li M, Hwang T. Dual roles of the sixth transmembrane segment of the CFTR chloride channel in gating and permeation. The Journal of General Physiology 2010;136(3):293-309.

13. Bai Y, Li M, Hwang TC. Structural basis for the channel function of a degraded ABC transporter, CFTR (ABCC7). The Journal of General Physiology 2011;138(5):495-507.

14. Baker JM, Hudson RP, Kanelis V, Choy W, Thibodeau PH, Thomas PJ, et al. CFTR regulatory region interacts with NBD1 predominantly via multiple transient helices. Nature structural & molecular biology 2007;14(8):738-745.

15. Baldursson O, Berger HA, Welsh MJ. Contribution of R domain phosphoserines to the function of CFTR studied in Fischer rat thyroid epithelia. American Journal of Physiology-Lung Cellular and Molecular Physiology 2000;279(5):L835-L841.

16. Basso C, Vergani P, Nairn AC, Gadsby DC. Prolonged nonhydrolytic interaction of nucleotide with CFTR's NH2-terminal nucleotide binding domain and its role in channel gating. The Journal of General Physiology 2003;122(3):333-348.

17. Bear CE, Li C, Kartner N, Bridges RJ, Jensen TJ, Ramjeesingh M, et al. Purification and functional reconstitution of the cystic fibrosis transmembrane conductance regulator (CFTR). Cell 1992;68(4):809-818.

18. Becq F, Auzanneau C, Norez C, Derand R, Bulteau-Pignoux L. Radiotracer flux method to study CFTR channel activity: regulation, pharmacology and drug discovery. European Working Group on CFTR Expression 2003;D5:1-13.

19. Berger HA, Travis SM, Welsh MJ. Regulation of the cystic fibrosis transmembrane conductance regulator Cl- channel by specific protein kinases and protein phosphatases. Journal Biological Chemistry 1993;25;268(3):2037-2047.

20. Berkower C, Michaelis S. Mutational analysis of the yeast a-factor transporter STE6, a member of the ATP binding cassette (ABC) protein superfamily. EMBO Journal 1991;10(12):3777-3785.

21. Bertrand CA, Zhang R, Pilewski JM, Frizzell RA. SLC26A9 is a constitutively active, CFTR-regulated anion conductance in human

bronchial epithelia. The Journal of General Physiology 2009;133(4):421-438.

22. Biemans-Oldehinkel E, Doeven MK, Poolman B. ABC transporter architecture and regulatory roles of accessory domains. FEBS Letters 2006;580(4):1023-1035.

23. Billet A, Jia Y, Jensen T, Riordan JR, Hanrahan JW. Regulation of the cystic fibrosis transmembrane conductance regulator anion channel by tyrosine phosphorylation. The FASEB Journal 2015;29(9):3945-3953.

24. Billet A, Jia Y, Jensen TJ, Hou Y, Chang X, Riordan JR, et al. Potential sites of CFTR activation by tyrosine kinases. Channels 2016;10(3):247-251.

25. Bompadre SG, Ai T, Cho JH, Wang X, Sohma Y, Li M, et al. CFTR gating I: Characterization of the ATP-dependent gating of a phosphorylation-independent CFTR channel (DeltaR-CFTR). The Journal of General Physiology 2005;125(4):361-375.

26. Bompadre SG, Sohma Y, Li M, Hwang TC. G551D and G1349D, two CF-associated mutations in the signature sequences of CFTR, exhibit distinct gating defects. The Journal of General Physiology 2007;129(4):285-298.

27. Bovell D. The human eccrine sweat gland: structure, function and disorders. Journal of Local and Global Health Science 2015:5.

28. Boyle MP, De Boeck K. A new era in the treatment of cystic fibrosis: correction of the underlying CFTR defect. The Lancet Respiratory Medicine 2013;1(2):158-163.

29. Bozoky Z, Krzeminski M, Muhandiram R, Birtley JR, Al-Zahrani A, Thomas PJ, et al. Regulatory R region of the CFTR chloride channel is a dynamic integrator of phospho-dependent intra-and intermolecular interactions. Proceedings of the National Academy of Sciences of the United States of America 2013;110(47):E4427-E4436.

30. Burgel PR, Bellis G, Olesen HV, Viviani L, Zolin A, Blasi F, et al. Future trends in cystic fibrosis demography in 34 European countries. European Respiratory Journal 2015;46(1):133-141.

31. Caputo A, Caci E, Ferrera L, Pedemonte N, Barsanti C, Sondo E, et al. TMEM16A, a membrane protein associated with calcium-dependent chloride channel activity. Science 2008;322(5901):590-594.

32. Castellani C, Assael BM. Cystic fibrosis: a clinical view. Cellular and Molecular Life Sciences 2017;74(1):129-140.

33. Chan KW, Csanady L, Seto-Young D, Nairn AC, Gadsby DC. Severed molecules functionally define the boundaries of the cystic fibrosis transmembrane conductance regulator's NH(2)-terminal nucleotide binding domain. The Journal of General Physiology 2000;116(2):163-180.

34. Chang X, Cui L, Hou Y, Jensen TJ, Aleksandrov AA, Mengos A, et al. Removal of multiple arginine-framed trafficking signals overcomes misprocessing of ΔF508 CFTR present in most patients with cystic fibrosis. Molecular Cell 1999;4(1):137-142.

35. Chang XB, Tabcharani JA, Hou YX, Jensen TJ, Kartner N, Alon N, et al. Protein kinase A (PKA) still activates CFTR chloride channel after mutagenesis of all 10 PKA consensus phosphorylation sites. Journal of Biological Chemistry 1993;268(15):11304-11311.

36. Chappe V, Hinkson DA, Howell LD, Evagelidis A, Liao J, Chang X, et al. Stimulatory and inhibitory protein kinase C consensus sequences regulate the cystic fibrosis transmembrane conductance regulator. Proceedings of the National Academy of Sciences of the United States of America 2004;101(1):390-395.

37. Chappe V, Irvine T, Liao J, Evagelidis A, Hanrahan JW. Phosphorylation of CFTR by PKA promotes binding of the regulatory domain. EMBO Journal 2005;24(15):2730-2740.

38. Chappe V, Hinkson DA, Zhu T, Chang X-, Riordan JR, Hanrahan JW. Phosphorylation of protein kinase C sites in NBD1 and the R domain control CFTR channel activation by PKA. The Journal of Physiology 2003;548(1):39-52.

39. Cheng SH, Gregory RJ, Marshall J, Paul S, Souza DW, White GA, et al. Defective intracellular transport and processing of CFTR is the molecular basis of most cystic fibrosis. Cell 1990;63(4):827-834.

40. Cheng SH, Rich DP, Marshall J, Gregory RJ, Welsh MJ, Smith AE. Phosphorylation of the R domain by cAMP-dependent protein kinase regulates the CFTR chloride channel. Cell 1991;66(5):1027-1036.

41. Cheng Y, Patel DJ. An efficient system for small protein expression and refolding. Biochemical and Biophysical Research Communications 2004;317(2):401-405.

42. Cheng J, Moyer BD, Milewski M, Loffing J, Ikeda M, Mickle JE, et al. A Golgi-associated PDZ domain protein modulates cystic fibrosis transmembrane regulator plasma membrane expression. Journal of Biological Chemistry 2002;277(5):3520-3529.

43. Coakley RD, Grubb BR, Paradiso AM, Gatzy JT, Johnson LG, Kreda SM, et al. Abnormal surface liquid pH regulation by cultured cystic fibrosis bronchial epithelium. Proceedings of the National Academy of Sciences of the United States of America 2003;100(26):16083-16088.

44. Cohen TS, Prince A. Cystic fibrosis: a mucosal immunodeficiency syndrome. Nature Medicine 2012;18(4):509.

45. Cohen-Cymberknoh M, Kerem E, Ferkol T, Elizur A. Airway inflammation in cystic fibrosis: molecular mechanisms and clinical implications. Thorax 2013;68(12):1157-1162.

46. Csanady L, Chan KW, Nairn AC, Gadsby DC. Functional roles of nonconserved structural segments in CFTR's NH2-terminal nucleotide binding domain. The Journal of General Physiology 2005;125(1):43-55.

47. Csanady L, Chan KW, Seto-Young D, Kopsco DC, Nairn AC, Gadsby DC. Severed channels probe regulation of gating of cystic fibrosis transmembrane conductance regulator by its cytoplasmic domains. The Journal of General Physiology 2000;116(3):477-500.

48. Csanady L, Vergani P, Gadsby DC. Strict coupling between CFTR's catalytic cycle and gating of its Cl- ion pore revealed by distributions of open channel burst durations. Proceedings of the National Academy of Sciences of the United States of America 2010 Jan 19;107(3):1241-1246.

49. Cui L, Aleksandrov L, Chang X, Hou Y, He L, Hegedus T, et al. Domain interdependence in the biosynthetic assembly of CFTR. Journal of Molecular Biology 2007;365(4):981-994.

50. Davidson AL, Chen J. ATP-binding cassette transporters in bacteria. Annual Review of Biochemistry 2004;73(1):241-268.

51. Davis PB. Cystic fibrosis since 1938. American journal of respiratory and critical care medicine 2006;173(5):475-482.

52. Dawson RJ, Locher KP. Structure of a bacterial multidrug ABC transporter. Nature 2006;443(7108):180.

53. Day BJ, van Heeckeren AM, Min E, Velsor LW. Role for cystic fibrosis transmembrane conductance regulator protein in a glutathione response to bronchopulmonary pseudomonas infection. Infection and Immunity 2004;72(4):2045-2051.

54. Dean M, Annilo T. Evolution of the ATP-binding cassette (ABC) transporter superfamily in vertebrates. Annual Review of Genomics and Human Genetics. 2005;6:123-142.

55. Dean M, Rzhetsky A, Allikmets R. The human ATP-binding cassette (ABC) transporter superfamily. Genome Research 2001;11(7):1156-1166.

56. di Sant'Agnese PA. Fibrocystic disease of the pancreas, a generalized disease of exocrine glands. The Journal of the American Medical Association 1956;160(10):846-853.

57. di Sant'agnese PA, Darling RC, Perera GA, Shea E. Abnormal electrolyte composition of sweat in cystic fibrosis of the pancreas; clinical significance and relationship to the disease. Pediatrics 1953;12(5):549-563.

58. Du K, Lukacs GL. Cooperative assembly and misfolding of CFTR domains in vivo. Molecular Biology of the Cell 2009;20(7):1903-1915.

59. Dulhanty AM, Chang X, Riordan JR. Mutation of potential phosphorylation sites in the recombinant R domain of the cystic fibrosis transmembrane conductance regulator has significant effects on domain conformation. Biochemical and Biophysical Research Communications 1995;206(1):207-214.

60. Dulhanty AM, Riordan JR. Phosphorylation by cAMP-dependent protein kinase causes a conformational change in the R domain of the cystic fibrosis transmembrane conductance regulator. Biochemistry 1994;33(13):4072-4079

61. Dyson HJ, Wright PE. Intrinsically unstructured proteins and their functions. Nature Reviews Molecular Cell Biology 2005;6(3):197.

62. El Hiani Y, Negoda A, Linsdell P. Cytoplasmic pathway followed by chloride ions to enter the CFTR channel pore. Cellular and Molecular Life Sciences 2016;73(9):1917-1925.

63. El Hiani Y, Linsdell P. Functional Architecture of the Cytoplasmic Entrance to the Cystic Fibrosis Transmembrane Conductance Regulator Chloride Channel Pore. Journal of Biological Chemistry 2015;290(25):15855-15865.

64. El Hiani Y, Linsdell P. Changes in accessibility of cytoplasmic substances to the pore associated with activation of the cystic fibrosis transmembrane conductance regulator chloride channel. Journal of Biological Chemistry 2010;285(42):32126-32140.

65. Elborn JS. Cystic fibrosis. The Lancet 2016;388(10059):2519-2531.

66. Farinha CM, Canato S. From the endoplasmic reticulum to the plasma membrane: mechanisms of CFTR folding and trafficking. Cellular and Molecular Life Sciences 2017;74(1):39-55.

67. Farinha CM, Amaral MD. Most F508del-CFTR is targeted to degradation at an early folding checkpoint and independently of calnexin. Molecular and Cellular Biology 2005;25(12):5242-5252.

68. Farinha CM, Nogueira P, Mendes F, Penque D, Amaral MD. The human DnaJ homologue (Hdj)-1/heat-shock protein (Hsp) 40 co-chaperone is required for the in vivo stabilization of the cystic fibrosis transmembrane conductance regulator by Hsp70. Biochemical Journal 2002;366(3):797-806.

69. Fatehi M, Linsdell P. Novel residues lining the CFTR chloride channel pore identified by functional modification of introduced cysteines. The Journal of Membrane Biology 2009;228(3):151-164.

70. Fischer H, Machen TE. The tyrosine kinase p60c-src regulates the fast gate of the cystic fibrosis transmembrane conductance regulator chloride channel. Biophysical Journal 1996;71(6):3073-3082.

71. Flass T, Narkewicz MR. Cirrhosis and other liver disease in cystic fibrosis. Journal of Cystic Fibrosis 2013;12(2):116-124.

72. Fredriksson S, Gullberg M, Jarvius J, Olsson C, Pietras K, Gústafsdóttir SM, et al. Protein detection using proximity-dependent DNA ligation assays. Nature Biotechnology 2002;20(5):473.

73. French PJ, Bijman J, Edixhoven M, Vaandrager AB, Scholte BJ, Lohmann SM, et al. Isotype-specific activation of cystic fibrosis transmembrane conductance regulator-chloride channels by cGMP-dependent protein kinase II. Journal of Biological Chemistry 1995;270(44):26626-26631.

74. Frizzell RA, Hanrahan JW. Physiology of epithelial chloride and fluid secretion. Cold Spring Harbor Perspectives in Medicine 2012;2(6):a009563.

75. Gadsby DC, Nairn AC. Control of CFTR channel gating by phosphorylation and nucleotide hydrolysis. Physiological Reviews 1999;79(1):S77-S107.

76. Gajbhiye R, Gaikwad A. Cystic Fibrosis, CFTR Gene, and Male Infertility. Male Infertility: Understanding, Causes and Treatment: Springer; 2017. p.131-150.

77. Gao X, Bai Y, Hwang T. Cysteine scanning of CFTR's first transmembrane segment reveals its plausible roles in gating and permeation. Biophysical Journal 2013;104(4):786-797.

78. Gao X, Hwang TC. Localizing a gate in CFTR. Proceedings of the National Academy of Sciences of the United States of America 2015;112(8):2461-2466.

79. Gavet O, Pines J. Progressive activation of CyclinB1-Cdk1 coordinates entry to mitosis. Developmental cell 2010;18(4):533-543.

80. Gibson-Corley KN, Meyerholz DK, Engelhardt JF. Pancreatic pathophysiology in cystic fibrosis. The Journal of Pathology 2016;238(2):311-320.

81. Gowen C, Lawson E, Gingras-Leatherman J, Gatzy J, Boucher RC, Knowles MR. Increased nasal potential difference and amiloride sensitivity in neonates with cystic fibrosis. The Journal of Pediatrics 1986;108(4):517-521.

82. Gronenborn AM, Clore GM. Rapid screening for structural integrity of expressed proteins by heteronuclear NMR spectroscopy. Protein Science 1996;5(1):174-177.

83. Grubb BR, O'Neal WK, Ostrowski LE, Kreda SM, Button B, Boucher RC. Transgenic hCFTR expression fails to correct βENaC mouse lung disease. American Journal of Physiology-Heart and Circulatory Physiology 2011;302(2):L238-L247

84. Grubb BR, Gabriel SE. Intestinal physiology and pathology in gene-targeted mouse models of cystic fibrosis. American Journal of Physiology-Gastrointestinal and Liver Physiology 1997;273(2):G258-266.

85. Gullberg M, Gustafsdottir SM, Schallmeiner E, Jarvius J, Bjarnegard M, Betsholtz C, et al. Cytokine detection by antibody-based proximity ligation. Proceedings of the National Academy of Sciences of the United States of America 2004;101(22):8420-8424.

86. Gunderson KL, Kopito RR. Conformational states of CFTR associated with channel gating: the role of ATP binding and hydrolysis. Cell 1995;82(2):231-239.

87. Gunderson KL, Kopito RR. Effects of pyrophosphate and nucleotide analogs suggest a role for ATP hydrolysis in cystic fibrosis transmembrane regulator channel gating. Journal of Biological Chemistry 1994;269(30):19349-19353.

88. Haller W, Ledder O, Lewindon PJ, Couper R, Gaskin KJ, Oliver M. Cystic fibrosis: an update for clinicians. Part 1: nutrition and gastrointestinal complications. Journal of Gastroenterology and Hepatology 2014;29(7):1344-1355.

89. Hallows KR, Raghuram V, Kemp BE, Witters LA, Foskett JK. Inhibition of cystic fibrosis transmembrane conductance regulator by novel interaction

with the metabolic sensor AMP-activated protein kinase. Journal of Clinical Investigation 2000;105(12):1711-1721.

90. Hammond C, Braakman I, Helenius A. Role of N-linked oligosaccharide recognition, glucose trimming, and calnexin in glycoprotein folding and quality control. Proceedings of the National Academy of Sciences of the United States of America 1994;91(3):913-917.

91. Haynes C, Oldfield CJ, Ji F, Klitgord N, Cusick ME, Radivojac P, et al. Intrinsic disorder is a common feature of hub proteins from four eukaryotic interactomes. PLoS Computational Biology 2006;2(8):e100.

92. He L, Aleksandrov AA, Serohijos AW, Hegedus T, Aleksandrov LA, Cui L, et al. Multiple membrane-cytoplasmic domain contacts in the cystic fibrosis transmembrane conductance regulator (CFTR) mediate regulation of channel gating. Journal of Biological Chemistry 2008;283(39):26383-26390.

93. Hegedűs T, Serohijos AW, Dokholyan NV, He L, Riordan JR. Computational studies reveal phosphorylation-dependent changes in the unstructured R domain of CFTR. Journal of Molecular Biology 2008;378(5):1052-1063.

94. Higgins CF. ABC transporters: from microorganisms to man. Annual Review of Cell Biology 1992;8(1):67-113.

95. Hoegger MJ, Fischer AJ, McMenimen JD, Ostedgaard LS, Tucker AJ, Awadalla MA, et al. Impaired mucus detachment disrupts mucociliary transport in a piglet model of cystic fibrosis. Science 2014;345(6198):818-822.

96. Hong JH, Park S, Shcheynikov N, Muallem S. Mechanism and synergism in epithelial fluid and electrolyte secretion. Pflügers Archiv-European Journal of Physiology 2014;466(8):1487-1499.

97. Huang J, Shan J, Kim D, Liao J, Evagelidis A, Alper SL, et al. Basolateral chloride loading by the anion exchanger type 2: role in fluid secretion by the human airway epithelial cell line Calu-3. The Journal of Physiology 2012;590(21):5299-5316.

98. Hung L, Wang IX, Nikaido K, Liu P, Ames GF, Kim S. Crystal structure of the ATP-binding subunit of an ABC transporter. Nature 1998;396(6712):703.

99. Hwang TC, Lu L, Zeitlin PL, Gruenert DC, Huganir R, Guggino WB. Cl-channels in CF: lack of activation by protein kinase C and cAMP-dependent protein kinase. Science 1989;244(4910):1351-1353.

100. Hwang TC, Nagel G, Nairn AC, Gadsby DC. Regulation of the gating of cystic fibrosis transmembrane conductance regulator C1 channels by phosphorylation and ATP hydrolysis. Proceedings of the National Academy of Sciences of the United States of America 1994;91(11):4698-4702.

101. Hwang TC, Yeh JT, Zhang J, Yu YC, Yeh HI, Destefano S. Structural mechanisms of CFTR function and dysfunction. The Journal of General Physiology 2018;150(4):539-570.

102. Hyde SC, Gill DR, Higgins CF, Trezise AE, MacVinish LJ, Cuthbert AW, et al. Correction of the ion transport defect in cystic fibrosis transgenic mice by gene therapy. Nature 1993;362(6417):250.

103. Iakoucheva LM, Radivojac P, Brown CJ, O'Connor TR, Sikes JG, Obradovic Z, et al. The importance of intrinsic disorder for protein phosphorylation. Nucleic Acids Research 2004;32(3):1037-1049.

104. Irvine, Thomas (2002). Studies of split R domain deleted CFTR channels expressed in mammalian cells. Master Thesis. McGill University, Montreal, Canada.

105. Itani OA, Chen JH, Karp PH, Ernst S, Keshavjee S, Parekh K, et al. Human cystic fibrosis airway epithelia have reduced Cl- conductance but not increased Na+ conductance. Proceedings of the National Academy of Sciences of the United States of America 2011;108(25):10260-10265.

106. Jerabek-Willemsen M, André T, Wanner R, Roth HM, Duhr S, Baaske P, et al. MicroScale Thermophoresis: Interaction analysis and beyond. Journal of Molecular Structure 2014;1077:101-113.

107. Jia Y, Mathews CJ, Hanrahan JW. Phosphorylation by protein kinase C is required for acute activation of cystic fibrosis transmembrane conductance regulator by protein kinase A. Journal of Biological Chemistry 1997;272(8):4978-4984.

108. Jih KY, Sohma Y, Li M, Hwang TC. Identification of a novel post-hydrolytic state in CFTR gating. The Journal of General Physiology 2012a;139(5):359-370.

109. Jih KY, Sohma Y, Hwang TC. Nonintegral stoichiometry in CFTR gating revealed by a pore-lining mutation. The Journal of General Physiology 2012b;140(4):347-359.

110. Kanelis V, Hudson RP, Thibodeau PH, Thomas PJ, Forman-Kay JD. NMR evidence for differential phosphorylation-dependent interactions in WT and ΔF508 CFTR. EMBO Journal 2010;29(1):263-277.

111. Kelly A, Moran A. Update on cystic fibrosis-related diabetes. Journal of Cystic Fibrosis 2013;12(4):318-331.

112. Kim JY, Han W, Namkung W, Lee JH, Kim KH, Shin H, et al. Inhibitory regulation of cystic fibrosis transmembrane conductance regulator anion-transporting activities by Shank2. Journal of Biological Chemistry 2004;279(11):10389-10396.

113. King Jr JD, Fitch AC, Lee JK, McCane JE, Mak DD, Foskett JK, et al. AMP-activated protein kinase phosphorylation of the R domain inhibits PKA stimulation of CFTR. American Journal of Physiology-Cell Physiology 2009;297(1):C94-C101.

114. King S, Sorscher E. R-domain interactions with distal regions of CFTR lead to phosphorylation and activation. Biochemistry 2000;39(32):9868-9875.

115. Klein I, Sarkadi B, Váradi A. An inventory of the human ABC proteins. Biochimica et Biophysica Acta-Biomembranes 1999;1461(2):237-262.

116. Kleizen B, van Vlijmen T, de Jonge HR, Braakman I. Folding of CFTR is predominantly cotranslational. Molecular Cell 2005;20(2):277-287.

117. Ko SB, Zeng W, Dorwart MR, Luo X, Kim KH, Millen L, et al. Gating of CFTR by the STAS domain of SLC26 transporters. Nature Cell Biology 2004;6(4):343-350.

118. Kobelska-Dubiel N, Klincewicz B, Cichy W. Liver disease in cystic fibrosis. Przegląd Gastroenterologiczny 2014;9(3):136-141.

119. Kongsuphol P, Cassidy D, Hieke B, Treharne KJ, Schreiber R, Mehta A, et al. Mechanistic insight into control of CFTR by AMPK. Journal of Biological Chemistry 2009;284(9):5645-5653.

120. Kunzelmann K, Schreiber R, Hadorn HB. Bicarbonate in cystic fibrosis. Journal of Cystic Fibrosis 2017;16(6):653-662.

121. Lamprecht G, Heil A, Baisch S, Lin-Wu E, Yun CC, Kalbacher H, et al. The down regulated in adenoma (dra) gene product binds to the second PDZ domain of the NHE3 kinase A regulatory protein (E3KARP), potentially linking intestinal Cl-/HCO3-exchange to Na /H exchange. Biochemistry 2002;41(41):12336-12342.

122. Lazrak A, Jurkuvenaite A, Chen L, Keeling KM, Collawn JF, Bedwell DM, et al. Enhancement of alveolar epithelial sodium channel activity with decreased cystic fibrosis transmembrane conductance regulator expression in mouse lung. American Journal of Physiology-Heart and Circulatory Physiology 2011.

123. Ledder O, Haller W, Couper RT, Lewindon P, Oliver M. Cystic fibrosis: an update for clinicians. Part 2: hepatobiliary and pancreatic manifestations. Journal of Gastroenterology and Hepatology 2014;29(12):1954-1962.

124. Lee JH, Richter W, Namkung W, Kim KH, Kim E, Conti M, et al. Dynamic regulation of cystic fibrosis transmembrane conductance regulator by competitive interactions of molecular adaptors. Journal of Biological Chemistry 2007;282(14):10414-10422.

125. Levy H, Farrell PM. New challenges in the diagnosis and management of cystic fibrosis. The Journal of Pediatrics 2015;166(6):1337-1341.

126. Lewis HA, Buchanan SG, Burley SK, Conners K, Dickey M, Dorwart M, et al. Structure of nucleotide-binding domain 1 of the cystic fibrosis transmembrane conductance regulator. EMBO Journal 2004;23(2):282-293.

127. Lewis HA, Zhao X, Wang C, Sauder JM, Rooney I, Noland BW, et al. Impact of the deltaF508 mutation in first nucleotide-binding domain of human cystic fibrosis transmembrane conductance regulator on domain folding and structure. Journal of Biological Chemistry 2005;280(2):1346-1353.

128. Li J, Poulikakos PI, Dai Z, Testa JR, Callaway DJ, Bu Z. Protein kinase C phosphorylation disrupts Na+/H+ exchanger regulatory factor 1 autoinhibition and promotes cystic fibrosis transmembrane conductance regulator macromolecular assembly. Journal of Biological Chemistry 2007;282(37):27086-27099.

129. Li JD, Dohrman AF, Gallup M, Miyata S, Gum JR, Kim YS, et al. Transcriptional activation of mucin by Pseudomonas aeruginosa lipopolysaccharide in the pathogenesis of cystic fibrosis lung disease. Proceedings of the National Academy of Sciences of the United States of America 1997;94(3):967-972.

130. Liang X, Da Paula AC, Bozóky Z, Zhang H, Bertrand CA, Peters KW, et al. Phosphorylation-dependent 14-3-3 protein interactions regulate CFTR biogenesis. Molecular Biology of the Cell 2012;23(6):996-1009.

131. Linsdell P. Anion conductance selectivity mechanism of the CFTR chloride channel. Biochimica et Biophysica Acta-Biomembranes 2016;1858(4):740-747.

132. Linsdell P. Relationship between anion binding and anion permeability revealed by mutagenesis within the cystic fibrosis transmembrane conductance regulator chloride channel pore. The Journal of Physiology 2001;531(1):51-66.

133. Linsdell P, Evagelidis A, Hanrahan JW. Molecular determinants of anion selectivity in the cystic fibrosis transmembrane conductance regulator chloride channel pore. Biophysical Journal 2000;78(6):2973-2982.

134. Liu F, Zhang Z, Csanády L, Gadsby DC, Chen J. Molecular structure of the human CFTR ion channel. Cell 2017;169(1):85-95.e8.

135. Long KJ, Walsh KB. Iodide efflux measurements with an iodide-selective electrode: A non-radioactive procedure for monitoring cellular chloride transport. Methods in Cell Science 1997;19(3):207-212.

136. Loo TW, Clarke DM. Reconstitution of drug-stimulated ATPase activity following co-expression of each half of human P-glycoprotein as separate polypeptides. Journal of Biological Chemistry 1994;269(10):7750-5.

137. Loo MA, Jensen TJ, Cui L, Hou Y, Chang XB, Riordan JR. Perturbation of Hsp90 interaction with nascent CFTR prevents its maturation and accelerates its degradation by the proteasome. EMBO Journal 1998;17(23):6879-6887.

138. Luo J, Pato MD, Riordan JR, Hanrahan JW. Differential regulation of single CFTR channels by PP2C, PP2A, and other phosphatases. American Journal of Physiology-Cell Physiology 1998;274(5):C1397-C1410.

139. Luz S, Kongsuphol P, Mendes AI, Romeiras F, Sousa M, Schreiber R, et al. Contribution of casein kinase 2 and spleen tyrosine kinase to CFTR trafficking and protein kinase A-induced activity. Molecular and Cellular Biology 2011;31(22):4392-4404.

140. Ma J, Zhao J, Drumm ML, Xie J, Davis PB. Function of the R domain in the cystic fibrosis transmembrane conductance regulator chloride channel. Journal of Biological Chemistry 1997;272(44):28133.

141. Mall M, Grubb BR, Harkema JR, O'Neal WK, Boucher RC. Increased airway epithelial Na absorption produces cystic fibrosis-like lung disease in mice. Nature Medicine 2004;10(5):487.

142. Matsumura Y, Sakai J, Skach WR. Endoplasmic reticulum protein quality control is determined by cooperative interactions between Hsp/c70 protein and the CHIP E3 ligase. Journal of Biological Chemistry 2013;288(43):31069-31079.

143. McCarty NA, Zhang Z. Identification of a region of strong discrimination in the pore of CFTR. American Journal of Physiology-Lung Cellular and Molecular Physiology 2001;281(4):L852-L867.

144. McCloy RA, Rogers S, Caldon CE, Lorca T, Castro A, Burgess A. Partial inhibition of Cdk1 in G2 phase overrides the SAC and decouples mitotic events. Cell Cycle 2014;13(9):1400-1412.

145. Meacham GC, Lu Z, King S, Sorscher E, Tousson A, Cyr DM. The Hdj-2/Hsc70 chaperone pair facilitates early steps in CFTR biogenesis. EMBO Journal 1999;18(6):1492-1505.

146. Mendes AI, Matos P, Moniz S, Luz S, Amaral MD, Farinha CM, et al. Antagonistic regulation of cystic fibrosis transmembrane conductance regulator cell surface expression by protein kinases WNK4 and spleen tyrosine kinase. Molecular and Cellular Biology 2011;31(19):4076-4086.

147. Mense M, Vergani P, White DM, Altberg G, Nairn AC, Gadsby DC. In vivo phosphorylation of CFTR promotes formation of a nucleotide-binding domain heterodimer. EMBO Journal 2006;25(20):4728-4739.

148. Michelsen K, Yuan H, Schwappach B. Hide and run. Arginine-based endoplasmic-reticulum-sorting motifs in the assembly of heteromultimeric membrane proteins. EMBO Reports 2005;6(8):717-722.

149. Morales MM, Carroll TP, Morita T, Schwiebert EM, Devuyst O, Wilson PD, et al. Both the wild type and a functional isoform of CFTR are expressed in kidney. American Journal of Physiology-Renal Physiology 1996;270(6):F1038-F1048.

150. Mornon J, Lehn P, Callebaut I. Molecular models of the open and closed states of the whole human CFTR protein. Cellular and Molecular Life Sciences 2009;66(21):3469-3486.

151. Mornon J, Lehn P, Callebaut I. Atomic model of human cystic fibrosis transmembrane conductance regulator: membrane-spanning domains and coupling interfaces. Cellular and Molecular Life Sciences 2008;65(16):2594-2612.

152. Morris AP, Cunningham SA, Benos DJ, Frizzell RA. Glycosylation status of endogenous CFTR does not affect cAMP-stimulated Cl- secretion in epithelial cells. American Journal of Physiology-Cell Physiology 1993;265(3):C688-C694.

153. Naren AP, Nelson DJ, Xie W, Jovov B, Pevsner J, Bennett MK, et al. Regulation of CFTR chloride channels by syntaxin and Munc18 isoforms. Nature 1997;390(6657):302.

154. Naren AP, Cormet-Boyaka E, Fu J, Villain M, Blalock JE, Quick MW, et al. CFTR chloride channel regulation by an interdomain interaction. Science 1999;286(5439):544-548.

155. Naren AP, Di A, Cormet-Boyaka E, Boyaka PN, McGhee JR, Zhou W, et al. Syntaxin 1A is expressed in airway epithelial cells, where it modulates CFTR Cl(-) currents. Journal of Clinical Investigation 2000;105(3):377-386.

156. Norimatsu Y, Ivetac A, Alexander C, Kirkham J, O'Donnell N, Dawson DC, et al. Cystic fibrosis transmembrane conductance regulator: a molecular model defines the architecture of the anion conduction path and locates a "bottleneck" in the pore. Biochemistry 2012;51(11):2199-2212.

157. Ostedgaard LS, Baldursson O, Vermeer DW, Welsh MJ, Robertson AD. A functional R domain from cystic fibrosis transmembrane conductance regulator is predominantly unstructured in solution. Proceedings of the National Academy of Sciences of the United States of America 2000;97(10):5657-5662.

158. Ostedgaard LS, Rich DP, DeBerg LG, Welsh MJ. Association of domains within the cystic fibrosis transmembrane conductance regulator. Biochemistry 1997;36(6):1287-1294.

159. Ostedgaard LS, Randak C, Rokhlina T, Karp P, Vermeer D, Ashbourne Excoffon KJ, et al. Effects of C-terminal deletions on cystic fibrosis transmembrane conductance regulator function in cystic fibrosis airway epithelia. Proceedings of the National Academy of Sciences of the United States of America 2003;100(4):1937-1942.

160. Ousingsawat J, Kongsuphol P, Schreiber R, Kunzelmann K. CFTR and TMEM16A are separate but functionally related Cl- channels. Cellular Physiology and Biochemistry 2011;28(4):715-724.

161. Palmiter RD, Behringer RR, Quaife CJ, Maxwell F, Maxwell IH, Brinster RL. Cell lineage ablation in transgenic mice by cell-specific expression of a toxin gene. Cell 1987;50(3):435-443.

162. Paranjape SM, Mogayzel Jr PJ. Cystic Fibrosis. Pediatrics in Review 2014;35(5):194-205.

163. Park HW, Lee MG. Transepithelial bicarbonate secretion: lessons from the pancreas. Cold Spring Harbor Perspectives in Medicine 2012;2(10):a009571.

164. Patrick AE, Karamyshev AL, Millen L, Thomas PJ. Alteration of CFTR transmembrane span integration by disease-causing mutations. Molecular Biology of the Cell 2011;22(23):4461-4471.

165. Pezzulo AA, Tang XX, Hoegger MJ, Alaiwa MHA, Ramachandran S, Moninger TO, et al. Reduced airway surface pH impairs bacterial killing in the porcine cystic fibrosis lung. Nature 2012;487(7405):109.

166. Picciotto M, Cohn J, Bertuzzi G, Greengard P, Nairn A. Phosphorylation of the cystic fibrosis transmembrane conductance regulator. Journal of Biological Chemistry 1992;267(18):12742-12752.

167. Pind S, Riordan JR, Williams DB. Participation of the endoplasmic reticulum chaperone calnexin (p88, IP90) in the biogenesis of the cystic fibrosis transmembrane conductance regulator. Journal of Biological Chemistry 1994;269(17):12784-12788.

168. Pranke IM, Sermet-Gaudelus I. Biosynthesis of cystic fibrosis transmembrane conductance regulator. The International Journal of Biochemistry & Cell Biology 2014;52:26-38.

169. Qian F, El Hiani Y, Linsdell P. Functional arrangement of the 12th transmembrane region in the CFTR chloride channel pore based on functional investigation of a cysteine-less CFTR variant. Pflügers Archiv-European Journal of Physiology 2011;462(4):559.

170. Quinn DJ, Weldon S, Taggart CC. Antiproteases as therapeutics to target inflammation in cystic fibrosis. The Open Respiratory Medicine Journal 2010;4:20-31.

171. Quinton PM. Cystic fibrosis: impaired bicarbonate secretion and mucoviscidosis. The Lancet 2008;372(9636):415-417.

172. Quinton PM. Cystic fibrosis: lessons from the sweat gland. Physiology 2007;22(3):212-225.

173. Quinton PM. The neglected ion: HCO 3−. Nature Medicine 2001;7(3):292.

174. Quinton PM. Chloride impermeability in cystic fibrosis. Nature 1983;301(5899):421.

175. Reddy M, Quinton P. Functional interaction of CFTR and ENaC in sweat glands. Pflügers Archiv: European Journal of Physiology 2003;445(4):499-503.

176. Rich DP, Berger HA, Cheng SH, Travis SM, Saxena M, Smith AE, et al. Regulation of the cystic fibrosis transmembrane conductance regulator Cl-channel by negative charge in the R domain. Journal of Biological Chemistry 1993;268(27):20259.

177. Rich DP, Gregory RJ, Anderson MP, Manavalan P, Smith AE, Welsh MJ. Effect of Deleting the R Domain on CFTR-Generated Chloride Channels. Science 1991;253(5016):205-207.

178. Riordan JR, Rommens JM, Kerem B, Alon N, Rozmahel R, Grzelczak Z, et al. Identification of the cystic fibrosis gene: cloning and characterization of complementary DNA. Science 1989;245(4922):1066-1073.

179. Rottner M, Freyssinet J, Martínez MC. Mechanisms of the noxious inflammatory cycle in cystic fibrosis. Respiratory Research 2009;10(1):23.

180. Sagel SD, Sontag MK, Wagener JS, Kapsner RK, Osberg I, Accurso FJ. Induced sputum inflammatory measures correlate with lung function in children with cystic fibrosis. The Journal of Pediatrics 2002;141(6):811-817.

181. Saint-Criq V, Gray MA. Role of CFTR in epithelial physiology. Cellular and Molecular Life Sciences 2017;74(1):93-115.

182. Sato N, Funayama N, Nagafuchi A, Yonemura S, Tsukita S, Tsukita S. A gene family consisting of ezrin, radixin and moesin. Its specific localization at actin filament/plasma membrane association sites. Journal of Cell Science 1992;103(1):131-143.

183. Schubert T, Längst G. Studying epigenetic interactions using MicroScale Thermophoresis (MST). AIMS Biophysics 2015;2(3):370-380.

184. Seavilleklein G, Amer N, Evagelidis A, Chappe F, Irvine T, Hanrahan JW, et al. PKC phosphorylation modulates PKA-dependent binding of the R domain to other domains of CFTR. American Journal of Physiology-Cell Physiology 2008;295(5):C1366-C1375.

185. Sebastian A, Rishishwar L, Wang J, Bernard KF, Conley AB, McCarty NA, et al. Origin and evolution of the cystic fibrosis transmembrane regulator protein R domain. Gene 2013;523(2):137-146.

186. Seibert F, Chang X, Aleksandrov A, Clarke D, Hanrahan J, Riordan J. Influence of phosphorylation by protein kinase A on CFTR at the cell surface and endoplasmic reticulum. Biochimica et Biophysica Acta-Biomembranes 1999;1461(2):275-283.

187. Seibert FS, Linsdell P, Loo TW, Hanrahan JW, Riordan JR, Clarke DM. Cytoplasmic loop three of cystic fibrosis transmembrane conductance regulator contributes to regulation of chloride channel activity. Journal of Biological Chemistry 1996a;271(44):27493.

188. Seibert FS, Linsdell P, Loo TW, Hanrahan JW, Clarke DM, Riordan JR. Disease-associated mutations in the fourth cytoplasmic loop of cystic fibrosis transmembrane conductance regulator compromise biosynthetic processing and chloride channel activity. Journal of Biological Chemistry 1996b;271(25):15139-15145.

189. Seidel SA, Dijkman PM, Lea WA, van den Bogaart G, Jerabek-Willemsen M, Lazic A, et al. Microscale thermophoresis quantifies biomolecular interactions under previously challenging conditions. Methods 2013;59(3):301-315.

190. Sermet-Gaudelus I, Bianchi ML, Garabédian M, Aris RM, Morton A, Hardin DS, et al. European cystic fibrosis bone mineralisation guidelines. Journal of Cystic Fibrosis 2011;10:S16-S23.

191. Serohijos AW, Hegedus T, Aleksandrov AA, He L, Cui L, Dokholyan NV, et al. Phenylalanine-508 mediates a cytoplasmic-membrane domain contact in the CFTR 3D structure crucial to assembly and channel function. Proceedings of the National Academy of Sciences of the United States of America 2008;105(9):3256-3261.

192. Shan J, Liao J, Huang J, Robert R, Palmer ML, Fahrenkrug SC, et al. Bicarbonate-dependent chloride transport drives fluid secretion by the human airway epithelial cell line Calu-3. The Journal of Physiology 2012;590(21):5273-5297.

193. Sheppard DN, Ostedgaard LS, Rich DP, Welsh MJ. The amino-terminal portion of CFTR forms a regulated Cl− channel. Cell 1994;76(6):1091-1098.

194. Shevchenko A, Tomas H, Havli J, Olsen JV, Mann M. In-gel digestion for mass spectrometric characterization of proteins and proteomes. Nature protocols 2006;1(6):2856.

195. Shoemaker BA, Portman JJ, Wolynes PG. Speeding molecular recognition by using the folding funnel: the fly-casting mechanism. Proceedings of the National Academy of Sciences of the United States of America 2000;97(16):8868-8873.

196. Simonsen CC, Levinson AD. Isolation and expression of an altered mouse dihydrofolate reductase cDNA. Proceedings of the National Academy of Sciences of the United States of America 1983;80(9):2495-2499.

197. Skach WR. Defects in processing and trafficking of the cystic fibrosis transmembrane conductance regulator. Kidney International 2000;57(3):825-831.

198. Sly PD, Brennan S, Gangell C, de Klerk N, Murray C, Mott L, et al. Lung disease at diagnosis in infants with cystic fibrosis detected by newborn screening. American Journal of Respiratory and Critical Care Medicine 2009;180(2):146-152.

199. Söderberg O, Gullberg M, Jarvius M, Ridderstråle K, Leuchowius K, Jarvius J, et al. Direct observation of individual endogenous protein complexes in situ by proximity ligation. Nature Methods 2006;3(12):995.

200. Song Y, Salinas D, Nielson DW, Verkman A. Hyperacidity of secreted fluid from submucosal glands in early cystic fibrosis. American Journal of Physiology-Cell Physiology 2006;290(3):C741-C749.

201. Sosnay PR, Siklosi KR, Van Goor F, Kaniecki K, Yu H, Sharma N, et al. Defining the disease liability of variants in the cystic fibrosis transmembrane conductance regulator gene. Nature Genetics 2013;45(10):1160.

202. Sun F, Hug MJ, Bradbury NA, Frizzell RA. Protein kinase A associates with cystic fibrosis transmembrane conductance regulator via an interaction with ezrin. Journal of Biological Chemistry 2000;275(19):14360-14366.

203. Tabcharani JA, Chang X, Riordan JR, Hanrahan JW. Phosphorylation-regulated Cl− channel in CHO cells stably expressing the cystic fibrosis gene. Nature 1991;352:628-631.

204. Tang XX, Ostedgaard LS, Hoegger MJ, Moninger TO, Karp PH, McMenimen JD, et al. Acidic pH increases airway surface liquid viscosity in cystic fibrosis. Journal of Clinical Investigation 2016;126(3):879-891.

205. Tang AC, Turvey SE, Alves MP, Regamey N, Tummler B, Hartl D. Current concepts: host-pathogen interactions in cystic fibrosis airways disease. European Respiratory Review 2014 Sep;23(133):320-332.

206. Tarran R. Regulation of airway surface liquid volume and mucus transport by active ion transport. Proceedings of the American Thoracic Society 2004;1(1):42-46.

207. Taus T, Köcher T, Pichler P, Paschke C, Schmidt A, Henrich C, et al. Universal and confident phosphorylation site localization using phosphoRS. Journal of proteome research 2011;10(12):5354-5362.

208. ter Beek J, Guskov A, Slotboom DJ. Structural diversity of ABC transporters. The Journal of General Physiology 2014;143(4):419-435.

209. Thelin WR, Kesimer M, Tarran R, Kreda SM, Grubb BR, Sheehan JK, et al. The cystic fibrosis transmembrane conductance regulator is regulated by a direct interaction with the protein phosphatase 2A. Journal of Biological Chemistry 2005;280(50):41512-41520.

210. Theodoulou FL, Kerr ID. ABC transporter research: going strong 40 years on. Biochemical Society Transactions 2015;43(5):1033-1040.

211. Tirouvanziam R, Khazaal I, Péault B. Primary inflammation in human cystic fibrosis small airways. American Journal of Physiology-Lung Cellular and Molecular Physiology 2002;283(2):L445-L451.

212. Tompa P, Fuxreiter M. Fuzzy complexes: polymorphism and structural disorder in protein–protein interactions. Trends in Biochemical Science 2008;33(1):2-8.

213. Treharne KJ, Xu Z, Chen JH, Best OG, Cassidy DM, Gruenert DC, et al. Inhibition of protein kinase CK2 closes the CFTR Cl channel, but has no effect on the cystic fibrosis mutant deltaF508-CFTR. Cellular Physiology and Biochemistry 2009;24(5-6):347-360.

214. Trout L, King M, Feng W, Inglis SK, Ballard ST. Inhibition of airway liquid secretion and its effect on the physical properties of airway mucus. American Journal of Physiology-Lung Cellular and Molecular Physiology 1998;274(2):L258-L263.

215. Uversky VN. Intrinsically disordered proteins from A to Z. The International Journal of Biochemistry & Cell Biology 2011;43(8):1090-1103.

216. Vankeerberghen A, Cuppens H, Cassiman J. The cystic fibrosis transmembrane conductance regulator: an intriguing protein with pleiotropic functions. Journal of Cystic Fibrosis 2002;1(1):13-29.

217. Vastiau A, Cao L, Jaspers M, Owsianik G, Janssens V, Cuppens H, et al. Interaction of the protein phosphatase 2A with the regulatory domain of the cystic fibrosis transmembrane conductance regulator channel. FEBS Letters 2005;579(16):3392-3396.

218. Venerando A, Franchin C, Cant N, Cozza G, Pagano MA, Tosoni K, et al. Detection of phospho-sites generated by protein kinase CK2 in CFTR: mechanistic aspects of Thr1471 phosphorylation. PloS one 2013;8(9):e74232.

219. Verdugo P, Deyrup-Olsen I, Aitken M, Villalon M, Johnson D. Molecular mechanism of mucin secretion: I. The role of intragranular charge shielding. Journal of Dental Research 1987;66(2):506-508.

220. Vergani P, Lockless SW, Nairn AC, Gadsby DC. CFTR channel opening by ATP-driven tight dimerization of its nucleotide-binding domains. Nature 2005;433(7028):876.

221. Vergani P, Nairn AC, Gadsby DC. On the mechanism of MgATP-dependent gating of CFTR Cl- channels. The Journal of General Physiology 2003;121(1):17-36.

222. Verhaeghe C, Remouchamps C, Hennuy B, Vanderplasschen A, Chariot A, Tabruyn SP, et al. Role of IKK and ERK pathways in intrinsic inflammation of cystic fibrosis airways. Biochemical Pharmacology 2007;73(12):1982-1994.

223. Wang S, Raab RW, Schatz PJ, Guggino WB, Li M. Peptide binding consensus of the NHE-RF-PDZ1 domain matches the C-terminal sequence of cystic fibrosis transmembrane conductance regulator (CFTR). FEBS Letters 1998;427(1):103-108.

224. Wang S, Yue H, Derin RB, Guggino WB, Li M. Accessory protein facilitated CFTR-CFTR interaction, a molecular mechanism to potentiate the chloride channel activity. Cell 2000;103(1):169-179.

225. Wang W, Wu J, Bernard K, Li G, Wang G, Bevensee MO, et al. ATP-independent CFTR channel gating and allosteric modulation by phosphorylation. Proceedings of the National Academy of Sciences of the United States of America 2010;107(8):3888-3893.

226. Wang W, El Hiani Y, Rubaiy HN, Linsdell P. Relative contribution of different transmembrane segments to the CFTR chloride channel pore. Pflügers Archiv-European Journal of Physiology 2014;466(3):477-490.

227. Wang G. State-dependent regulation of cystic fibrosis transmembrane conductance regulator (CFTR) gating by a high affinity Fe3+ bridge between the regulatory domain and cytoplasmic loop 3. Journal of Biological Chemistry 2010;285(52):40438-40447.

228. Wang G, Duan DD. Regulation of activation and processing of the cystic fibrosis transmembrane conductance regulator (CFTR) by a complex electrostatic interaction between the regulatory domain and cytoplasmic loop 3. Journal of Biological Chemistry 2012;287(48):40484-40492.

229. Wang W, Bernard K, Li G, Kirk KL. Curcumin opens cystic fibrosis transmembrane conductance regulator channels by a novel mechanism that requires neither ATP binding nor dimerization of the nucleotide-binding domains. Journal of Biological Chemistry 2007;282(7):4533-4544.

230. Wang W, El Hiani Y, Linsdell P. Alignment of transmembrane regions in the cystic fibrosis transmembrane conductance regulator chloride channel pore. The Journal of General Physiology 2011;138(2):165-178.

231. Wang W, He Z, O'Shaughnessy TJ, Rux J, Reenstra WW. Domain-domain associations in cystic fibrosis transmembrane conductance regulator. American Journal of Physiology-Cell Physiology 2002;282(5):C1170-80.

232. Wang X, Matteson J, An Y, Moyer B, Yoo JS, Bannykh S, et al. COPII-dependent export of cystic fibrosis transmembrane conductance regulator from the ER uses a di-acidic exit code. Journal of Cell Biology 2004;167(1):65-74.

233. Wei L, Vankeerberghen A, Cuppens H, Eggermont J, Cassiman J, Droogmans G, et al. Interaction between calcium-activated chloride channels and the cystic fibrosis transmembrane conductance regulator. Pflügers Archiv-European Journal of Physiology 1999;438(5):635-641.

234. Weldon S, McNally P, McElvaney NG, Elborn JS, McAuley DF, Wartelle J, et al. Decreased levels of secretory leucoprotease inhibitor in the Pseudomonas-infected cystic fibrosis lung are due to neutrophil elastase degradation. Journal of Immunology 2009;183(12):8148-8156.

235. Wilkinson DJ, Strong TV, Mansoura MK, Wood DL, Smith SS, Collins FS, Dawson DC. CFTR activation: additive effects of stimulatory and inhibitory phosphorylation sites in the R domain. American Journal of Physiology-Lung Cellular and Molecular Physiology. 1997;273(1):L127-133.

236. Wine JJ. The development of lung disease in cystic fibrosis pigs. Science Translational Medicine 2010;2(29):29ps20.

237. Winter MC, Welsh MJ. Stimulation of CFTR activity by its phosphorylated R domain. Nature 1997;389(6648):294.

238. Wright PE, Dyson HJ. Intrinsically unstructured proteins: re-assessing the protein structure-function paradigm. Journal of Molecular Biology 1999;293(2):321-331.

239. Wright PE, Dyson HJ. Intrinsically disordered proteins in cellular signalling and regulation. Nature reviews Molecular cell biology. 2015;16(1):18.

240. Xie J, Zhao J, Davis PB, Ma J. Conformation, independent of charge, in the R domain affects cystic fibrosis transmembrane conductance regulator channel openings. Biophysical Journal 2000;78(3):1293-1305.

241. Xie J, Adams LM, Zhao J, Gerken TA, Davis PB, Ma J. A short segment of the R domain of cystic fibrosis transmembrane conductance regulator contains channel stimulatory and inhibitory activities that are separable by sequence modification. Journal of Biological Chemistry 2002;277(25):23019-23027.

242. Xu Y, Szep S, Lu Z. The antioxidant role of thiocyanate in the pathogenesis of cystic fibrosis and other inflammation-related diseases. Proceedings of the National Academy of Sciences of the United States of America 2009;106(48):20515-20519.

243. Yoo JS, Moyer BD, Bannykh S, Yoo HM, Riordan JR, Balch WE. Non-conventional trafficking of the cystic fibrosis transmembrane conductance regulator through the early secretory pathway. Journal of Biological Chemistry 2002;277(13):11401-11409.

244. Younger JM, Chen L, Ren H, Rosser MF, Turnbull EL, Fan C, et al. Sequential quality-control checkpoints triage misfolded cystic fibrosis transmembrane conductance regulator. Cell 2006;126(3):571-582.

245. Yuan H, Michelsen K, Schwappach B. 14-3-3 dimers probe the assembly status of multimeric membrane proteins. Current Biology 2003;13(8):638-646.

246. Zhang J, Hwang T. The fifth transmembrane segment of cystic fibrosis transmembrane conductance regulator contributes to its anion permeation pathway. Biochemistry 2015;54(24):3839-3850.

247. Zhang Z, Chen J. Atomic structure of the cystic fibrosis transmembrane conductance regulator. Cell 2016;167(6):1586-1597.e9.

248. Zhang Z, Liu F, Chen J. Conformational changes of CFTR upon phosphorylation and ATP binding. Cell 2017;170(3):483-491.e8.

249. Zhang Z, Liu F, Chen J. Molecular structure of the ATP-bound, phosphorylated human CFTR. Proceedings of the National Academy of Sciences of the United States of America 2018;115(50):12757-12762.

250. Zhou P, Lugovskoy AA, Wagner G. A solubility-enhancement tag (SET) for NMR studies of poorly behaving proteins. Journal of Biomolecular NMR 2001;20(1):11-14.

251. Zhou Z, Wang X, Liu HY, Zou X, Li M, Hwang TC. The two ATP binding sites of cystic fibrosis transmembrane conductance regulator (CFTR) play distinct roles in gating kinetics and energetics. The Journal of General Physiology 2006;128(4):413-422.

252. Zhu T, Dahan D, Evagelidis A, Zheng S, Luo J, Hanrahan JW. Association of cystic fibrosis transmembrane conductance regulator and protein phosphatase 2C. Journal of Biological Chemistry 1999;274(41):29102-29107.

# Appendix A: Copyright Agreement Letters

## Figure 1 permission

### AMERICAN ACADEMY OF PEDIATRICS LICENSE TERMS AND CONDITIONS

Jun 26, 2019

This Agreement between Dalhousie University -- Diogo Poroca ("You") and American Academy of Pediatrics ("American Academy of Pediatrics") consists of your license details and the terms and conditions provided by American Academy of Pediatrics and Copyright Clearance Center.

| | |
|---|---|
| License Number | 4615511399585 |
| License date | Jun 24, 2019 |
| Licensed Content Publisher | American Academy of Pediatrics |
| Licensed Content Publication | Pediatrics in Review |
| Licensed Content Title | Cystic Fibrosis |
| Licensed Content Author | Shruti M. Paranjape,Peter J. Mogayzel |
| Licensed Content Date | May 1, 2014 |
| Licensed Content Volume | 35 |
| Licensed Content Issue | 5 |
| Licensed Content Pages | 12 |
| Type of Use | Dissertation/Thesis |
| Requestor type | Individual |
| Format | Print and Electronic |
| Portion | Figures/tables/images |
| Number of figures/tables/images | 1 |
| Use of a photo? | No |
| Original AAP figure/table/image number(s) | Figure 2 |
| Order reference number | |
| Requestor Location | Dalhousie University<br>6299 South St |

Halifax, NS B3H 4R2
Canada
Attn: Dalhousie University

Total 0.00 USD

Terms and Conditions

**AAP TERMS ANDCONDITIONS**

The American Academy of Pediatrics grants permission to use the content cited above for the purpose stated. This letter shall serve as a receipt for payment of the permissions fee(s) and as an approval agreement.

1. The following credit line must appear:
   **Reproduced with permission from Journal <Journal>, Vol. <Vol>, Page(s) <Pages>, Copyright © <Year> by the AAP**
2. The requester guarantees to reprint the materials exactly as originally published. Obvious typographical errors maybe corrected. No deletions, alterations, or other changes may be made to the information or statistical data without the written consent of the American Academy of Pediatrics.
3. Rights granted herein are not exclusive and the American Academy of Pediatrics reserves the right to grant the same permission to others. Permission is granted for only the reproduction media specified.
4. Original artwork or copies of articles cannot be supplied, but PDF files may be downloaded from www.aappublications.org . Quantities of reprints and eprints can be obtained by contacting Terry Dennsteadt, Reprint Sales Manager – AAP Journals, The Walchli Tauber Group, Inc., 2225 Old Emmorton Road, Suite 201, Bel Air, MD 21046. 443.512.8899 x 112 office, 443.512.8909 fax, terry.dennsteadt@wt-group.com.
5. This permission is granted on a one-time, annual basis only. Reproduction of this material is confined to the purpose and/or media for which permission is hereby given. Future use of this material is subject to the conditions stated herein. *Gratis permissions are not issued for use in materials available for commercial sale, even for educational use.*
6. If the permission fee for the requested use of our material is waived in this instance, please be aware future requests for AAP materials are subject to fees.
7. Reservation of Rights: Publisher reserves all rights not specifically granted in the combination of (i) the license details provided by you and accepted in the course of this licensing transaction, (ii) these terms and conditions and (iii) CCC's Billing and Payment terms and conditions.
8. License Contingent Upon Payment. Provided that you have disclosed complete and accurate details of your proposed use, no license is effective unless and until full payment is received from you(either by publisher or by CCC) as provided in the CCC's Billing and Payment terms and conditions. If full payment is not received on a timely basis, then any license preliminarily granted shall be deemed automatically revoked and shall be void as if never granted. Further, in the event that you breach terms and conditions or any of CCC's Billing and Payment terms

and conditions, the license is automatically revoked and shall be void as if never granted.

9. Warranties: Publisher makes no representations or warranties of any kind, express or implied, including but not limited to, accuracy, timeliness or completeness of the information contained in the licensed materials, or merchantability, title or fitness of a use for a particular purpose.
10. Indemnity: You hereby indemnify and agree to hold harmless publisher and CCC, and their respective officers, directors, employees and agents, from and against any and all claims arising out of your use of the licensed material other than specifically authorized pursuant to this license.
11. No Transfer of License: This license is personal to you and may not be sublicensed, assigned or transferred by you to any other person without publisher's written permission.
12. No Amendment Except in Writing: This license may not be amended except in writing signed by both requestor and publisher.
13. This permission, if permission has been granted for use of figures/tables/images, does not cover any third party copyrighted work which may appear in the material requested and does not apply to materials credited to publications other than American Academy of Pediatrics (AAP) journals. For materials credited to non-AAP journal publications, you will need to obtain permission from the publication referenced in the material legend or credit line before proceeding with usage of the materials. You agree to hold harmless and indemnify the AAP against any claims arising from your use of any content in your work that is credited to non-AAP sources.
14. This permission does not apply to and is not valid for photographs depicting identifiable individuals, including images where individuals' eyes have been blacked out or images depicting victims of abuse.
15. If the requester is translating the material, the following translation disclaimer must be included:
    **The materials reused with permission from the American Academy of Pediatrics ("AAP") appeared originally in English, published by the AAP. The AAP assumes no responsibility for any inaccuracy or error in the contents of these materials, including any inaccuracy or error arising from the translation from English.**
16. **Other Terms and Conditions:**

v1.4

## Figure 2 Permission

**ELSEVIER LICENSE**
**TERMS AND CONDITIONS**

Jun 26, 2019

This Agreement between Dalhousie University -- Diogo Poroca ("You") and Elsevier ("Elsevier") consists of your license details and the terms and conditions provided by Elsevier and Copyright Clearance Center.

| | |
|---|---|
| License Number | 4615520504384 |
| License date | Jun 24, 2019 |
| Licensed Content Publisher | Elsevier |
| Licensed Content Publication | The Lancet Respiratory Medicine |
| Licensed Content Title | A new era in the treatment of cystic fibrosis: correction of the underlying CFTR defect |
| Licensed Content Author | Michael P Boyle,Kris De Boeck |
| Licensed Content Date | Apr 1, 2013 |
| Licensed Content Volume | 1 |
| Licensed Content Issue | 2 |
| Licensed Content Pages | 6 |
| Start Page | 158 |
| End Page | 163 |
| Type of Use | reuse in a thesis/dissertation |
| Portion | figures/tables/illustrations |
| Number of figures/tables/illustrations | 1 |
| Format | both print and electronic |
| Are you the author of this Elsevier article? | No |
| Will you be translating? | No |
| Original figure numbers | Figure 1 |
| Title of your thesis/dissertation | PHOSPHORYLATION-DEPENDENT CHANGES IN THE R-REGION INTERACTIONS |

| | |
|---|---|
| | CONTRIBUTE TO REGULATION OF THE CFTR CHLORIDE CHANNEL |
| Expected completion date | Aug 2019 |
| Estimated size (number of pages) | 200 |
| Requestor Location | Dalhousie University<br>6299 South St<br><br>Halifax, NS B3H 4R2<br>Canada<br>Attn: Dalhousie University |
| Publisher Tax ID | GB 494 6272 12 |
| Total | 0.00 USD |

Terms and Conditions

**INTRODUCTION**

1. The publisher for this copyrighted material is Elsevier. By clicking "accept" in connection with completing this licensing transaction, you agree that the following terms and conditions apply to this transaction (along with the Billing and Payment terms and conditions established by Copyright Clearance Center, Inc. ("CCC"), at the time that you opened your Rightslink account and that are available at any time at http://myaccount.copyright.com).

**GENERAL TERMS**

2. Elsevier hereby grants you permission to reproduce the aforementioned material subject to the terms and conditions indicated.
3. Acknowledgement: If any part of the material to be used (for example, figures) has appeared in our publication with credit or acknowledgement to another source, permission must also be sought from that source. If such permission is not obtained then that material may not be included in your publication/copies. Suitable acknowledgement to the source must be made, either as a footnote or in a reference list at the end of your publication, as follows:
"Reprinted from Publication title, Vol /edition number, Author(s), Title of article / title of chapter, Pages No., Copyright (Year), with permission from Elsevier [OR APPLICABLE SOCIETY COPYRIGHT OWNER]." Also Lancet special credit - "Reprinted from The Lancet, Vol. number, Author(s), Title of article, Pages No., Copyright (Year), with permission from Elsevier."
4. Reproduction of this material is confined to the purpose and/or media for which permission is hereby given.
5. Altering/Modifying Material: Not Permitted. However figures and illustrations may be altered/adapted minimally to serve your work. Any other abbreviations, additions, deletions and/or any other alterations shall be made only with prior written authorization of Elsevier Ltd. (Please contact Elsevier at permissions@elsevier.com). No

modifications can be made to any Lancet figures/tables and they must be reproduced in full.
6. If the permission fee for the requested use of our material is waived in this instance, please be advised that your future requests for Elsevier materials may attract a fee.
7. Reservation of Rights: Publisher reserves all rights not specifically granted in the combination of (i) the license details provided by you and accepted in the course of this licensing transaction, (ii) these terms and conditions and (iii) CCC's Billing and Payment terms and conditions.
8. License Contingent Upon Payment: While you may exercise the rights licensed immediately upon issuance of the license at the end of the licensing process for the transaction, provided that you have disclosed complete and accurate details of your proposed use, no license is finally effective unless and until full payment is received from you (either by publisher or by CCC) as provided in CCC's Billing and Payment terms and conditions. If full payment is not received on a timely basis, then any license preliminarily granted shall be deemed automatically revoked and shall be void as if never granted. Further, in the event that you breach any of these terms and conditions or any of CCC's Billing and Payment terms and conditions, the license is automatically revoked and shall be void as if never granted. Use of materials as described in a revoked license, as well as any use of the materials beyond the scope of an unrevoked license, may constitute copyright infringement and publisher reserves the right to take any and all action to protect its copyright in the materials.
9. Warranties: Publisher makes no representations or warranties with respect to the licensed material.
10. Indemnity: You hereby indemnify and agree to hold harmless publisher and CCC, and their respective officers, directors, employees and agents, from and against any and all claims arising out of your use of the licensed material other than as specifically authorized pursuant to this license.
11. No Transfer of License: This license is personal to you and may not be sublicensed, assigned, or transferred by you to any other person without publisher's written permission.
12. No Amendment Except in Writing: This license may not be amended except in a writing signed by both parties (or, in the case of publisher, by CCC on publisher's behalf).
13. Objection to Contrary Terms: Publisher hereby objects to any terms contained in any purchase order, acknowledgment, check endorsement or other writing prepared by you, which terms are inconsistent with these terms and conditions or CCC's Billing and Payment terms and conditions. These terms and conditions, together with CCC's Billing and Payment terms and conditions (which are incorporated herein), comprise the entire agreement between you and publisher (and CCC) concerning this licensing transaction. In the event of any conflict between your obligations established by these terms and conditions and those established by CCC's Billing and Payment terms and conditions, these terms and conditions shall control.
14. Revocation: Elsevier or Copyright Clearance Center may deny the permissions described in this License at their sole discretion, for any reason or no reason, with a full refund payable to you. Notice of such denial will be made using the contact information provided by you. Failure to receive such notice will not alter or invalidate the denial. In

no event will Elsevier or Copyright Clearance Center be responsible or liable for any costs, expenses or damage incurred by you as a result of a denial of your permission request, other than a refund of the amount(s) paid by you to Elsevier and/or Copyright Clearance Center for denied permissions.

**LIMITED LICENSE**

The following terms and conditions apply only to specific license types:

15. **Translation**: This permission is granted for non-exclusive world **English** rights only unless your license was granted for translation rights. If you licensed translation rights you may only translate this content into the languages you requested. A professional translator must perform all translations and reproduce the content word for word preserving the integrity of the article.

16. **Posting licensed content on any Website**: The following terms and conditions apply as follows: Licensing material from an Elsevier journal: All content posted to the web site must maintain the copyright information line on the bottom of each image; A hyper-text must be included to the Homepage of the journal from which you are licensing at http://www.sciencedirect.com/science/journal/xxxxx or the Elsevier homepage for books at http://www.elsevier.com; Central Storage: This license does not include permission for a scanned version of the material to be stored in a central repository such as that provided by Heron/XanEdu.

Licensing material from an Elsevier book: A hyper-text link must be included to the Elsevier homepage at http://www.elsevier.com . All content posted to the web site must maintain the copyright information line on the bottom of each image.

**Posting licensed content on Electronic reserve**: In addition to the above the following clauses are applicable: The web site must be password-protected and made available only to bona fide students registered on a relevant course. This permission is granted for 1 year only. You may obtain a new license for future website posting.

17. **For journal authors:** the following clauses are applicable in addition to the above:

**Preprints:**

A preprint is an author's own write-up of research results and analysis, it has not been peer-reviewed, nor has it had any other value added to it by a publisher (such as formatting, copyright, technical enhancement etc.).

Authors can share their preprints anywhere at any time. Preprints should not be added to or enhanced in any way in order to appear more like, or to substitute for, the final versions of articles however authors can update their preprints on arXiv or RePEc with their Accepted Author Manuscript (see below).

If accepted for publication, we encourage authors to link from the preprint to their formal publication via its DOI. Millions of researchers have access to the formal publications on ScienceDirect, and so links will help users to find, access, cite and use the best available version. Please note that Cell Press, The Lancet and some society-owned have different preprint policies. Information on these policies is available on the journal homepage.

**Accepted Author Manuscripts:** An accepted author manuscript is the manuscript of an article that has been accepted for publication and which typically includes author-incorporated changes suggested during submission, peer review and editor-author communications.

Authors can share their accepted author manuscript:

- immediately
    - via their non-commercial person homepage or blog
    - by updating a preprint in arXiv or RePEc with the accepted manuscript
    - via their research institute or institutional repository for internal institutional uses or as part of an invitation-only research collaboration work-group
    - directly by providing copies to their students or to research collaborators for their personal use
    - for private scholarly sharing as part of an invitation-only work group on commercial sites with which Elsevier has an agreement
- After the embargo period
    - via non-commercial hosting platforms such as their institutional repository
    - via commercial sites with which Elsevier has an agreement

In all cases accepted manuscripts should:

- link to the formal publication via its DOI
- bear a CC-BY-NC-ND license - this is easy to do
- if aggregated with other manuscripts, for example in a repository or other site, be shared in alignment with our hosting policy not be added to or enhanced in any way to appear more like, or to substitute for, the published journal article.

**Published journal article (JPA):** A published journal article (PJA) is the definitive final record of published research that appears or will appear in the journal and embodies all value-adding publishing activities including peer review co-ordination, copy-editing, formatting, (if relevant) pagination and online enrichment.

Policies for sharing publishing journal articles differ for subscription and gold open access articles:

**Subscription Articles:** If you are an author, please share a link to your article rather than the full-text. Millions of researchers have access to the formal publications on ScienceDirect, and so links will help your users to find, access, cite, and use the best available version.

Theses and dissertations which contain embedded PJAs as part of the formal submission can be posted publicly by the awarding institution with DOI links back to the formal publications on ScienceDirect.

If you are affiliated with a library that subscribes to ScienceDirect you have additional private sharing rights for others' research accessed under that agreement. This includes use for classroom teaching and internal training at the institution (including use in course packs and courseware programs), and inclusion of the article for grant funding purposes.

**Gold Open Access Articles:** May be shared according to the author-selected end-user license and should contain a CrossMark logo, the end user license, and a DOI link to the formal publication on ScienceDirect.

Please refer to Elsevier's posting policy for further information.

18. **For book authors** the following clauses are applicable in addition to the above: Authors are permitted to place a brief summary of their work online only. You are not allowed to download and post the published electronic version of your chapter, nor may you scan the printed edition to create an electronic version. **Posting to a**

**repository:** Authors are permitted to post a summary of their chapter only in their institution's repository.

19. **Thesis/Dissertation**: If your license is for use in a thesis/dissertation your thesis may be submitted to your institution in either print or electronic form. Should your thesis be published commercially, please reapply for permission. These requirements include permission for the Library and Archives of Canada to supply single copies, on demand, of the complete thesis and include permission for Proquest/UMI to supply single copies, on demand, of the complete thesis. Should your thesis be published commercially, please reapply for permission. Theses and dissertations which contain embedded PJAs as part of the formal submission can be posted publicly by the awarding institution with DOI links back to the formal publications on ScienceDirect.

**Elsevier Open Access Terms and Conditions**

You can publish open access with Elsevier in hundreds of open access journals or in nearly 2000 established subscription journals that support open access publishing. Permitted third party re-use of these open access articles is defined by the author's choice of Creative Commons user license. See our open access license policy for more information.

**Terms & Conditions applicable to all Open Access articles published with Elsevier:**

Any reuse of the article must not represent the author as endorsing the adaptation of the article nor should the article be modified in such a way as to damage the author's honour or reputation. If any changes have been made, such changes must be clearly indicated. The author(s) must be appropriately credited and we ask that you include the end user license and a DOI link to the formal publication on ScienceDirect.

If any part of the material to be used (for example, figures) has appeared in our publication with credit or acknowledgement to another source it is the responsibility of the user to ensure their reuse complies with the terms and conditions determined by the rights holder.

**Additional Terms & Conditions applicable to each Creative Commons user license:**

**CC BY:** The CC-BY license allows users to copy, to create extracts, abstracts and new works from the Article, to alter and revise the Article and to make commercial use of the Article (including reuse and/or resale of the Article by commercial entities), provided the user gives appropriate credit (with a link to the formal publication through the relevant DOI), provides a link to the license, indicates if changes were made and the licensor is not represented as endorsing the use made of the work. The full details of the license are available at http://creativecommons.org/licenses/by/4.0.

**CC BY NC SA:** The CC BY-NC-SA license allows users to copy, to create extracts, abstracts and new works from the Article, to alter and revise the Article, provided this is not done for commercial purposes, and that the user gives appropriate credit (with a link to the formal publication through the relevant DOI), provides a link to the license, indicates if changes were made and the licensor is not represented as endorsing the use made of the work. Further, any new works must be made available on the same conditions. The full details of the license are available at http://creativecommons.org/licenses/by-nc-sa/4.0.

**CC BY NC ND:** The CC BY-NC-ND license allows users to copy and distribute the Article, provided this is not done for commercial purposes and further does not permit distribution of the Article if it is changed or edited in any way, and provided the user

## Figure 3 Permission

| SPRINGER NATURE LICENSE TERMS AND CONDITIONS | |
|---|---|
| Jun 26, 2019 | |
| This Agreement between Dalhousie University -- Diogo Poroca ("You") and Springer Nature ("Springer Nature") consists of your license details and the terms and conditions provided by Springer Nature and Copyright Clearance Center. | |
| License Number | 4615521202154 |
| License date | Jun 24, 2019 |
| Licensed Content Publisher | Springer Nature |
| Licensed Content Publication | Cellular and Molecular Life Sciences |
| Licensed Content Title | From the endoplasmic reticulum to the plasma membrane: mechanisms of CFTR folding and trafficking |
| Licensed Content Author | Carlos M. Farinha, Sara Canato |
| Licensed Content Date | Jan 1, 2016 |
| Licensed Content Volume | 74 |
| Licensed Content Issue | 1 |
| Type of Use | Thesis/Dissertation |
| Requestor type | academic/university or research institute |
| Format | print and electronic |
| Portion | figures/tables/illustrations |
| Number of figures/tables/illustrations | 1 |
| Will you be translating? | no |
| Circulation/distribution | <501 |
| Author of this Springer Nature content | no |
| Title | PHOSPHORYLATION-DEPENDENT CHANGES IN THE R-REGION INTERACTIONS CONTRIBUTE TO REGULATION OF THE CFTR CHLORIDE CHANNEL |
| Institution name | Dalhousie University |
| Expected presentation date | Aug 2019 |
| Portions | Figure 3 |
| Requestor Location | Dalhousie University<br>6299 South St<br><br>Halifax, NS B3H 4R2 |

| | |
|---|---|
| | Canada<br>Attn: Dalhousie University |
| Total | 0.00 USD |

Terms and Conditions

**Springer Nature Customer Service Centre GmbH**
**Terms and Conditions**

This agreement sets out the terms and conditions of the licence (the **Licence**) between you and **Springer Nature Customer Service Centre GmbH** (the **Licensor**). By clicking 'accept' and completing the transaction for the material (**Licensed Material**), you also confirm your acceptance of these terms and conditions.

1. **Grant of License**

    1. The Licensor grants you a personal, non-exclusive, non-transferable, world-wide licence to reproduce the Licensed Material for the purpose specified in your order only. Licences are granted for the specific use requested in the order and for no other use, subject to the conditions below.
    2. The Licensor warrants that it has, to the best of its knowledge, the rights to license reuse of the Licensed Material. However, you should ensure that the material you are requesting is original to the Licensor and does not carry the copyright of another entity (as credited in the published version).
    3. If the credit line on any part of the material you have requested indicates that it was reprinted or adapted with permission from another source, then you should also seek permission from that source to reuse the material.

2. **Scope of Licence**

    1. You may only use the Licensed Content in the manner and to the extent permitted by these Ts&Cs and any applicable laws.
    2. A separate licence may be required for any additional use of the Licensed Material, e.g. where a licence has been purchased for print only use, separate permission must be obtained for electronic re-use. Similarly, a licence is only valid in the language selected and does not apply for editions in other languages unless additional translation rights have been granted separately in the licence. Any content owned by third parties are expressly excluded from the licence.
    3. Similarly, rights for additional components such as custom editions and derivatives require additional permission and may be subject to an additional fee. Please apply toJournalpermissions@springernature.com/bookpermissions@springernature.com for these rights.
    4. Where permission has been granted **free of charge** for material in print, permission may also be granted for any electronic version of that work, provided that the material is incidental to your work as a whole and that

the electronic version is essentially equivalent to, or substitutes for, the print version.

5. An alternative scope of licence may apply to signatories of the STM Permissions Guidelines, as amended from time to time.

**Duration of Licence**

1. A licence for is valid from the date of purchase ('Licence Date') at the end of the relevant period in the below table:

| Scope of Licence | Duration of Licence |
|---|---|
| Post on a website | 12 months |
| Presentations | 12 months |
| Books and journals | Lifetime of the edition in the language purchased |

**Acknowledgement**

1. The Licensor's permission must be acknowledged next to the Licenced Material in print. In electronic form, this acknowledgement must be visible at the same time as the figures/tables/illustrations or abstract, and must be hyperlinked to the journal/book's homepage. Our required acknowledgement format is in the Appendix below.

**Restrictions on use**

1. Use of the Licensed Material may be permitted for incidental promotional use and minor editing privileges e.g. minor adaptations of single figures, changes of format, colour and/or style where the adaptation is credited as set out in Appendix 1 below. Any other changes including but not limited to, cropping, adapting, omitting material that affect the meaning, intention or moral rights of the author are strictly prohibited.
2. You must not use any Licensed Material as part of any design or trademark.
3. Licensed Material may be used in Open Access Publications (OAP) before publication by Springer Nature, but any Licensed Material must be removed from OAP sites prior to final publication.

**Ownership of Rights**

1. Licensed Material remains the property of either Licensor or the relevant third party and any rights not explicitly granted herein are expressly reserved.

**Warranty**

IN NO EVENT SHALL LICENSOR BE LIABLE TO YOU OR ANY OTHER PARTY OR ANY OTHER PERSON OR FOR ANY SPECIAL, CONSEQUENTIAL, INCIDENTAL OR INDIRECT DAMAGES, HOWEVER CAUSED, ARISING OUT OF OR IN CONNECTION WITH THE DOWNLOADING, VIEWING OR USE OF THE MATERIALS REGARDLESS OF THE FORM OF ACTION, WHETHER FOR BREACH OF CONTRACT, BREACH OF WARRANTY, TORT, NEGLIGENCE, INFRINGEMENT OR OTHERWISE (INCLUDING, WITHOUT LIMITATION,

DAMAGES BASED ON LOSS OF PROFITS, DATA, FILES, USE, BUSINESS OPPORTUNITY OR CLAIMS OF THIRD PARTIES), AND
WHETHER OR NOT THE PARTY HAS BEEN ADVISED OF THE POSSIBILITY OF SUCH DAMAGES. THIS LIMITATION SHALL APPLY NOTWITHSTANDING ANY FAILURE OF ESSENTIAL PURPOSE OF ANY LIMITED REMEDY PROVIDED HEREIN.

**Limitations**

1. ***BOOKS ONLY:***Where **'reuse in a dissertation/thesis'** has been selected the following terms apply: Print rights of the final author's accepted manuscript (for clarity, NOT the published version) for up to 100 copies, electronic rights for use only on a personal website or institutional repository as defined by the Sherpa guideline (www.sherpa.ac.uk/romeo/).

**Termination and Cancellation**

1. Licences will expire after the period shown in Clause 3 (above).
2. Licensee reserves the right to terminate the Licence in the event that payment is not received in full or if there has been a breach of this agreement by you.

**Appendix 1 — Acknowledgements:**

**For Journal Content:**
Reprinted by permission from [**the Licensor**]: [**Journal Publisher** (e.g. Nature/Springer/Palgrave)] [**JOURNAL NAME**] [**REFERENCE CITATION**(Article name, Author(s) Name), [**COPYRIGHT**] (year of publication)
For **Advance Online Publication papers:**
Reprinted by permission from [**the Licensor**]: [**Journal Publisher** (e.g. Nature/Springer/Palgrave)] [**JOURNAL NAME**] [**REFERENCE CITATION**(Article name, Author(s) Name), [**COPYRIGHT**] (year of publication), advance online publication, day month year (doi: 10.1038/sj.[JOURNAL ACRONYM].)
**For Adaptations/Translations:**
Adapted/Translated by permission from [**the Licensor**]: [**Journal Publisher** (e.g. Nature/Springer/Palgrave)] [**JOURNAL NAME**] [**REFERENCE CITATION**(Article name, Author(s) Name), [**COPYRIGHT**] (year of publication)
**Note: For any republication from the British Journal of Cancer, the following credit line style applies:**
Reprinted/adapted/translated by permission from [**the Licensor**]: on behalf of Cancer Research UK: : [**Journal Publisher** (e.g. Nature/Springer/Palgrave)] [**JOURNAL NAME**] [**REFERENCE CITATION** (Article name, Author(s) Name), [**COPYRIGHT]** (year of publication)
For **Advance Online Publication** papers:
Reprinted by permission from The [**the Licensor**]: on behalf of Cancer Research UK: [**Journal Publisher** (e.g. Nature/Springer/Palgrave)] [**JOURNAL NAME**] [**REFERENCE CITATION** (Article name, Author(s)

## Figure 6A Permission

**ELSEVIER LICENSE**
**TERMS AND CONDITIONS**

Aug 26, 2019

This Agreement between Dalhousie University -- Diogo Poroca ("You") and Elsevier ("Elsevier") consists of your license details and the terms and conditions provided by Elsevier and Copyright Clearance Center.

| | |
|---|---|
| License Number | 4656620423176 |
| License date | Aug 26, 2019 |
| Licensed Content Publisher | Elsevier |
| Licensed Content Publication | Cell |
| Licensed Content Title | Molecular Structure of the Human CFTR Ion Channel |
| Licensed Content Author | Fangyu Liu,Zhe Zhang,László Csanády,David C. Gadsby,Jue Chen |
| Licensed Content Date | Mar 23, 2017 |
| Licensed Content Volume | 169 |
| Licensed Content Issue | 1 |
| Licensed Content Pages | 19 |
| Start Page | 85 |
| End Page | 95.e8 |
| Type of Use | reuse in a thesis/dissertation |
| Portion | figures/tables/illustrations |
| Number of figures/tables/illustrations | 1 |
| Format | electronic |
| Are you the author of this Elsevier article? | No |
| Will you be translating? | No |
| Original figure numbers | Figure 1. |
| Title of your thesis/dissertation | PHOSPHORYLATION-DEPENDENT CHANGES IN THE R-REGION INTERACTIONS CONTRIBUTE TO REGULATION OF THE CFTR CHLORIDE CHANNEL |

| | |
|---|---|
| Publisher of new work | Dalhousie University |
| Expected completion date | Aug 2019 |
| Estimated size (number of pages) | 200 |
| Requestor Location | Dalhousie University<br>6299 South St<br><br>Halifax, NS B3H 4R2<br>Canada<br>Attn: Dalhousie University |
| Publisher Tax ID | GB 494 6272 12 |
| Total | 0.00 CAD |

Terms and Conditions

## INTRODUCTION

1. The publisher for this copyrighted material is Elsevier. By clicking "accept" in connection with completing this licensing transaction, you agree that the following terms and conditions apply to this transaction (along with the Billing and Payment terms and conditions established by Copyright Clearance Center, Inc. ("CCC"), at the time that you opened your Rightslink account and that are available at any time at http://myaccount.copyright.com).

## GENERAL TERMS

2. Elsevier hereby grants you permission to reproduce the aforementioned material subject to the terms and conditions indicated.
3. Acknowledgement: If any part of the material to be used (for example, figures) has appeared in our publication with credit or acknowledgement to another source, permission must also be sought from that source. If such permission is not obtained then that material may not be included in your publication/copies. Suitable acknowledgement to the source must be made, either as a footnote or in a reference list at the end of your publication, as follows:
"Reprinted from Publication title, Vol /edition number, Author(s), Title of article / title of chapter, Pages No., Copyright (Year), with permission from Elsevier [OR APPLICABLE SOCIETY COPYRIGHT OWNER]." Also Lancet special credit - "Reprinted from The Lancet, Vol. number, Author(s), Title of article, Pages No., Copyright (Year), with permission from Elsevier."
4. Reproduction of this material is confined to the purpose and/or media for which permission is hereby given.
5. Altering/Modifying Material: Not Permitted. However figures and illustrations may be altered/adapted minimally to serve your work. Any other abbreviations, additions, deletions and/or any other alterations shall be made only with prior written authorization of Elsevier Ltd. (Please contact Elsevier at permissions@elsevier.com). No modifications can be made to any Lancet figures/tables and they must be reproduced in full.
6. If the permission fee for the requested use of our material is waived in this instance, please be advised that your future requests for Elsevier materials may attract a fee.
7. Reservation of Rights: Publisher reserves all rights not specifically granted in the combination of (i) the license details provided by you and accepted in the course of this

licensing transaction, (ii) these terms and conditions and (iii) CCC's Billing and Payment terms and conditions.
8. License Contingent Upon Payment: While you may exercise the rights licensed immediately upon issuance of the license at the end of the licensing process for the transaction, provided that you have disclosed complete and accurate details of your proposed use, no license is finally effective unless and until full payment is received from you (either by publisher or by CCC) as provided in CCC's Billing and Payment terms and conditions. If full payment is not received on a timely basis, then any license preliminarily granted shall be deemed automatically revoked and shall be void as if never granted. Further, in the event that you breach any of these terms and conditions or any of CCC's Billing and Payment terms and conditions, the license is automatically revoked and shall be void as if never granted. Use of materials as described in a revoked license, as well as any use of the materials beyond the scope of an unrevoked license, may constitute copyright infringement and publisher reserves the right to take any and all action to protect its copyright in the materials.
9. Warranties: Publisher makes no representations or warranties with respect to the licensed material.
10. Indemnity: You hereby indemnify and agree to hold harmless publisher and CCC, and their respective officers, directors, employees and agents, from and against any and all claims arising out of your use of the licensed material other than as specifically authorized pursuant to this license.
11. No Transfer of License: This license is personal to you and may not be sublicensed, assigned, or transferred by you to any other person without publisher's written permission.
12. No Amendment Except in Writing: This license may not be amended except in a writing signed by both parties (or, in the case of publisher, by CCC on publisher's behalf).
13. Objection to Contrary Terms: Publisher hereby objects to any terms contained in any purchase order, acknowledgment, check endorsement or other writing prepared by you, which terms are inconsistent with these terms and conditions or CCC's Billing and Payment terms and conditions. These terms and conditions, together with CCC's Billing and Payment terms and conditions (which are incorporated herein), comprise the entire agreement between you and publisher (and CCC) concerning this licensing transaction. In the event of any conflict between your obligations established by these terms and conditions and those established by CCC's Billing and Payment terms and conditions, these terms and conditions shall control.
14. Revocation: Elsevier or Copyright Clearance Center may deny the permissions described in this License at their sole discretion, for any reason or no reason, with a full refund payable to you. Notice of such denial will be made using the contact information provided by you. Failure to receive such notice will not alter or invalidate the denial. In no event will Elsevier or Copyright Clearance Center be responsible or liable for any costs, expenses or damage incurred by you as a result of a denial of your permission request, other than a refund of the amount(s) paid by you to Elsevier and/or Copyright Clearance Center for denied permissions.

## LIMITED LICENSE

The following terms and conditions apply only to specific license types:
15. **Translation**: This permission is granted for non-exclusive world **English** rights only unless your license was granted for translation rights. If you licensed translation rights you

may only translate this content into the languages you requested. A professional translator must perform all translations and reproduce the content word for word preserving the integrity of the article.
16. **Posting licensed content on any Website**: The following terms and conditions apply as follows: Licensing material from an Elsevier journal: All content posted to the web site must maintain the copyright information line on the bottom of each image; A hyper-text must be included to the Homepage of the journal from which you are licensing at http://www.sciencedirect.com/science/journal/xxxxx or the Elsevier homepage for books at http://www.elsevier.com; Central Storage: This license does not include permission for a scanned version of the material to be stored in a central repository such as that provided by Heron/XanEdu.
Licensing material from an Elsevier book: A hyper-text link must be included to the Elsevier homepage at http://www.elsevier.com . All content posted to the web site must maintain the copyright information line on the bottom of each image.

**Posting licensed content on Electronic reserve**: In addition to the above the following clauses are applicable: The web site must be password-protected and made available only to bona fide students registered on a relevant course. This permission is granted for 1 year only. You may obtain a new license for future website posting.
17. **For journal authors:** the following clauses are applicable in addition to the above:
**Preprints:**
A preprint is an author's own write-up of research results and analysis, it has not been peer-reviewed, nor has it had any other value added to it by a publisher (such as formatting, copyright, technical enhancement etc.).
Authors can share their preprints anywhere at any time. Preprints should not be added to or enhanced in any way in order to appear more like, or to substitute for, the final versions of articles however authors can update their preprints on arXiv or RePEc with their Accepted Author Manuscript (see below).
If accepted for publication, we encourage authors to link from the preprint to their formal publication via its DOI. Millions of researchers have access to the formal publications on ScienceDirect, and so links will help users to find, access, cite and use the best available version. Please note that Cell Press, The Lancet and some society-owned have different preprint policies. Information on these policies is available on the journal homepage.
**Accepted Author Manuscripts:** An accepted author manuscript is the manuscript of an article that has been accepted for publication and which typically includes author-incorporated changes suggested during submission, peer review and editor-author communications.
Authors can share their accepted author manuscript:

- immediately
    - via their non-commercial person homepage or blog
    - by updating a preprint in arXiv or RePEc with the accepted manuscript
    - via their research institute or institutional repository for internal institutional uses or as part of an invitation-only research collaboration work-group

    - directly by providing copies to their students or to research collaborators for their personal use
    - for private scholarly sharing as part of an invitation-only work group on commercial sites with which Elsevier has an agreement
- After the embargo period
    - via non-commercial hosting platforms such as their institutional repository
    - via commercial sites with which Elsevier has an agreement

In all cases accepted manuscripts should:

- link to the formal publication via its DOI
- bear a CC-BY-NC-ND license - this is easy to do
- if aggregated with other manuscripts, for example in a repository or other site, be shared in alignment with our hosting policy not be added to or enhanced in any way to appear more like, or to substitute for, the published journal article.

**Published journal article (JPA):** A published journal article (PJA) is the definitive final record of published research that appears or will appear in the journal and embodies all value-adding publishing activities including peer review co-ordination, copy-editing, formatting, (if relevant) pagination and online enrichment.
Policies for sharing publishing journal articles differ for subscription and gold open access articles:
**Subscription Articles:** If you are an author, please share a link to your article rather than the full-text. Millions of researchers have access to the formal publications on ScienceDirect, and so links will help your users to find, access, cite, and use the best available version.
Theses and dissertations which contain embedded PJAs as part of the formal submission can be posted publicly by the awarding institution with DOI links back to the formal publications on ScienceDirect.
If you are affiliated with a library that subscribes to ScienceDirect you have additional private sharing rights for others' research accessed under that agreement. This includes use for classroom teaching and internal training at the institution (including use in course packs and courseware programs), and inclusion of the article for grant funding purposes.
**Gold Open Access Articles:** May be shared according to the author-selected end-user license and should contain a CrossMark logo, the end user license, and a DOI link to the formal publication on ScienceDirect.
Please refer to Elsevier's posting policy for further information.
18. **For book authors** the following clauses are applicable in addition to the above: Authors are permitted to place a brief summary of their work online only. You are not allowed to download and post the published electronic version of your chapter, nor may you scan the printed edition to create an electronic version. **Posting to a repository:** Authors are permitted to post a summary of their chapter only in their institution's repository.

19. **Thesis/Dissertation**: If your license is for use in a thesis/dissertation your thesis may be submitted to your institution in either print or electronic form. Should your thesis be published commercially, please reapply for permission. These requirements include permission for the Library and Archives of Canada to supply single copies, on demand, of the complete thesis and include permission for Proquest/UMI to supply single copies, on demand, of the complete thesis. Should your thesis be published commercially, please reapply for permission. Theses and dissertations which contain embedded PJAs as part of the formal submission can be posted publicly by the awarding institution with DOI links back to the formal publications on ScienceDirect.

**Elsevier Open Access Terms and Conditions**

You can publish open access with Elsevier in hundreds of open access journals or in nearly 2000 established subscription journals that support open access publishing. Permitted third party re-use of these open access articles is defined by the author's choice of Creative Commons user license. See our open access license policy for more information.

**Terms & Conditions applicable to all Open Access articles published with Elsevier:**

Any reuse of the article must not represent the author as endorsing the adaptation of the article nor should the article be modified in such a way as to damage the author's honour or reputation. If any changes have been made, such changes must be clearly indicated. The author(s) must be appropriately credited and we ask that you include the end user license and a DOI link to the formal publication on ScienceDirect.

If any part of the material to be used (for example, figures) has appeared in our publication with credit or acknowledgement to another source it is the responsibility of the user to ensure their reuse complies with the terms and conditions determined by the rights holder.

**Additional Terms & Conditions applicable to each Creative Commons user license:**

**CC BY:** The CC-BY license allows users to copy, to create extracts, abstracts and new works from the Article, to alter and revise the Article and to make commercial use of the Article (including reuse and/or resale of the Article by commercial entities), provided the user gives appropriate credit (with a link to the formal publication through the relevant DOI), provides a link to the license, indicates if changes were made and the licensor is not represented as endorsing the use made of the work. The full details of the license are available at http://creativecommons.org/licenses/by/4.0.

**CC BY NC SA:** The CC BY-NC-SA license allows users to copy, to create extracts, abstracts and new works from the Article, to alter and revise the Article, provided this is not done for commercial purposes, and that the user gives appropriate credit (with a link to the formal publication through the relevant DOI), provides a link to the license, indicates if changes were made and the licensor is not represented as endorsing the use made of the work. Further, any new works must be made available on the same conditions. The full details of the license are available at http://creativecommons.org/licenses/by-nc-sa/4.0.

**CC BY NC ND:** The CC BY-NC-ND license allows users to copy and distribute the Article, provided this is not done for commercial purposes and further does not permit distribution of the Article if it is changed or edited in any way, and provided the user gives appropriate credit (with a link to the formal publication through the relevant DOI), provides a link to the license, and that the licensor is not represented as endorsing the use made of the work. The full details of the license are available